MODELLING NEUTROPHIL TRANSIT THROUGH THE HUMAN PULMONARY CIRCULATION

by

BARRY JAMES RYDER WIGGS

BSc (UBC) 1982, MSc (UBC) 1989

A THESIS SUBMITTED IN PARTIAL FULFILMENT OF THE REQUIREMENTS

FOR THE DEGREE OF DOCTOR OF PHILOSOPHY

in

THE FACULTY OF GRADUATE STUDIES

DEPARTMENT OF EXPERIMENTAL MEDICINE

We accept this thesis as conforming to the required standard

THE UNIVERSITY OF BRITISH COLUMBIA

August, 1993

In presenting this thesis in partial fulfilment of the requirements for an advanced degree at the University of British Columbia, I agree that the Library shall make it freely available for reference and study. I further agree that permission for extensive copying of this thesis for scholarly purposes may be granted by the head of my department or by his or her representatives. It is understood that copying or publication of this thesis for financial gain shall not be allowed without my written permission.

Department of EXPERIMENTAL MEDICINE

The University of British Columbia
Vancouver, Canada

Date DEC 23/93

DE-6 (2/88)

Abstract

The object of this thesis was to construct a model to simulate the arterial, capillary and venous networks of the pulmonary circulation and to compute transit times of red blood cells and neutrophils through the human lung. A complete model of the arterial system was constructed using existing anatomical data for the arterial branching system combined with a set of probabilities to describe the branching nature of the arterial network beyond the existing data. Flow continuity and energy balance equations were used to estimate the total pressure drops through a wide range of possible pathways in this network. When flow had reached the capillary bed, a strictly stochastic model of cell transit through a randomly generated grid network was used to simulate capillary flow. Finally, the flow was returned to the left atrium by modifying the arterial network to represent the venous system.

Studies in several species have shown that neutrophils have much longer transit times than red blood cells in the pulmonary circulation. The model described above was used to test the hypothesis that this delay is due to the greater deformability of red blood cells with respect to neutrophils. The results show that erythrocyte transit times are accurately predicted from physical data using the model. However, the neutrophil transit times predicted from the delay which neutrophils experience as they deform to enter smaller capillary segments are shorter than current experimental results. This suggests that factors additional to those that result from cell deformation times delay the neutrophils. These factors could include either receptor-mediated neutrophil adhesion to endothelial cells or the time required for neutrophils to actively move through segments with very low driving pressures. It further suggests that these components are responsible for a major time delay of neutrophils in the pulmonary microcirculation which could

not be modelled with currently available data. The results obtained with the model also suggests that the fall in pulmonary vascular resistance and rise in circulating neutrophil count associated with increased pulmonary blood flow could be related to the flushing of neutrophils out of the pulmonary capillary bed.

Table of Contents

List of Tables

List of Figures

Acknowledgements

I wish to gratefully acknowledge the contributions that so many people have made in conducting this research. It will be a strong foundation from which to build a future of scientific inquiry.

The questions posed by this work are a start to a lifetime dedicated to unravelling the mysteries that are held, unsolved within the pulmonary vasculature. It is believed that the knowledge and skills learned through my program of studies will provide me with the tools needed to navigate the tough journey ahead.

To my committee, all the excellent researchers at the Pulmonary Research Lab, and my scientific colleagues - thank you. Without your guidance, critique and assistance this would not have been possible. Most of all to my wife, Veronica, who has been beside me through all the good times and the not so good times.

Hey folks .... IT IS DONE!!!!!!!!!!!!!!!!!!!!!

1 Objective

The modelling of biological systems has increased our understanding of structure and function at the molecular, cellular and organ level. This is well illustrated by Watson and Cricks' (94) structural model of DNA which revolutionized biology by providing new insight into DNA function. Similar, if less dramatic, advances have been provided by modelling of the cellular functions of transport (97), volume control (86) and mobility (51). The understanding of organ function has also been advanced, particularly in the lung, by the model of pulmonary blood flow introduced by West et al. (98), the model of ventilation distribution by Milic Emili et al. (67), and by the model of gas exchange across the alveolar capillary membrane provided by Wagner and associates (89).

The introduction of the computer into biology enhanced the sophistication of the modelling process by providing the rapid calculation capability required when anatomically based models are used to predict function. In a previous series of studies which formed the basis of my MSc degree (101, 103), a computational model of airway structure and function was developed which has been useful in predicting the effect of structural changes on airway function. The model allowed quantitative anatomic data obtained from normal and diseased airways to be entered and used to predict their effects on airways function. The information obtained from the model was then used to construct new hypotheses that are being tested either in whole animals or in isolated in vitro systems.

The model presented in this thesis was developed to investigate cell traffic through the lung vasculature. It is based on studies in both animals (18,19,20,21,42,62) and man (8,59,60) where a double indicator dilution technique was used to compare erythrocyte (RBC), platelet and neutrophil (PMN) traffic during a single transit through the pulmonary vascular bed. These studies showed that PMN were delayed with respect to RBC with only 20-30% of PMN appearing at the outflow with the RBC. They also showed that the lung capillary bed is uniquely designed to accommodate these difference in PMN and RBC transit time because it provides a vast network of short interconnecting capillary segments that allow the faster moving RBC to stream around segments filled with slower moving PMN (41). Unfortunately, indicator dilution technology does not allow a complete analysis of this system because the much longer transit time of PMN with respect to RBC allow substantial recirculation of RBC before all of the PMN have completed a single pass through the lung. Although this problem might have been overcome by using an isolated organ system that prevented recirculation, construction of a computer model based on existing anatomic and physiologic data was chosen in an attempt to understand the large body of experimental data.

The complexity of the pulmonary vasculature can be appreciated by examining the angiograms shown in Figures 1, 2 and 3. These images, from a normal human subject, taken 3, 8 and 20 seconds after dye injection, show the arterial tree filled at 3 seconds, the venous tree at 8 seconds with only a small amount of dye remaining in the pulmonary vessels. These images provide an overview of the very complex branching network and range of transit in the pulmonary circulation. At least two approaches are available for obtaining the information

needed to construct a model of this complex system. The first involves the application of a theoretical knowledge of branching systems based on a knowledge of fractals. The second is based on existing information about the anatomic structure of the lung where behaviour of the branching system is represented by stochastic rules.

The available morphometric data from the arterial trees of dogs, humans and cats have been used to graph the relationship between the number of vessels at any given order vs the average diameter of a vessel at that particular order (109). Typically, these plots are drawn on a log-log scale and show a remarkedly linear relationship between these two parameters suggesting a scale independent nature of the branching structure. The use of fractal analysis to describe physiological phenomena has been effectively employed by Bassingthwaite et al. (4,5) to investigate the spatial heterogeneity of blood flow in the heart and by Glenny et al (34,35) to investigate the relative contribution of gravity to regional variation in pulmonary flow. While the use of fractals allows the very complex systems to be simplified to an extremely small number of parameters it also loses some of the anatomical feel for the physiological system being investigated. Although it is possible to study the human vasculature using an analytical approach based on fractals, the present thesis is based on an anatomical approach to this problem. Principally, this decision was based on the fact that the pathologists, physiologists and clinicians with whom I collaborated to collect much of the data that stimulated the development of the model, found it easier to consider problems when posed in anatomical rather than abstract frameworks.

The starting point for construction of the model was the knowledge that: PMN are delayed with respect to RBC in a single pass through the canine (10,41,57,62,63), rabbit (18, 19,20) and human lungs (42,59,60,68). Using indicator dilution studies, Martin et al (62, 63) labelled both RBC and PMN in order to compare how these cells traverse the pulmonary circulation. When RBC labelled with either ^{99m}Tc or ^{51}Cr were simultaneously injected into the right atrium and collected at the aorta, there was no difference in how the cells traversed the pulmonary circulation (Figure 4). However, a similar injection where ^{99m}Tc RBC are compared to ^{51}Cr PMN showed that the PMN are markedly delayed in the lung with respect to the RBC (Figure 5). A series of studies subsequently showed that from 60 - 80% of PMN are delayed with respect to RBC in the human, rabbit and dog respectively (42).

Although PMN have similar maximum diameters to RBC, they deform much more slowly (13,23). This difference in deformability has been used to explain the observed difference in PMN and RBC transit time (40,41,42). However, the vast parallel arrangement of the pulmonary capillary segments means that the pressure drop across individual capillary segments must be small and raises the question as to where the large forces required to move PMN into single capillaries (23) are generated. The fact that it is difficult, if not impossible to measure the pressure across individual segments of the pulmonary capillary bed, led us to consider creating a model of the pulmonary vasculature to estimate the delay that PMN experience with respect to RBC. The anatomic data for the model comes from several sources. The data for the large vessels was generously provided by Dr. Keith Horsfield from existing published and unpublished information obtained from a human pulmonary vascular cast studied in his

laboratory. This information allowed us to obtain adequate data to construct a reasonable model of the arterial supply and to infer the venous drainage of the pulmonary capillary bed. The data on the PMN and capillary segment dimensions was based on Weibels' (95,96) original reports that were supplemented by independent studies from our own laboratory (21).

The goal was to construct a model of the arterial, capillary and venous systems of the human pulmonary vasculature that would provide realistic RBC and PMN transit times. It involved the construction of a set of probabilities to describe the branching nature of the arterial network that allowed the pressure drop through the system to be estimated using flow continuity and energy balance equations. A strictly stochastic model of cell transit was then used to simulate capillary flow through a randomly generated grid network. The flow was then returned to the left atrium by modifying the arterial network to represent the venous system.

The results suggest that the model accurately predicts RBC transit times but underestimates the delay which PMN experience with respect to the RBC during a single transit through the lung. This suggests that factors such as receptor mediated PMN endothelial interactions and the ability of trapped PMN to actively move through restrictions provided by the capillary bed may be important determinants of their transit time. The computational model that has been constructed provides a framework in which to think about the problem of cell transit through the pulmonary circulation and suggests new experiments to try in order to achieve a better understanding of this problem.

2. The Large Vessels

2.1 Introduction

Horsfield and his colleagues (44,45,47,78,79) made detailed measurements of the arterial and venous branching system on a cast of the pulmonary vascular system obtained from the lungs of a 32-year old woman who died of uremia and was free from any known respiratory disease. The complete process for preparing the cast was described in detail by Singhal et al (78). Briefly, the trachea and main pulmonary vessels were washed free of secretions and blood clots and then cannulated. The airspaces were inflated with carbon dioxide momentarily and then allowed to deflate by their own elastic recoil. This process of inflation and deflation was continued to replace the air in the lung with carbon dioxide. The lungs were then floated in a tank of boiled air-free tap water and a plastic tube was attached to the bronchial cannula. The free end of the tube was left in that tank below water level and a deBakey roller pump was used to pump water from the tank into the lungs. Water easily passed through the lung tissue and returned to the tank via the pulmonary blood vessels and the pleural surface. By adjusting pump speed, any level of lung inflation could be obtained.

The lungs were inflated to the top of their pressure-volume curve and then deflated down to a volume corresponding to functional residual capacity. Pumping was continued until the lungs sank to the bottom of the tank, implying that most of the carbon dioxide had been replaced by air-free tap water. Formaldehyde solution (40%) was added to the tank to make a 2%

formalin solution, which circulated through the lungs for 48 hours. During fixation, 0.9% sodium chloride solution was pumped through the arterial cannula at a constant pressure of 25 cm H_2O. After fixation, the lung volume was 5.01 ± 0.10L.

The method for casting the vasculature tree was that of Tompsett (87). A mixture of monomer, resin, catalyst and accelerator was allowed to flow into the arterial cannula from a height of 25 cm above the formalin level. During casting, the lungs remained submerged and the density of the casting material was 1.125 g/ml, similar to water, so that little if any pressure difference existed between different regions of the fluid filled lung. The casting mixture flowed easily through the arteries, capillary bed and venous system. After four minutes, the resin gelled and it was allowed to harden for eight days. The surrounding lung tissue was corroded from the cast with concentrated hydrochloric acid and the cast washed clean in tap water. No shrinkage was detected during the setting or cleaning process.

The data subsequently published from observations on this cast was useful but the goals of the authors differed significantly from the objectives of this study. Horsfield et al wanted to provide detailed anatomical information about the branching structure of the arterial and venous trees in a normal human lung. They chose to order the complex branching network of the arterial and venous trees using a Strahler ordering system. This system has been widely used by geomorphologists to describe the branching patterns of rivers (85) and has the unique property of producing a branching structure with the minimum number of orders.

Figure 6 shows a simple network ordered according to Strahler rules. In this branching scheme, all identifiable terminal endpoints are denoted as order 1. When two branches of the

same order meet at a junction, the resulting parent branch increases in order by one. If two branches of different orders join, the order of the parent branch remains the order of the largest ordered branch. Unfortunately, this branching scheme, while efficient, loses a great deal of information. In particular, estimates of length and fluid flow from the main pulmonary artery to the terminal arterioles are impossible when modelled using the Strahler ordering system since many divisions will occur where the length from the parent branch to the division is not recorded.

Alternative branching schemes are possible and the most frequently considered are the Weibel symmetric branching scheme and the Horsfield asymmetric scheme. Figure 7 shows the result of symmetric ordering of the tree in Figure 6. In this method, the main pulmonary artery would be labelled order 0 and at each division the two daughter branches would each be designated one order larger than the parent. This branching method obviously relies on a highly symmetric branching pattern and cannot be reasonably considered as a viable scheme for ordering the very asymmetric vascular tree shown in Figures 1-3. The system which Horsfield and Cumming used to describe the branching network of the bronchial tree (46) is similar to Strahler ordering where each terminal branch is identified as an order 1 vessel. However, as any two vessels join, the parent vessel is ordered as one order larger than the largest daughter. Figure 8 shows the same tree as in Figures 6 and 7 with Horsfield orders.

Several points can be made from the investigation of these different ordering methods. First, Weibel ordering is a "top down" while Horsfield and Strahler are "bottom up" methods. In this regard, Weibel ordering has clear advantages for recording cast information. It is not

necessary with a Weibel symmetric (96) structure to locate all the terminal endpoints which can be extremely difficult when using casts. Secondly, Weibel structures are uniform bifurcating systems where Horsfield and Strahler systems need not be. The angiograms shown in Figures 1-3 clearly show a high degree of disparity between the size of daughter branches from a single parent. Third, Strahler ordering has a fundamental flaw which renders it unusable for any investigations of transit time. Looking closely at Figure 6, we see that on the right side of the figure, there is a single branch labelled "2" with a branch "1" offshoot. Since the entire vessel 2 is recorded as a single unit rather than as a parent and a daughter, it is impossible to record the correct path length for any blood travelling down the branch "1" offshoot. The number of segments, and therefore bifurcations, traversed in a branching structure cannot be determined using this ordering scheme. Also, since Strahler ordering loses vital length information, it is not possible to estimate the pressure drop along a length of vessel.

Because of the unique nature of the casts prepared and studied by Dr. Horsfield, he was approached for permission to study the original data. The purpose was to completely reorder all cast data using the Horsfield branching system so that true vessel length and diameter of each vessel segment could be modelled. Unfortunately, the original casts, now some 20 years old, had been destroyed but Dr. Horsfield was able to provide the data sheets showing the original vessel identification and methods used for cataloguing the branches of the cast. He also allowed us to study copies of many drawings of the cast branches. Using both the drawings and the vessel identification charts, the casts were reconstructed in a computer that allowed any ordering scheme to be applied.

The available data was in four distinct regions and the number of individual branches available in each region is summarized in Table 1. These four regions divided the available cast data into sets of vessels of decreasing diameter. The first task was to study the original drawings since these were the only visual link back to the original cast, and several observations were made. First, it became apparent, both from the drawings and from angiographic images, that the pulmonary vasculature consisted not only of bifurcating but also trifurcating branches. The number of trifurcations were sufficient that they could not be ignored and would have to be included to obtain an accurate model. Second, within each zone, a large number of smaller vessels were broken or lost at the end of the casts. This artifact tends to lower the numbers of branches recorded for the very small orders as they broke more easily than larger branches. Third, studies of the drawings in relation to the angiograms showed that it was possible for daughter branches from a single parent to have very different diameters. Finally, the model was further complicated by the presence of numerous 15 μm vessels which appeared to extend out from many vessels at a nearly right angle. These tiny vessels were distributed throughout the cast and do not appear to be merely ruptures in the vessel walls giving fine strands of casting material. These vessels were eliminated from the dataset and not considered in modelling pressure drops, flows and transit times.

2.2 Arterial Branching Pattern

Each of the four data regions (Table 1) where information was available were ordered as follows. First, all terminal branches were labelled as order 1 vessels. Then a computer program was written to track each daughter pair to the appropriate parent and ordered the parent branch one order higher than the largest daughter. Trifurcations could be easily handled using this branching scheme, as could the vast difference between the orders of daughter branches from a single parent. This process required that all terminal branches be of a set size. The smallest remaining broken cast branches were assigned an order based on their diameter in relation to the already ordered branches. The computer program then attempted to reorder as much of the remaining tree as possible using an iterative process, returning to order unbroken branches as required, until every available branch in each of the four regions was ordered. The final branch ordering was determined to be the scheme with the smallest diameter coefficient of variation when data were represented on a log scale.

Once each region was ordered, the individual regions were connected to generate a single ordering system from 15μm to 3cm vessels. The rough Horsfield ordering can be seen in Figure 9 where each region has been artificially placed on a scale from 0 to 80 so that some gap is left between regions. Note from this figure that as the smaller regions of each zone are approached, diameters appear to decline in a curvilinear manner. The reason for this curvilinear drop was that whole cast portions had been destroyed, resulting in biased estimates. It was very difficult, as Horsfield noted, to use the cast and not have whole sections break away. The remaining

unbroken sections had been preserved and tended to have a greater number of larger vessels since portions with smaller vessels were trimmed off to aid counting. This loss artificially increased the estimated vessel diameter. The original zones were carefully selected by Horsfield and his colleagues to overlap each other by a few orders. The diameter of the smallest vessels in one region were compared to the diameters of the largest vessels in the next region. The large vessels of this more distal region were given orders similar to the same diameter vessels in the more proximal region. Once it was established how one region's orders related to all others, the complete dataset was reordered.

The results using a modified Horsfield ordering scheme to order the arterial branches of the pulmonary circulation are shown in Figure 10. There were 48 orders from the main pulmonary artery to the precapillary vessels of approximately 15μm in diameter. The log(diameter) was related to vessel order using a weighted regression analysis (Systat, Evanston, IL) where the data at each order were weighted inversely by the variability about the mean of that order and the results fitted to the relationship:

$$\log(\text{diameter}) = A + B*\text{Order} \qquad \text{[EQN 1]}$$

where:

Estimate	Value	Standard Error
A=Intercept	2.64	0.04
B=Slope	0.15	0.01

The overall model had a fit, R^2, of 0.995 for the relation between log(average diameter) versus order. The estimates for slope and intercept correspond to a precapillary estimated diameter of 15μm at order 1 and each order's mean diameter increases by about 25% for each single order increase.

Once the vessels had been ordered, further information regarding how the vessels branched was required to estimate path lengths, pressure drops and transit times. Horsfield ordering systems, as already mentioned, are "bottom up" ordering systems. However, "top down" branching rules would be preferred so computations could begin at the main pulmonary artery and terminate at precapillary vessels. To formulate a "top down" ordering scheme, two pieces of information were recorded for each branching site. First, whether the vessel bifurcated or trifurcated (or divided an even greater number of times) was recorded. Second, the decreases in order for each daughter from the parent branch (parent branch order minus daughter branch order) was recorded. This second piece of information was recorded for every daughter while keeping track of which daughter had the largest, second largest, etc, diameter. The data from the four regions were combined to give two major cast regions, 3cm to 100μm, and 100μm to 10μm, since two regions had relatively few branches (Table 1).

Table 2 shows the results for bifurcations and trifurcations in these regions. In large vessels, 82% of the branches were bifurcations. There were a significant number of trifurcations, and the fraction of branches that were trifurcations increased in the smaller vessels. Table 3 shows how the daughters branched, relative to the parent, in large vessels and table 4 shows the same results for the small vessels. In these tables, a bifurcation would have

a largest and a smallest daughter while a trifurcation would have a largest, second largest and smallest daughter. The data for the bifurcations and trifurcations were combined as there was no difference between their branching patterns, the difference in orders between the parent and daughter branches was not affected by a division being a bifurcation or trifurcation. It is of interest to note that the largest daughter branched relatively slowly, dropping typically 1 or at most 2 orders smaller than the parent, while the smaller daughters dropped several orders relative to the parent branch. These data show that the path lengths from the main pulmonary artery to the 15μm precapillary vessels vary considerably and are likely to result in the wide range of transit times through the vascular tree.

The probabilities displayed in tables 2,3 and 4 provide a set of branching rules which can be used to reconstruct a model of the arterial branching system. One very important piece of information which will be required is the relationship between branch length and vessel order. Because the data for this work was reconstructed from drawings and old files, the valuable length data contained in the original cast was largely lost. Only about 600 vessels, ordered by our new system, had length information available, and most of these were larger vessels. Singhal et al found a linear relationship between the log(length) and vessel diameter (78). This relationship is likely to be a function of the branch ordering scheme they selected, and we could not accurately estimate any relationship between length and order. In this study the ratio of length to diameter was plotted versus order and the relationship showed that the ratio was similar for all orders. Realizing that this is a potential weakness, but without the original cast to either consult or measure, we took all values for which both length and diameter were available and

estimated an average value for length relative to diameter, regardless of order to be 140%±30%.

The actual large vessel model was constructed using the anatomical measurements from the cast data for all branches from order 45 to 48 (the largest vessels). The reason for this was that the estimated lengths, diameters and branching probabilities for these first few divisions were not accurately represented by the prediction methods proposed. Table 5 shows the branching scheme and dimensions for these larger vessels. Once order 44 was reached, the probabilities from tables 2, 3 and 4 were continually applied until all vessels terminated in an order 1 vessel. To terminate the tree, a vessel was not allowed to branch beyond order 1. Table 6 shows the resulting branching pattern for the orders from order 44 to 1. Figure 11 shows the relationship between the model's estimate of the number of branches at any given order from the main pulmonary artery to the 15μm order 1 precapillary vessels. At order 1, the model predicts $3x10^8$ terminal arterioles.

In Figure 12, the relationship between cross-sectional area available for blood flow and anatomical order from the main pulmonary artery to precapillary vessels is shown. There is a vast increase in the available cross-sectional area as flow approaches the capillary bed. This large increase is required to obtain a sufficient area for gas exchange between the alveolar airspaces and the capillary blood. Also of interest in Figure 12 is the reduction in cross-sectional area between orders 40 to 45. A corresponding reduction in the cross-sectional area available for airflow has been noted by Weibel and Gomez (96) and Horsfield and Cumming (46). Unfortunately, since simultaneous cast information on both airways and pulmonary vessels

is not available, it is difficult to state with certainty that both cross-sectional area reductions occur at the same anatomical location.

Using the branching probabilities estimated in this section, a realistic model of the arterial tree based on anatomical information can be computed.

2.3 Estimation of Flow in Arterial Vessels

The calculation for available cross-sectional area in Figure 12 is based on an assumption that the entire cardiac output passed through each order so that all branches of a given order contributed to the available cross-sectional area. This is clearly incorrect because the cast data show that at most branches one daughter branch is markedly smaller than the other. This inequality in daughter branches implies that some fraction of the flow arrived at a more distal location in the arterial tree without flowing through a vessel of every order. The consequence of this result is that estimations of the path length from main pulmonary artery to the capillary bed, the fraction of flow in a given branch and the expected pressure drop in the arterial tree must be made with consideration as to how flow divides at each bifurcation.

As previously stated, the division of flow at a bifurcation can not be determined simply by assuming that the flow to a given order branch is equal to the total cardiac output divided by the total number of branches of that order. This technique has been used by others to map airflow flow in the lung (72,102) and to map blood flow in the cat lung (110) but the marked asymmetry in the human pulmonary arterial tree makes this approach questionable. Instead, continuity equations were used to determine the possible range of flows that could exist in a branch of any given order. Consider the possibilities for bifurcating branching patterns of a vessel with a given order. We will denote the division of a parent into its two daughters as 2:(1,1), indicating that a parent of order 2 has divided into two daughters, each of order 1. This is the only possible choice for an order 2 branch as it has already been assumed that the arterial

tree terminates at order 1 vessels. Another assumption will be that the entire cardiac output is evenly distributed to the terminal arterioles so that each order 1 branch carries 1 unit of the flow. Continuity states that the total flow into the daughter vessels must equal the total flow in the parent vessel. Therefore, each order 2 branch must carry 2 units of order 1 vessel flow. The branching choices for an order 3 branch are 3:(1,1), 3:(1,2), and 3:(2,1). Recall that the 3:(1,1) is possible since daughters may be up to 5 orders smaller than the parent branch and the largest daughter can branch either one or two orders from the parent. Since each order 2 branch carries 2 units of flow and each order 1 branch 1 unit, order 3 branch vessels can carry either 3 or 2 units of flow. The possibilities at order 4 are: 4:(3,3), 4:(3,2), 4:(3,1), 4:(2,3), 4:(2,2) and 4:(2,1) and the resulting flows are either 2,3,4,5,6,7 or 8 units of flow. While these examples deal only with bifurcations, trifurcations can also be considered and every possible combination for any branch order can be determined.

Figure 13 shows the possible distribution of flows in branches of given orders relative to order 1 branches if all pathways are equally likely. As the branch increases in order, it carries, on average, a higher flow rate but the variability of the flow rate quickly increases as the number of available pathways increases. Using a computer to track the flows, it was possible to map every possible pathway up to an order 20 vessel. Beyond this order, the number of available pathways was so immense that they could no longer be stored for analysis using available equipment.

Figure 14 shows the average flow through each vessel for each order as a fraction of the total cardiac output. Using the average flow in a vessel and the total number of vessels of

each order, it is possible to estimate the average flow through an entire order. The estimated average flow through each order was computed to be approximately 50% of the total cardiac output. Also, from the data in Figure 13 used to generate Figure 14 each order also has a standard deviation about the mean of the flow. The average flow and the standard deviation of the average flow through a branch of a given order were fit to an exponential equation for orders 44 to 2:

$$\text{average flow (ml/s)} = \exp(-14.682 + 0.397 * \text{Order}) \quad \text{[EQN 2]}$$

$$\text{SD Flow (ml/s)} = \exp(-15.682 + 0.403 * \text{Order}) \quad \text{[EQN 3]}$$

Based on estimates of the possible flow to branches of an arterial tree where each terminal branch receives a uniform fraction of the total cardiac output, equations 2 and 3 will be used to estimate the flow in a branch for any given order.

2.4 Calculation of Arterial Pressure Drop

Bernoulli's equation states that, in conditions of steady flow for a frictionless incompressible fluid, that the energy stored in the fluid is a constant (28,71). The equation is:

$$\frac{P}{\gamma} + Z + \alpha\frac{V^2}{2g} = constant \qquad [EQN\ 4]$$

where:

P/γ	=	energy stored in the fluid due to the pressure the fluid is under per unit weight of the fluid
Z	=	vertical height of the fluid
$V^2/(2g)$	=	kinetic energy stored in the fluid
P	=	pressure
γ	=	specific weight of the fluid = ρg
ρ	=	density of the fluid
g	=	acceleration of gravity
V	=	average velocity
α	=	kinetic energy coefficient

The height effect, Z, in this equation is negligible for a single bifurcation and can be eliminated allowing [EQN 4] to be rewritten as:

$$P/\rho + \alpha V^2/2 = \text{constant} \qquad \text{[EQN 5]}$$

At a single bifurcation or trifurcation the Bernoulli equation between any two points in a pipe network must be related according to the energy or head loss between these two points. As an example of the calculation procedure consider a simple bifurcation (a trifurcation was handled in an analogous manner) where the parent branch is denoted by the subscript 1 and the daughters by the subscripts 2 and 3. The energy balance equations are then:

$$\left(\frac{P_1}{\rho} + \alpha_1\frac{V_1^2}{2}\right) - \left(\frac{P_2}{\rho} + \alpha_2\frac{V_2^2}{2}\right) = H_{Lt} \qquad \textit{[EQN 6]}$$

$$\left(\frac{P_1}{\rho} + \alpha_1\frac{V_1^2}{2}\right) - \left(\frac{P_3}{\rho} + \alpha_3\frac{V_3^2}{2}\right) = H_{Lt} \qquad \textit{[EQN 7]}$$

where H_{Lt} is the total head loss for the route from the parent through the bifurcation to either daughter 2 or daughter 3 and represents the unwanted conversion of mechanical energy to thermal energy.

Head loss can be separated into a major, h_L, and minor, h_{LM}, component. The major head loss component is due to friction and if the change in height between the two network locations is negligible, as we are assuming, then:

$$h_L = f\frac{L}{D}\frac{V^2}{2} \qquad [EQN\ 8]$$

where L=pipe length; D=pipe diameter; V=velocity and f is a nondimensional parameter used for describing fluid behaviour and is equal to 64/(Reynold's Number) for laminar flow (28). Reynold's Number is equal to:

$$Re = \rho\frac{VD}{\nu} = \rho\frac{4Q}{\Pi\nu D} \qquad [EQN\ 9]$$

where:

V	=	velocity
D	=	pipe diameter
Q	=	flow rate
ν	=	viscosity
ρ	=	density

The minor losses are related to changes in pipe geometry, the most important factor in this model being the bifurcation itself. These losses can then be calculated as:

$$H_{LM} = f\frac{Le}{D}\frac{V^2}{2} \qquad [EQN10]$$

where Le is the equivalent pipe length that would represent a frictional loss as severe as the geometry change and is typically determined experimentally. Gelin (32) made several detailed investigations into the pressure drop in tubes past a trifurcation point. In his experiments, flow with an entrance pressure of 160,000 dynes/cm^2 was calculated to have a drop of 116,850 dynes/cm^2 in the lead vessel and 17,040 dynes/cm^2 in the branch vessels. This left an unaccounted drop, from the input to the parent vessel to the output of each daughter, of 26,110 dynes/cm^2 (160,000-116,850-17,040). These pressures were modelled by Charm and Kurland (12) using laminar flow assumptions, and they obtained results very nearly identical to those determined experimentally by Gelin. Charm and Kurland proposed that the remaining unaccounted for 26,110 dynes/cm^2 was due to the division in flow itself. This value would indicate that the bifurcation or trifurcation contributed at least as much to the pressure drop as did the pressure drop along the daughter branch. Using Gelin's results, a value of 1.5 was used for Le/D in the equation for minor head losses (26,110/17,040). The calculated losses due to flow division were included in the calculation of pressure drops only if the estimated Reynold's Number exceeded 100, since pressure drops at a low Reynolds numbers will be determined solely by the viscous losses (72).

Equations 6,8 and 10 can be combined to give:

$$\left(\frac{P_1}{\rho} + \alpha_1\frac{V_1^2}{2}\right) - \left(\frac{P_2}{\rho} + \alpha_2\frac{V_2^2}{2}\right) = f\frac{L_2}{D_2}\frac{V_2^2}{2} + f\frac{Le_2}{D_2}\frac{V_2^2}{2} \qquad \textit{[EQN 11]}$$

The ideal solution to this equation would be to compute the pressures and flows using the combinations of the continuity equation and energy balance equation through the entire pulmonary arterial tree. This, however, is impossible because of the vast number of branches involved. Instead, each order was considered as a complete unit in much the same manner as Zhuang et al (109). Equation 11 can be rewritten as:

$$P_1 = \frac{\rho}{2}(V_2^2 - V_1^2) + f\rho\frac{L_2\, V_2^2}{D_2\, 2} + f\rho\frac{Le_2\, V_2^2}{D_2\, 2} P_2 \qquad [EQN\ 12]$$

$$OR$$

$$P_1 = \Delta P + P_2$$

Obviously, the pressure difference between any two orders, ΔP, is made of three components: $(\rho/2)(V_2^2-V_1^2)$ is the change in kinetic energy; $f\rho(L_2V_2^2)/(D_22)$ is the major head loss; $f\rho(Le_2V_2^2)/(D_22)$ is the minor head loss. Each order has approximately 50% of the total cardiac output flowing through it and this flow divides into the next 5 orders. The velocity of flow in each order will be estimated as the total flow divided by the cross-sectional area available for flow. The major head loss will be then be computed directly using equation 8. The minor head loss is computed using equation 10 with $Le/D=1.5$. The kinetic energy change is estimated for the difference in velocities between the parent order and each of the next five daughter orders. Each daughter order will then have 5 different possible values for this equation and a weighted average based on the probabilities in tables 2 to 4 will be used to estimate an average kinetic energy transfer.

It is well known (29) that the viscosity of whole blood is affected by the size of vessel through which it flows. The change in viscosity, commonly termed the Fahraeus-Lindquist effect (24) is a reduction in the viscosity as vessel diameter decreases. Kiani and Hudetz (50) have developed an empirical model to estimate the dependence of blood viscosity on vessel diameter and hematocrit. The model they developed, for tubes larger than 10μm is:

$$\mu_{app} = \mu_p[1-(1-\mu_p/\mu_c)(1-2\delta/d)^4]^{-1}\,[1-(D_m/d)^4]^{-1} \qquad \text{[EQN 13]}$$

where:

μ_{app} = apparent viscosity of blood relative to plasma

μ_p = viscosity of plasma

μ_c = core apparent viscosity = exp(0.48 + 2.35*hematocrit)

δ = marginal layer width (microns)= 2.03 - 2*hematocrit

d = tube diameter in microns

D_m = effective diameter of a single red blood cell in the vessel and was assumed to be constant at 3 microns but this has little effect for vessels of sizes greater than 15 microns.

The pressure drops in the arterial tree were then computed as follows:

1) The probabilities in tables 2, 3 and 4 were used to compute the arterial tree and determine the number of vessels of a given order.

2) The diameters and lengths of vessels were assigned to branches at each order with a coefficient of variation of 30%.

3) The total flow through all branches at each order from 44 to 4 was assumed to be 50% of the total cardiac output. Orders 48 to 44 have 23 endpoints (Table 5), it was assumed that each of these endpoints carried 1/23 of the cardiac output. Similarly the orders from 4 to 1 were mapped assuming that all possible branching patterns to order 1 vessels were equally likely.

4) Using the geometry in 2) and the flows in 3) the velocity of flow was estimated.

5) The viscosity was estimated using equation 13.

6) The distribution of Reynolds number at each order was estimated

7) The friction factor was estimated as 64/Reynold's Number

8) The major head loss due to friction was computed

9) The loss of kinetic energy due to varying flow velocities was computed as: $(V_i^2 - V_{i-1}^2)\rho/2$

10) The entire pressure drop for each order was estimated

11) The average pressure drop for the entire arterial tree was estimated by summing the pressure drop for each order.

The simulation program was written in Gauss VM (Aptech Systems, Kent WA) and all calculations were made on an IBM 30386 based computer.

Therefore, the following sequence is followed to estimate the pressure drop of a particular pathway through the arterial tree. Starting at the main pulmonary artery, the

probabilities from tables 2 to 4 were used to predict the orders of the daughter branches. The daughters were assigned diameters and lengths using equation 1. Flows were purposely assigned to either one daughter in a bifurcation or 2 daughters in a trifurcation based on equations 2 and 3. The continuity equation was used to compute the flow in the remaining daughter. Equation 12 was then solved for the pressure drop from parent to each daughter. One daughter was randomly chosen as the parent for the next division and the process continued until an order 1 vessel was reached. Using this technique, the average pressure drop from main pulmonary artery to terminal arteriole averaged 1.8mmHg and ranged from 0.2 mmHg to 4 mmHg. The interquartile range of arterial pressure drops for a random path from the main pulmonary artery to the precapillary terminal arterioles was 1.5 to 2.5 mmHg. The distribution of total pressure drops is shown in Figure 15. Figure 16 shows the distribution of pathlengths using the simulation results. The average pathlength is 5.3cm ranging from 2.1cm to 11.2cm. In Figure 17 the estimated velocity of blood flow at the precapillary level is shown.

Using equations to balance the energy contained in a volume of flowing fluid and the mass of the fluid; accounting for pressure losses due to a division of flow; a changing viscosity; the total pressure drop through a model of the arterial tree can be calculated.

2.5 Pulmonary Venous Circulation

Although the remaining drawings of the cast of the venous tree were more limited than those available from the arterial system. Previous work by Horsfield and Gordon (47) included a detailed Strahler ordering of the pulmonary veins in man. Using Strahler ordering, they found that the veins contained only 15 orders as compared to the 17 orders found in the arterial tree. Some of the difference between the number of orders is due to the venous return to the left atrium actually arriving as 4 distinct vessels, effectively cutting off the top two orders of the venous tree. Table 7 shows the ratio between arterial and venous trees for the number of vessels, the diameter and the length for each Strahler order. There are 5 times as many terminal venules as there are arterioles but the average diameter and length for vessels at each order is within the individual vessel variation recorded for the arterial tree (about $\pm 30\%$) (Figure 10).

Table 8 shows the percent reduction in the number of branches for each order relative to the order immediately distal to it. Both the arterial and venous trees appear to converge from order 1 to order 15 or 17 in a similar pattern. Since no actual information was available on how the branches of the venous tree divided, no tables of probabilities could be constructed as for the arterial system. However, because of the striking similarity between the Strahler ordering of both the arterial and venous trees, we decided to use tables 2 to 4 to describe the structure of the venous tree. The only minor difference was that the top 4 Horsfield orders in the tree were eliminated as was the single bottom order. By trimming the tree in this manner, 78×10^6 terminal venules were recorded in contrast to 73×10^6 actually estimated by Horsfield and Gordon

(47). Table 9 shows the branch orders, number of branches and average diameters for the venous tree structure similar to Table 6.

The calculations to estimate geometry and pressure drops was exactly as for the arterial tree. Figure 18 shows a histogram of the pathlengths through the venous tree. The distribution of the total pressure drop along these pathlengths is shown in Figure 19. The average venous pressure drop is estimated to be 1.2mmHg with a range from 0.01 to 4.1mmHg. The maximum cumulative pressure drop for both the arterial and venous systems is displayed in Figure 20. This maximum pressure drop was obtained from the longest possible pathway, one that involves every order through the arterial and venous tree. Also shown in Figure 20 is the average pressure drop for each order. If the total pressure drop across the pulmonary circulation is 8 mmHg then only about on half of this drop is due to pressure drops in each of the large vessel regions and the rest of the pressure drop must be located in the capillary bed.

In this model it is was assumed that the branching structure of the venous tree is identical to that of the arterial tree with exception of fewer orders being present in the venous system.

3 The Capillary Bed

3.1 Capillary Dimensions and Their Relation to Neutrophil Size

As early as 1963, Weibel (95) reported measurements on the size of capillaries in the human lung. He found that the average capillary segment diameters were $8.36 \pm 2.96 \mu m$ (range 2-14μm) and the capillary segment lengths were 12.30 ± 4.72 μm (range 3-25μm). In addition Schmid-Schonbein et al (75) measured the diameter of leukocytes to be 7.25μm. Using a technique similar to Schmid-Schonbein et al (75) and modified by Williams (104) a pure population of human neutrophils and a random sample of human capillaries were measured to obtain the dimensions of these structures and to verify published values from several different laboratories. The purpose was to provide direct dimensional comparisons between neutrophils and capillaries so that these values could be used to develop a computational model of the capillary network.

Lung tissue from patients undergoing lung resection (59) for small peripheral tumours was used for the measurement of capillary structure. Briefly, the surgery proceeded until the vasculature of the lobe to be resected was isolated. The lung was then inflated and ventilated at a constant rate for approximately 10 minutes. The artery and vein supplying the lobe were tied off and the resection completed. The lobe was immediately inflated with 7.0% glutaraldehyde at a constant pressure of 25cm of fixative through the bronchus. The specimens were submersed in fixative overnight, sliced in the gravitational plane and random tissue samples from normal regions of lung were removed and processed for both light and electron microscopy.

Tissue sections were randomly selected for light microscopy from the available blocks and were dehydrated in graded alcohols and embedded in paraffin. The dimensions of the blocks had been previously recorded so that any shrinkage due to the dehydration could be corrected for. Light microscope sections 25μm thick were cut from these blocks and stained with toluidine blue O. Capillary segment diameters and lengths were measured at 400X magnification with a Nikon microscope equipped with a camera lucida and digitizing tablet interfaced to a microcomputer. Only whole capillaries that were entirely within a single focal plane were measured. These measurements were then corrected for linear shrinkage by comparing the dimensions of the cut sections to the original block dimensions.

The PMN dimensions were recorded on three human subjects undergoing lung resection for cancer. RBC were sedimented from the whole blood using dextran (molecular weight 100-200KD) and the leukocyte rich plasma was then removed and gently mixed with 7% glutaraldehyde for fixation. These fixed cells were suspended in 20% bovine serum albumin which was then cross-linked with 0.5% glutaraldehyde to form a rigid structure. Finally, this cell block was cut into 1mm cubes, post fixed with 1% osmium tetroxide, dehydrated with graded alcohols and embedded in epoxy resin. Sections 60-90nm thick were cut using a diamond knife on an ultramicrotome (Reichart Ultra Cut II) and stained with uranyl acetate and Satos lead for examination by electron microcopy (Philips 400). Photographs of 75-135 sections were sequentially obtained for each human sample at 10,000X magnification.

Unlike the measurements of the capillary segments, direct measurements of the neutrophil diameters can not be made. It is, however, possible to formulate a set of probability rules

(75,104) that consider the neutrophils as a system of polydispersed spheres. Any single random section through a sphere will provide (if the section is thin enough) a single circular cross-sectioned profile with a measurable diameter. The profiles can be grouped by diameter into one of perhaps 30 bins, each with a designated diameter range. These profiles in the largest diameter bin represent the population of neutrophils that are the largest and have been sectioned at or near their exact centre. If 50 profiles of 500 measured profiles fall into this largest bin, the expected number of profiles that should be found in the bin with the next smallest range of diameters can be estimated. If more profiles are found in the second bin than expected based on the number found in the first bin, then a second population of neutrophils of a slightly smaller maximum diameter than the ones in the first bin must exist. If less profiles than expected are found then not enough total profiles have been sampled. This process of matching expected to observed number of profiles is continued until the last bin size is reached.

Important assumptions for this technique are that the suspended and fixed neutrophils that were sectioned are spherical and that no neutrophil is sampled twice. While the exact 3-dimensional structure can not be determined the cells did in fact appear quite spherical. The sections were guaranteed to never contain profiles from the same neutrophil by trimming the blocks between section cuts by a thickness larger than any expected neutrophil diameter.

This process was verified by simulating random sections through a computer generated system of spheres. A collection of random polydispersed spheres, diameter 6.39 ± 0.70, was sectioned in the described way yielding a calculated diameter of 5.74 ± 1.25 when only 300 profiles were used. The technique appeared to systematically underestimate the diameters by

10% and neither increasing the number of profiles measured nor narrowing the dispersion of the simulated spheres had any effect. Therefore, our measurement of PMN diameter is likely to be an underestimate of the actual value.

The frequency distribution of neutrophil diameters in the pooled data of the three humans studied is shown in Figure 21. Also shown in Figure 21 is the frequency distribution of capillary segment diameters. The estimated human neutrophil diameter when the neutrophil assumed a spherical shape was $6.8 \pm 0.8 \mu m$(N=308) with an estimated volume of 174 fL. In contrast to the neutrophil diameter, the capillary segment diameter was $7.48 \pm 2.31 \mu m$ with a length of $14.4 \pm 5.84 \mu m$ (N=352), a volume of 632.5fL. Approximately 38% of the capillary segments were smaller than the mean spherical neutrophil diameter. This fraction is probably underestimated because the neutrophil diameter is slightly underestimated. Finally, no bivariate relationship between the capillary segment lengths and capillary segment diameters was evident.

These data show that the PMN diameter is larger than the capillary segment diameter and that some type of PMN deformation is required for the PMN to enter most capillary segments. Figure 22 shows an entire alveolar wall with its associated capillary network. What is immediately obvious from the examination of this and other such sections is the immense number of potential pathways that a cell could travel while traversing the capillary bed. Therefore, it would be of interest to know the effect of obstruction of individual segments of the capillary bed on the flow through those that remain open and on the pressure drop across the network of segments containing the obstructed units.

3.2 Effect of Plugging in the Capillary Network

Staub and Schultz (83) found that between 10 and 20 alveolar walls of 5-8 alveoli are crossed when travelling from a terminal arteriole to a venule in the canine lung. This means that the network of capillary segments in an individual alveolar wall such as that shown in Fig. 22 must connect with a similar network in other alveolar walls to form an interconnecting grid of 10-20 walls which provide passage from the terminal arterioles to venules. Figure 23 shows an example of how each wall was conceptualized for computational purposes. Each alveolar wall was arranged as a small grid of interconnecting pipes and the walls themselves were considered to be interconnected by corner vessels which had diameters larger than the neutrophils. The input to each of these simulated walls was taken to be either an arteriole or corner vessel and the exit was another corner vessel or venule. Two of the bordering sides were taken to be inputs and the remaining two were outputs, these sides were always randomly chosen for each alveolar wall in the model.

The development of a computational model of the entire capillary network is obviously an impossible task. Instead, either small representative sections must be modelled or a single cell must be able to pass through the pulmonary circulation without any need to worry about the 'history' of previous cells. If the previous passage of cells has little or no effect on subsequent cells then a model can be designed that dynamically constructs the capillary bed in front of each cell as it traverses the microcirculation.

Therefore, determining if a cell trapped within the alveolar wall would alter the effective resistance between any site in the wall and the exit became a major focus of these studies. Examination of enface sections of alveolar walls similar to Figure 22 showed that each alveolar wall contained between 40 and 80 segments. If the alveolar wall is constructed as a square matrix of interconnecting pipes using a 5 by 5 array (Figure 23) it contains 60 individual capillary segments. Array sizes of 4 by 4 contain 40 segments and 6 by 6 contain 84 segments, the upper and lower limits for the number of segments in each alveolar wall. For each array size, blood flow can be modelled as current by considering each segment as a resistor, the input sides (either the arteriole or corner vessels) as a voltage source and the output side (either corner vessel or venule) as ground. If a neutrophil was to become stuck, effectively eliminating a segment from the network for a finite period of time, then that segment would appear to have an infinite resistance.

With each segment in Figure 23 replaced by a resistance, an electrical circuit model was simulated using the electrical circuit simulator PSPICE (version 5.1, January 1992,, MicroSim Corp., Irvine CA). The exact values used for resistances and voltages are unimportant as they can be easily scaled to realistic values, and our goal was to compare the matrix sizes and characteristics. Each resistance was modelled as a 10 ohm ideal resistor with a tolerance of 50%. This ensured that a random pattern of resistors between 5 and 15 ohm populated the circuit. The input voltage was set at 10 volts. In this model a node is the junction of individual capillary segments within a single alveolar wall. Surprisingly, the different network sizes, 4x4 5x5 and 6x6, had little effect on the total resistance across the network. The larger the grid size, the

smaller the total resistance, due to the vast number of parallel pathways, but the total resistance across the 5x5 grid was 90% of that across the 4x4 grid and the 6x6 was 83% of the 4x4 grid.

Table 10 shows the resistances from each node to the output ground in each of the three configurations. In all of the circuits, the location of the input "walls" and output "walls" in each configuration has been held constant to allow for easier comparison of the tables but this has no effect on the qualitative outcome. In all examples, the resistance within the network is a maximum of about 7 ohms in the upper left corner and falls to about 3 ohms in the lower right corner. Therefore, the actual network size has very little, if any, effect on the resistance across the network.

To model the effect of neutrophil plugging, multiple simulations were run in which 10% or 25% of all the resistors in the network were randomly eliminated and replaced with open circuits. Figure 24 shows the location of the resistors eliminated in the 5x5 network. Multiple simulations were performed in which the locations of the plugs were randomly shifted. The results showed that plug location had no effect on the qualitative pattern of changes in resistances across each segment. The relative increase in total resistance between a plugged and unplugged network was approximately 1.2 for the 4x4, 5x5 and 6x6 networks with 10% plugs and between 2.0 and 3.5 relative increase for 25% plugs. In this model the resistance from each node to the output has not reached infinity because while certain segments are occluded, many alternative pathways still exist from each node to the output. Once again the network size had no effect on total resistance and the wider range for 25% blockages merely reflects the greater possibilities to remove entire portions of the network. Table 11 shows the relative increase from

each node to the output for the three grid sizes for 10% blockages and Table 12 for 25% blockages. These tables show that, the relative increase in resistance for each segment is the same throughout the grid, indicating that even with 25% blockages, the pattern of resistance drops within the network has not been affected by blockages. To show this more clearly, table 13 has scaled the values for the 5x5 network in the following manner:

Rn = resistance from each node to the output without blockages

R* = total resistance without blockages from input to output

rn = resistance from each node to the output with blockages

r* = total resistance with blockages from input to output

Rn/R* = resistance at each node (without blockages) scaled to total resistance

rn/r* = resistance at each node (with blockages) scaled to the total resistance

The values shown in Table 13 are:

$$(rn/r^*)/(Rn/R^*)$$

If this value equal 1, then the pattern of resistance, with blockages, has not been altered relative to the pattern without blockages. The values in table 13 are all between 0.8 and 1.1, indicating that 10% and even 25% blockages have virtually no affect on the resistance pattern within the network.

The direction of flow must also be considered when modelling the capillary network. At each node in the model shown in Figure 23, it is reasonable to assume that 2 vessels would flow into the node and two would flow out from the node, at least on average across time and space. To model this situation, the model was designed to allow unidirectional flow through the

network. Obviously, this reduces the number of available pathways for current flow (blood flow by analogy) through the model. The relative total network resistance produced by adding this constraint was 1.5 times regardless of network size. The remarkable features of this new network can be seen in table 14 which shows the relative increase in resistance between a model with 10% blockages and a model with no blockages. The node at position 3,3 in the 6x6 grid has an infinite resistance because both paths leading from this node were blocked. This a worst case example of a blockage. Notice that relative increase in the surrounding nodes has increased by a factor of 1.7 or 1.8 and that 2 segments away from the plug have relative increases in resistance of 1.3 to 1.4. In the smaller grid, 4x4, the relative increases in resistance become 2 to 3 times that without blockages. The corresponding result for 25% blockages is shown in table 15 where very high local resistances are seen around neutrophil blockages with little effect on areas a short distance away.

These results suggest that while local areas of increased resistance occur in the region of PMN plugs, most capillary segment resistances within a single alveolar wall are unaffected. Therefore, the presence of a PMN plug within a single alveolar wall can be ignored and it can be assumed that moving PMN will flow around segments that are blocked.

3.3 Modelling the Effect of Lung Height on Capillary Size

Glazier et al (33) have measured the difference in capillary segment diameters at various lung heights in dog lungs under Zone III conditions. His data, redrawn in Figure 25, clearly demonstrates a plateau in the size of the capillary diameter at a location which corresponds to the bottom of the dog lung. This relationship between height and capillary pathway diameter is paralleled by an increase in the margination of PMN in the upper lung regions relative to the lower lung regions (62,63). However, the available measurements of capillary segment diameters (Figure 21) were made on tissue taken from lungs where the arteries and venous blood supply was simultaneously occluded under Zone III conditions and the lung was filled with liquid fixative. In animals this procedure fixes the capillaries in a distended state but there is no variation with lung height as there is liquid pressure on both sides of the vessel wall. This means that the capillary segment diameters from Figure 21 must be scaled to account for the differences in diameter in the gravitational plane observed in air filled lungs (33).

In Figure 26, a smooth curve has been fit to Glazier's data which has been rescaled and shown to plateau at 100%. The total vertical gradient studied by Glazier (Figure 25) was 47cm, larger than the vertical height of a normal human lung in the upright position. Assuming that a normal lung measures 30cm in height from the top to the bottom, five sections of 6cm each were taken from the centre of Glazier's data. The dotted lines on Figure 26 indicate the location of these even divisions to divide the regions from the top of the lung down towards the lung base in an upright human. The midpoint value of the curve in each of these regions was taken to

represent the percentage the average capillary segment in that region would be relative to fully distended capillaries in the bottom of the lung. Taking values from the middle of Glazier's data meant that the very small values and the very largest values for capillary segment diameters were not used. Table 16 shows the values used for regional capillary sizes up and down the lung based on Glazier's data.

When modelling flow through capillary networks in each of these five regions it will be assumed that all capillary segment diameters are from a uniformly distributed population with a mean and standard deviation as given in Table 16.

3.4 Neutrophil Deformation Time

The amount of flow through a network is based upon the pressure drop across the network and the resistance of the vessels within the network. Due to the wide discrepancy in capillary segment diameters and PMN diameters, many PMN will obviously encounter vessels too small to pass through without deformation. The time required for the PMN to deform from its current diameter to a diameter equal to that of the capillary segment will delay the PMN relative to faster deforming RBC. The actual time required for the PMN to deform is likely a function of the PMN diameter/capillary segment diameter and the pressure drop across the PMN.

Warnke and Skalak (90,91) and Skalak (81) have made a network model of the systemic capillary bed. Their model was based on a grid system of 260 nodes with a single feeding arteriole and a single collecting venule. In Warnke and Skalak's work, they computed the pressure in each of the 260 nodes and estimated the added pressure across a single WBC when it became plugged in a capillary segment. This study has used a similar approach to Warnke and Skalak (92) and that of Lipowsky and Zweifach (58) to model the pulmonary microcirculation.

Needham and Hochmuth (70) have calculated the duration a WBC is present in a plugged situation while entering a small diameter pipet as a function of pipet size, cell viscosity and the pressure drop across the cell to be:

$$T_{deform}\ (\text{seconds}) = R^3(4/3)\eta_{WBC}\{1 - (1 + \ln R^3)/R^3\}/\Delta P_{WBC} \qquad \text{EQN[14]}$$

where

R = WBC diameter / capillary segment diameter

η_{WBC} = viscosity of WBC

ΔP_{WBC} = pressure drop across WBC

To confidently use this equation information must be available on the viscosity of PMN and the pressure drop across the PMN and PMN viscosity when plugging occurs. Warnke and Skalak (90) have made many measurements on WBC viscosity and found values ranging from 45 to 3000Poise. Several other authors (14,22,80) have also attempted to measure WBC viscosity but actual published values vary considerably and Warnke and Skalak finally used a mean value of 1200Poise in their models. The pressure drop across a plugged PMN is also very difficult to estimate. Schmid-Schonbein (76) has estimated the required pressure drop across a granulocyte to clear the cell from a capillary segment to be in the range of 6-8cmH_2O. Under these conditions, where the available pressure is considerably less than the required pressure, the estimated pressure drop across the plugged cell would be equal to the pressure drop in neighbouring segments that remain unplugged (76).

In section 2.5 the total pressure drop across all large vessels was estimated to be 3mmHg leaving a pressure drop of 5mmHg across the pulmonary capillary network if the total pressure drop is 8mmHg. Staub and Schultz (83) has shown that the minimum number of capillary segments between an arteriole and a venule is equal to about 100 capillary segment lengths. If the pressure drop across the capillary bed is uniformly distributed across all capillary segments then the maximum pressure drop across each segment is 5mmHg/100 segments = 0.05mmHg/segment. If, in equation 14, the pressure drop across the plugged cell is then just

the pressure drop in adjacent capillary segments, 0.05mmHg, and the minimum estimated cell viscosity of 45Poise is assumed then extremely long plug durations of hours or days are predicted.

Fenton et al (26) have also investigated the time required for a WBC to be aspirated into a pipet. In their studies the time required for WBC of various diameters to enter pipets ranging in diameter from 4-7μm was recorded. The aspiration pressures used ranged from 200 to 400Pa or 1.5 to 3 mmHg. This pressure is likely high relative to the actual pressure drop across the plugged cell but this should then estimate plug durations which are shorter than expected. The empirically derived equation proposed by Fenton et al (26) was:

time to deform (seconds) = (1/1.6)exp(3.68*R-4.77) EQN [15]

where:

R = WBC diameter / pipet diameter

In this equation, a log relationship was found between the time to deform to enter an aspiration pipet (slope=3.68, intercept=4.77). A correction factor of 1/1.6 was also empirically derived to correct for the temperature difference between the majority of the experiments (made at room temperature) and a smaller collection of studies at physiological temperatures (37 degrees).

Figure 27 shows the estimated deformation times versus the WBC/pipet diameter ratio. It was also evident that the estimates of deformation times of Fenton et al (26) varied by approximately 30% over the entire range of pressures and WBC/pipet diameters recorded. No pressure effect was noted.

The model presented in this work uses equation 15 to estimate the required time to deform a PMN from a starting spherical cell diameter to the diameter of the capillary segment.

3.5 Capillary Bed Network Model

Using the preceding information, it is now possible to propose a model that can be used to simulate the capillary network. The electrical circuit simulations provide reasonable evidence that capillary plugs have little if any affect on resistances to most capillary segments within a single alveolar wall. While local areas of high resistance likely occur, it is reasonable to assume that these elevated resistances appear not to extend to other capillary segments. This model therefore, ignores the effect of neutrophil plugging and assumes that any plugs within individual capillary segments merely redirects flow to unplugged regions of alveolar walls without any change in capillary pathway resistance. The flow chart for modelling the capillary bed was as follows:

1) A PMN of random size based on the morphometric measurements was chosen.
2) This PMN was assigned a fixed, constant velocity, between 750um/s and 2000um/s throughout the capillary bed. Previous work by Staub and Schultz (83) has shown that this range of velocity of blood is reasonable. Work by Lien et al (56,57) using intravital videomicroscopy has demonstrated that the PMN move rapidly through the capillary bed, stop completely, then return to a relatively rapid velocity. Figure 17 from the large vessel portion of this simulation also show precapillary blood velocities within this range.

3) A random number of alveolar walls between 10 and 20 was assigned to this PMN for it to pass through based on the data of Staub and Schultz (83).

4) Each wall was randomly assigned a size of 4x4, 5x5 or 6x6 with equal probability.

5) Each alveolar wall had two sides randomly chosen as inputs and two as outputs.

6) All capillary segments in each wall were randomly assigned a length based on morphometric measurements.

7) All capillary segments in each wall were assigned diameters such that the minimum pathway diameters approximated the beta distribution and the total capillary diameter distribution matched morphometric results after they had been scaled to account for lung height. To force a beta distribution for the minimum capillary pathway diameter a uniform distribution of capillary segment diameters was assumed ranging from the mean value in table 18 to ± 2 standard deviations of the mean. The distribution shown in Figure 21 for capillary segment diameter appears quite broad so a uniform distribution does not seem unreasonable. This step determines whether the simulation will represent a collection of pathways from the upper or lower lung regions.

8) The PMN randomly entered the grid along either of the input walls.

9) If the cell diameter was less than the capillary segment diameter then the length of the capillary segment traversed is recorded. If the PMN was larger than the capillary segment then the time to deform was computed using [EQN 15] and this time, and capillary segment length was recorded. Previous work by Evans (23) has

shown that the time for a granulocyte to recover back to its spherical shape after aspiration into a pipet exceeds 12 seconds. Therefore, once a PMN had deformed to a size smaller than its full spherical diameter it remained at that size until a still narrower capillary segment was encountered.

10) PMN travelled through the model in a unidirectional manner where only two capillary segments from each node were possible exits.

11) Yen and Fung (108) have studied the separation of gelatin pellets in relatively large (0.32cm-0.64cm diameter) branching tubes. They found that the discharge tube haematocrits of gelatin pellets could be related to the feed tube haematocrits and the discharge tube velocities by the following equation (derived empirically):

$$H1/H2-1 = a(v1/v2-1)$$

where:

H1 and H2 are the discharge tube haematocrits

v1 and v2 are the discharge tube velocities

a is a nondimensional parameter meant to account for cell diameter/tube diameter ratio, feed tube haematocrit, cell shape and cell viscosity.

Yen and Fung (108) found that when the discharge tube flow velocity ratios were less than a critical ratio of 3:1, the above equation predicted the experimental results. Unfortunately, no experimental data are available which provide the simultaneous flow velocity ratios in capillaries at a given time point. Therefore, we assigned a constant velocity to each cell as it traversed the capillary bed. Furthermore, it was assumed that the velocity of adjacent capillaries was identical. Under these conditions, the data of Yen and Fung show that the discharge tube haematocrits of the capillaries would be identical. Unfortunately, it is not possible to infer from the work of Yen and Fung how a PMN would behave in such a system. With these factors under consideration, RBC and PMN would enter the branches of a bifurcation (where discharge tubes had identical lengths) in proportion to the ratio of the cross-sectional areas of the branches. Mayrovitz and Rubin (65) have made a more physiologically appropriate investigation into the distribution of leukocytes at small (5-20um diameter) branches by imaging cells flowing through systemic vessels. In their studies, only a very slight dependence was seen between flow and cell concentration and no critical threshold was observed as in the studies of Yen and Fung.

It was arbitrarily decided in the current study that for two vessels of cross-sectional area A1 and A2, a cell would enter vessel A1 with probability: A1^2/(A1^2+A2^2), which would divide cell flow relative to flow velocity. This equation likely overestimates the division of PMN into branch vessels but the true cell distributions into branches at division are not known. This equation is arbitrary but does not seem unreasonable. It is

also interesting to note, as indicated in the thesis, that all of these studies which estimate flow division at a bifurcation are only crude approximations of the true situations. In a true branching network such as the pulmonary vasculature there is little relationship between how flow divides at a bifurcation and the size of the vessels of the bifurcation. The dominant factor ruling how flow will divide at any division is the apparent resistance of each pathway. This resistance is obviously a complex function of all distal branches of the network at a particular bifurcation.

12) Once a PMN had completely traversed a single alveolar wall it immediately arrived at the next with no time delay.

Using the above flow chart to control how cells travelled through the capillary bed a computer program was written in Gauss VM386 (Aptech Systems, WA) which generated a capillary network in front of a PMN as it passed from a terminal arteriole to a venule.

Figure 28 shows a histogram of the number of segments a PMN, or RBC traversed in each pathway and Figure 29 the total path length travelled. The distribution of transit times for RBC, which were assumed to require no time for deformation, is shown in Figure 30. The median transit time for RBC was 0.8s with an interquartile range of (0.6-1.1) seconds.

As expected, the PMN transit times shown in Figure 31 are much longer than those for RBC (Figure 30). Figure 31 also shows the effect of regional differences in capillary segment diameters in the upper and lower lung regions. PMN taking longer than 10,000 seconds are not shown. Figure 32 shows the distribution of the number of stops for both the upper and lower

lung regions and Figure 33 the average time per stop. The values for time per stop, total capillary transit time and number stops for the five regions of the lung are summarized in table 17.

4 Total Pulmonary Transit Time

The calculation of total pulmonary transit time requires that the three separate models, arterial, venous and capillary, be combined into a single system. The arterial and venous trees have very fast transit times and PMN should have no difficulty traversing these regions because the vessels are much larger than the PMN. The distribution of RBC transit times for the arterial system is shown in Figure 34 and for the venous system in Figure 35. The median arterial and venous transit times were about 0.7 and 0.8 seconds respectively. Once the distribution of transit times through each of the three regions was known, the total pulmonary RBC transit times was taken to be the mathematical convolution of the large vessel transit time and the capillary bed transit time. It was also assumed that short arterial pathways are joined with short venous pathways but that no preference in capillary path length was seen for any length of arterial or venous path.

In order to determine the amount of flow that should be delivered to each of the five gravitationally determined regions of the lung it is necessary to know the relative flow to each lung region. Anthonisen and Milic-Emili (3) have mapped the regional distribution of pulmonary perfusion in upright humans. This data was used to partition the fraction of the cardiac output to each of the five lung regions. Table 18 shows the proportion of flow to each of the lung regions.

For computational purposes 10,000 RBC and PMN were passed through the arterial, capillary and venous beds and these cells were delivered into the five possible regions based on

the fraction of blood flow distribution described in table 18. Figure 36 shows the estimated transit time distribution of RBC and PMN through the entire pulmonary circulation where the median RBC transit time is 2.1 seconds and the median PMN transit time is 8.6 seconds. The differences in transit time for PMN in each of the lung regions is summarized in Table 17 where the median PMN transit time was ~64 seconds at the top and 5.3 seconds at the bottom of the lung.

The results of the model were compared to the experimental results reported by MacNee et al from our laboratory (59) where we obtained an estimate of the distribution of RBC transit times in the resected human lung specimens. These subjects, all of whom required lung surgery for lung cancer, were studied preoperatively where they received a bolus injection of ^{99m}Tc labelled RBC into the median basilic vein of the arm. The radiolabelled cells were observed passing through the right and left ventricles using a Siemens ZLC 3700 gamma camera with a wide field of view. The distribution of RBC transit times calculated by deconvolution of the time-activity curves recorded over the right and left ventricles compared favourably to those determined from measurements of blood volume and flow made on individual pieces of resected lung. Figure 37 shows the pooled frequency distribution for 718 samples from eight lungs from this study where the mean and median transit times for RBC were 4.9 and 3.5s respectively.

More recently, Hogg et al. (43) have used a similar approach to calculate the capillary transit times of both RBC and PMN using quantitative histological techniques to determine the number of RBC and PMN/ml of capillary blood and ^{99Tc}MAA to measure regional blood flow. The number of RBC or PMN delivered to the capillaries of each lung sample was calculated

from the isotopic determination of blood flow and the peripheral blood RBC or PMN count. The regional transit time obtained by dividing cells/ml by cells/ml/sec) showed a distribution of transit times that ranged from 0.03 to 14.5seconds with a median of 1.2 s for RBC and from 3.3-935 seconds with a median value of 129s for PMN with 18% overlap of the values for each cell type. These experimental values for RBC PMN capillary transit will be compared to those obtained by the model as well as others that are available in the literature in the discussion section.

5 Discussion

The computational model described in the thesis allows the transit time of red blood cells and neutrophils in the arterial, capillary and venous components of the human pulmonary vascular bed to be estimated. A large vessel model based on anatomical data for the arterial branching system was used to construct a set of probabilities which would describe the branching nature of the arterial network. With the arterial network specified, flow continuity and energy balance equations were used to estimate the total pressure drops through a wide range of possible pathways in this system. When flow had reached the capillary bed, a strictly stochastic model of cell transit through a randomly generated grid network was used to simulate capillary flow. Finally the flow was returned to the left atrium by making a slight modification on the arterial network to represent the venous system.

The information required to develop the model was accumulated from several different sources and the net result was based on anatomical geometry, fluid flow mechanics and probability theory. The results obtained with the model were then compared to experimental observations from our own and other laboratories.

5.1 Large Vessel Model

The anatomical structure of the human pulmonary arterial tree shown in the angiogram in Figures 1, 2 and 3 is extremely complex. The model presented in this thesis is based on the assumption that a modified Horsfield branching structure could be used to represent this very asymmetric tree. However, any number of asymmetric patterns could have been proposed that would have resulted in similar path length distributions and pressure drops.

This model uses a set of branching probabilities which detail whether a division is a bifurcation or trifurcation, and the relative size of the daughter vessels in relation to the parent vessel, based on anatomical measurements. The probabilities in tables 2,3 and 4 were estimated from the available cast data and strictly determine the number of branches the model estimates at a given order. If these probabilities are incorrect then the estimated number of vessels in the orders will be in error, also, the estimated relationship between parent and daughter branch sizes will also be incorrect. Detailed Horsfield ordering of the human arterial tree has not been previously published so no direct comparison between this work and others can be made. However, an important feature of many naturally occurring branching systems is a linear relationship between the log of the number of vessels and the order (78). Figure 10 clearly shows that the proposed model has this important feature. Furthermore, the number of terminal arteriole endpoints (order 1 vessels) estimated from the model can be compared to available morphometric estimates made by Weibel (95). Even small shifts in the probabilities shown in tables 2,3 and 4 result in dramatic changes in the number of terminal arterioles, the most

sensitive probability being the relative fraction of bifurcations in the arterial tree. Since the number of estimated precapillary arterioles closely match those of Weibel (95), it has been assumed that these values provide a valid set of branching rules which accurately describe the arterial tree.

The method used to represent the branching structure of the pulmonary vasculature is one which can be best described as a random model. Other investigators have made models of the pulmonary vasculature which have included detailed mathematical descriptions of the observed branching network. Two alternative methods for representing the branching nature of this system are Woldenberg's spatial hierarchy (105, 106, 107) and the fractal descriptions of Krenz (52,53) and Glenny (36, 37).

In Woldenberg's (105,106,107) representation of systems of rivers, or pulmonary vessels, he noted that streams (or areas) join to form larger rivers and that using the ordering schemes described earlier in this thesis that as the stream, or vessel order, increase (larger vessels) the number of these vessels declines geometrically. Also, the ratio of areas between successive orders can be related to the branching ratio of these orders. Hierarchial structures such as these can be described as stochastic models, random models such as used in this thesis, or, as Woldenberg uses, work related space filling models based on the hexagon theory of Christaller (15). Christaller developed a theory of central economic places (towns) and their associated market areas and discovered that the optimum partitioning of the space was achieved using hexagonal shapes. Larger areas, or structures, are then represented by larger groups or collections of hexagons. Christaller proposed that a large hexagon may contain 3,4 or 7 smaller

hexagons but Woldenberg has extended this to much larger sizes. The best description of the hexagonal area is given by Woldenberg (105,107):

Suppose we are given a hexagonal area. Let us divide the area into equal hexagonal areas. When the ratio of these areas, R_A, equals three, space may be filled with hexagons. Ratios of less than three have been observed in the human airway. R_A can be less than three, if one cuts the surface and excises some area. This is possible in the lung, which can be though of as a cut surface, which is folded into alveoli and connected to tubes. A river flows on a bent, but continuous, surface. Thus no area is excluded, and the river must have $R_A \geq 3$.

The value of R_A can never be less than two because for branching systems two branches of equal order are required to elevate a branch to higher order. $R_A < 7$, because small outside branches tending to flow to the centre would eventually join with branches in the ring of six hexagons surrounding the centre and create higher order branches before R_A could exceed seven. For analogous reasons R_A for market areas cannot be less than three (unless there are unobserved areas) nor greater than seven. In the latter case the intervening towns would become higher order.

This model may be extended to organic branching systems. Rivers are three-dimensional systems, although they appear planar on the map. While rivers, trees, lungs etc., are three-dimensional, functionally each system operates on or through surfaces. For instance, operationally the lung is considered to be a surface through

which CO_2 and O_2 are exchanged and is served by channels which may be compared topologically to a river system. In the capillary bed in the lung, the network vasculature is clearly hexagonal. At the centre of each hexagon is a point most completely removed from the surrounding hexagonal syncytium. Since we must fill space, circular channels are not allowed and this length of capillary channel surrounding each centre point is a minimum for the area enclosed; however, the size of the perimeter is adjusted to allow the centre point to be perfused with oxygen. Allow a branching network to be attached to the syncytium, only the small branches are connected to the synctium. These small branches join to form large branches, uniting small hexagonal areas into larger ones, and this process continues until only one branch is left so that all flows to or from the whole area are united in this one branch. The model resembles a tree trunk with its roots exposed, the smallest rootlets touching the hexagonal capillary system.

These remarks are still speculative, yet perhaps they are operationally correct, since the available evidence seems to support the hypothesis of hexagonal hierarchies in urban, fluvial and organic systems.

The spatial analysis proposed by Woldenberg is based on a geometrical approach that allows for the description of large structures by applying inter-connected series of shapes (hexagons). These shapes are considered to be self similar regardless of whether one is looking at the structure as a whole or only a small piece of the structure. Fractal structures are those that

display a self similarity that is invariant to scaling and therefore a logical extension of the work of Woldenberg is to consider the pulmonary vasculature as a fractal structure. Glenny (36, 37) and Krenz (52,53) have utilized fractal analysis to look respectively at pulmonary blood flow and the pulmonary arterial tree.

Krenz et al (52,53) modelled the relationship between the number of vessels at a given order, Nj, and diameter of vessels at that order, Dj,and related these two values through a third constant term β_1 :

$$N_j = a_1 D_j^{-\beta_1}$$

where a_1 is the dimension of the largest vessel. They were able to further define the resistance at each generation and the volume at generation all in terms of the descriptive parameter β_1. In their analysis they estimated values of β_1 between 2 and 3, smaller than the value of 3 which would be used by implicating Murray's law (69) yet slightly larger than previous values found by Horsfield and Woldenberg. Unfortunately, as noted by Krenz et al. (52), the estimates they obtained for resistance and volume of the pulmonary vasculature are very sensitive to the available morphometric data and they conclude, as this work has, that far more detailed investigations to acquire this information would be a great benefit.

Other investigations of the arterial tree (78,110) have used Strahler ordering schemes. While Strahler ordering is a convenient method of describing complex networks this method has, as already described, the drawback that individual pathway lengths can not be estimated. However, in the arterial cast data of Horsfield (44), much of the individual vessel length data was also missing. The small number of vessels for which length was available were dispersed

over a range of orders located in the large vessel region. No obvious relationship between vessel length and order could be clearly identified. The relationship between the ratio of vessel length and diameter also showed no obvious pattern. It was decided, based on the little length information available, that an average ratio between length and diameter, and the standard deviation of this ratio, would be used to estimate length from diameter throughout the arterial tree. This is clearly a simplification that will effect path length and pressure drop calculations throughout this work. A 10% error in vessel length, if it was always in either the positive or negative direction from the mean value, would result in a 10% error in the pathway length. A similar error in pressure drops would also occur. It seems unlikely that all vessels of a particular pathway would be uniformly shorter or longer and the standard deviation of $\pm$30% allowed vessels lengths to vary between 80% and 200% of the vessel diameter 95% of the time. While the distribution of arterial, and venous, pathways is not known, Figures 16 and 18 provide values that seem reasonable for a human lung 30cm tall.

This model has made the assumption that the venous system can be represented by the same branching probabilities as were used for the arterial system. No cast data was available on the venous tree which could be used to compare to an equivalently ordered arterial system using a Horsfield scheme. However, previously published results, for both arterial and venous networks are available using Strahler ordering (47,78) and a comparison of these networks shows a strong similarity between branching structures. As with the arterial tree proposed in this work, the exact system used to describe the venous network is likely unimportant given that at least the essential asymmetric pattern is maintained.

Future investigations are required to obtain more detailed anatomical data. Ideal information for modelling would include vessel lengths, diameters, branching angles and true spatial position within the lung. A convenient, non-invasive technique may now be available to obtain this information. Hatabu (39) has shown that high-resolution magnetic resonance imagers (MRI) can be used to obtain extremely detailed images of the pulmonary vasculature. These images have a high sensitivity to fluid flow and are therefore ideal for the investigation of the pulmonary vasculature. When these techniques have been perfected they should allow rapid analysis of the pulmonary vasculature under many different conditions.

Flow through vessels in this work was assumed to be Newtonian, steady and incompressible. Blood is not a simple fluid, but a complex two phase fluid of cells suspended in plasma. An important feature of blood is that its apparent viscosity changes as vessel diameter changes. In this work the equations of Kiana and Hudetz (50) were used to correct for this effect. Because of the relatively large vessel diameters used in this model (even at the precapillary level) equation 13 had virtually no affect and could be eliminated completely from the methods. Time-varying, pulsatile flow patterns also exists in the pulmonary circulation (29) and extend into the capillary bed. In addition, while the blood can be considered incompressible, the vessels through which it flows are themselves distendable. These effects have not been considered in this work as the major goal was to first develop a framework upon which these refinements could be made in later investigations.

In the current work flow was assumed to vary as a function of the radius to the fourth power (7,9,17,29,30,31,77). Uylings (88) has expanded upon the earlier work of Murray (69)

to present an alternative proposal where flow more closely relates to flow to the third power. In these studies flow through a vessel is modelled as strictly Hagen-Poisseuille flow with a work cost equal to the flow (proportional to the fourth power of the radius) times the pressure drop. An arbitrary additional energy requirement for the "maintenance of the blood" is added which Murray (69) argues as follows:

> *To study the antagonism between the friction and the volume of blood the latter factor must be multiplied by a dimensional constant. Let b, then, be the cost of blood in ergs per second per cubic centimetre of whole blood of average composition (and let B be the cost in calories per day per cc. of blood). There is, as far as I can see, nothing arbitrary about this step: it is certain that the maintenance of blood requires fuel. (The cost of blood may, however, be a complex account distributed among such factors as the small metabolism of the blood itself, the cost of upkeep of all the constituents, perhaps especially of hemaglobin, the cost of containing vessels, and the burden placed upon the body in general by the mere weight of blood).*

These issues are not of a fluid dynamic nature. Furthermore, the studies of Murray (69), Uylings (88), Woldenberg (105,106,107) and Fung (29) in this area are not supported by empirical evidence of actual pressure flow relationships in blood vessels. Both Murray and Fung themselves comment that the use of these cost functions is arbitrary. In the modelling results

of Fung only flow proportional to radius to the fourth power laws are considered. The data used in this model, most notably those of Gelin (32) and Lipowsky (58) are experimental results that support the use of flow as being proportional to flow to the fourth power and are consistent with current findings in this area.

The division of flow through an arbitrary bifurcation or trifurcation is extremely difficult to compute and usually empirical approaches are used. In this work flow was randomly chosen for one of the daughter branches in a bifurcation (two of the branches in a trifurcation) and flow continuity (the flow in a parent branch must equal the sum of the flows in the daughter branches) was used to estimate the flow in the remaining branch. The distribution from which flows were randomly selected was based on mapping all possible flow patterns in branches up to order 20. It was assumed that each terminal arteriole carried one unit of the total cardiac output, each unit being equal to the cardiac output divided by the number of terminal arterioles. This estimation obviously depends on each order 1 vessel having 1 unit of flow and no data is available on this. Previous studies (72,102,110) have taken a somewhat similar approach but they allowed only a single flow to exist for branches at each order. This method, for the division of flow, is simplistic and has likely resulted in incorrect estimates of pressure drops. It is difficult to predict exactly how this has affected the results in the current work. It may be possible to select small portions of the model presented here and solve exactly a set of equations which would show, at least in small portions of the network, possible flow patterns. This may be another area where MRI could provide useful quantitative results to assist in formulating a method for flow division. Work by Fei (25) and Ku (54) has shown that MRI can be used to map steady and non-steady

flow patterns both with and without pulsatile flows. While these kinds of studies have not yet been done on humans, their results show that very complex flow velocity profiles can be obtained and from these, pressure drops estimated.

In the study of Yen and Fung (108) an optimal cost (minimal) is considered in relation to branch angle. Their studies find that there exists, given that all their assumptions hold (especially Murray's (693) study), a set of angles that would minimize the energy loss through the bifurcation. Once again these studies are not supported by experimental evidence. In very recent study, Collins et al (16) have investigated the pressure losses through a bifurcating network experimentally and theoretically. Their studies show that at the low Reynold's numbers under consideration in models of either the airways or pulmonary vasculature, virtually no pressure loss is associated with the bifurcation. This finding is completely consistent with fluid dynamic findings that pressure losses to divergent flow at low Reynolds numbers are negligible. This being the case, a minor pressure loss correction has been implemented for larger vessels based on the experimental study of Gelin (32).

As previously mentioned, the lack of exact length information affects the accuracy of the model predictions concerning pressure drops in the large vessels. However, this model estimates that only 3 to 4 mmHg of the total pulmonary pressure drop is located in the large vessels, approximately 50% of the pressure drop across the pulmonary circulation. Zhuang et al. (110) used an asymmetric bifurcating model where flow was always divided 2/3 to one daughter and 1/3 to another at each division but pathway length was estimated from a Strahler-ordered branching scheme. In their study, they estimated that a total pressure drop 11.2 mmHg occurred

in the large vessels with very little remaining pressure drop across the capillary network. Direct measurement of microvascular pressure obtained by Bhattacharya and Staub (6) show that at least 46.4% of the total pulmonary vascular resistance was located across the capillary bed which agrees well with results of the current study. The discrepancy between Zhuang et al and this work is likely due to how large vessel pathways are predicted. In Zhaung et al. (110) every pathway contained vessels of each order, while the study presented here estimates that each order has only a 1/3 probability of being located in a given path. If, at every order in Zhuang's model, the probability that any particular order was present in a given pathway is set to 1/3, then the total estimated large vessel pressure drop is between 3 and 4 mmHg, the exact value found in this work which agrees with Bhattacharya and Staub's measurements (6).

5.2 Capillary Network Model

The model of the capillary bed presented in this thesis is based on the anatomic observations that the lung parenchyma consists of an interconnecting network of alveolar walls where each wall contains a network of short capillary segments. The size of the individual capillary segments and the numbers of these segments in each alveolar wall are based on Weibel's (95) data which were recently confirmed in our laboratory (21). The minimum capillary pathway lengths predicted by the model (Figure 32) roughly correspond to the distance between terminal arteriole and proximal venule reported by Staub and Schultz (83) who measured the linear distance between arterioles and venules in planar sections of the lung.

The alveolar wall capillary network was assumed to be a square grid (Figure 23). Two sides of the grid were arbitrarily assigned as flow inputs (arterioles or corner vessels) and two sides as flow outputs (venules or corner vessels). Each intersection between capillaries was always assume to involve four individual capillary segments. Comparison of the grid and the real alveolar wall (Figure 22) shows that the grid is a simplification of the actual structure. The thick sections examined showed that a single alveolar wall could easily have more than 4 sides and that capillary segments meet in junctions of three as well as 4. Furthermore, the possibility of many flow inputs around the outside of a single alveolar wall could allow local regions of a single alveolar wall to have reduced or stopped flow with flow entering the alveolar wall from adjacent arterioles or corner vessels. The presence of trifurcations in the alveolar wall also

increases the possibility of a single PMN temporarily blocking more than a single segment. This could occur if two vessels flow into a third, and this third vessel became occluded by a PMN.

It was also assumed that as either RBC or PMN traversed the capillary bed, no effect of plugged capillary segments would be seen. Hogg (40) has estimated the size of the marginating pool in man and has determined that even if the entire marginated pool was located within the lung capillary network then only 10% of all segments would contain a PMN. The resistor network simulations presented here indicate that blocking 10% of the capillary segments within a single alveolar, would result in very little increase in total resistance across the network of segments in that wall. Furthermore, the resistance around the plugged segments would not increase dramatically due to the vast number of alternative pathways available. Even when flow is restricted so that each capillary segment carries flow in a single direction, the increased resistance resulting from a plugged segment is transmitted to only a few other capillary segments in an alveolar wall. If the number of plugged segments approaches very high values, 25% of all capillary segments, then more significant increases in resistances are possible. Based on the data suggesting that only 10% of the capillary segments would be blocked at any point in time (39), it seemed reasonable to ignore the presence of plugged segments and assume that any cells traversing an alveolar wall would avoid capillary segments filled with PMN.

Lien et al. (57) have simulated the pulmonary capillary bed as a large network of interconnecting segments. They found that only 1% of the segments were required to be blocked to trap nearly 50% of the neutrophils at least once. In their work, cells traversed the capillary bed by a system of random walks, however, cells were allowed to attempt to enter a plugged

capillary which would then impede the passage of the following PMN. In the present study, it was found that ten times the blockages (10%) suggested by Lien et al (57) would not affect the resistances of surrounding capillary segments and therefore cells would not be impeded as they travelled around occluded segments. This finding agrees with that of Warnke and Skalak (88) who also found that leukocyte plugging had little effect on blood flow resistance in a single capillary network. From the present model, we estimate that 25% of the segments would need to be occluded before sufficient areas of impediment would be created to delay following cells. This suggests that the delay of PMN in the lung is not affected by capillary plugging by other neutrophils but is a function of the geometric difference in neutrophil and capillary segment diameter.

The equation of Fenton et al (26) used to predict the time required for a PMN to deform sufficiently to enter smaller diameter capillary segments was determined experimentally and does not contain a pressure term. This makes the equation suitable for this study where no estimates of pressure were available. Fenton developed this equation by aspirating WBC into pipets at pressures several times larger than those likely to be present in the pulmonary microcirculation, where the vast number of parallel pathways that exist in the capillary bed make it very unlikely that any significant pressure difference exists across a capillary segment plugged by a PMN. Indeed, the calculations made by Schmid-Schonbein (76) show that the large pressure required to clear a PMN through the capillary segment that it has plugged must exceed the available pressure drop across individual segments in the lung. For example, if the pressure drop across a single PMN plugged in a capillary segment is equal to the pressure drop in adjacent open

capillary segments (76) and the total pressure drop across the entire pulmonary capillary bed is only 4 mmHg, then a typical pathway containing 100 capillary segments would have a pressure drop of only 0.04 mmHg across each segment. This strongly suggests that the deformation which the PMN must undergo to negotiate narrow segments is an active rather than a passive process.

The time required for deformation is very sensitive to the ratio between neutrophil diameter and capillary diameter. The capillary and neutrophil sizes used in this study are in agreement with the previous measurements of Weibel (95) and Schmid-Schonbein (75) and extend that work by establishing the entire distribution of cell and capillary size fixed under similar conditions. Since the ratio of cell to vessel size is of prime importance to this model, the validity of the regional changes based on Glazier's work (33) are also critical. Sobin (82) and Fung and Sobin (30) measured the changes in alveolar sheet thickness as a function of capillary-alveolar pressure differences in cat lungs and report changes that exceed those determined by Glazier by approximately 15%. If Sobin's data are correct, then the transit time differences due to gravitational effect in capillary size would be even greater than currently estimated, but the difference between the two data sets may be due to species effects. Unfortunately, no detailed information is available on gravitationally related differences in human capillary size.

Using thoracic windows in dogs, Lien (57) has shown that about 40% of fluorescently labelled PMN pass through the lungs at approximately the same velocity as RBC and do not stop, while about 60% of the PMN are delayed by one or more stops. The results obtained with

the model show that the median number of stops for even the lower lung regions was 4. While it is difficult to determine why the results reported here differ from those of Lein et al, a recent report showing that the capillary network on the interior of the lung has narrower segments than those on the pleural surface (11) would be consistent with this difference. Another possible explanation is that the numerous short stops predicted by the model are related to an underestimate of the rate of deformation provided by equation 15. Alternatively, the neutrophil could rapidly deform down to some smaller diameter very quickly, maintain this diameter and therefore encounter fewer restrictions that would cause it to stop. Indeed, allowing the neutrophil to deform rapidly down to a diameter of 4.6μm reduced the number of stops by 2 but had little effect on transit time. With this rapid deformation, 30% of the cells were able to traverse the lower lung region with a single stop of only 1 second which may have been beyond the measurement abilities of Lien et al. (57).

Harris and Heath's (38) review of the data on total pulmonary blood volume and provide six separate estimates in humans where the group mean value is 250 and the range of 211-311 ml/m^2 BSA. Dividing this mean by an average cardiac output of 2.5-3 l/min/m^2 provides a total pulmonary transit times of between 5 and 6 sec. MacNee et al (59) from our laboratory reported similar values when pulmonary transit times obtained with a gamma camera technique in the pre-operative period were compared to measurements of blood volume and flow made on individual pieces of resected lung post-operatively. This data showed good agreement between the pre and post operative measurements with both methods yielding mean values of between 4 and 5 sec. The post-operative measurements also provided a frequency distribution of transit times based

on 7.8 samples from 8 resected lungs with a mean of 4.9 and a median of 3.5 s. In an extension of this approach, Hogg et al. (43) used quantitative histology to measure the concentration of RBC and PMN/ml of capillary blood and estimated the transit times by dividing this concentration by the flow of cells. This method estimated the median capillary transit time for RBC to be 1.2 s with a range of 0.3 to 14.5 sec and PMN capillary transit times with a median value of 129 sec with a range of 3.3 - 935 sec. These values for RBC transit time are slightly larger than those obtained with the model (med 0.8 range 0.5-4.5 sec) but are reasonable considering the experimental results were obtained on elderly subjects with mild COPD who were under general anesthesia. Also, the capillary blood volume estimates of Hogg et al. (43) are larger than those obtained by physiological techniques (49,55,64,66) and this would have the effect of making the model results agreeing closer with experimental results. However, the distribution of PMN capillary transit times estimated using the model is shifted much more markedly to the left of the experimentally determined results (median 7.8 vs 129 sec). This suggests that the model underestimates the time the majority of the PMN spend in the pulmonary capillary bed because it does not consider all of the factors which control the time PMN spend in the capillaries.

One possibility is that PMN must actively deform and become motile to pass through the restrictions they encounter in the capillary bed. In an investigation of the random migration of PMN, Manderino et al. (61) showed that PMN can travel approximately 1600 μm in 2 hours or 0.22 μm/second in the absence of a chemotactic gradient. If a PMN managed to force itself partially into a capillary segment before it occluded flow in that segment, at least half of the

capillary segment would remain to be traversed. Travelling at a rate of 0.22 μm/second, a PMN would require approximately 34 sec to travel half the length of a 15 μm capillary segment which would bring the model predictions much closer to the experimental result.

If active cell deformation and movement are required for PMN through capillary restrictions, any intervention in the motility of PMN would increase PMN margination. Preliminary evidence in support of the concept has been provided by Inano et al (46) who reported studies using colchicine to inhibit the microtubule assembly of the PMN and found that this reduced their ability to move through filters and increased their margination in the lung.

Under normal physiological conditions, the number of neutrophils entering the pulmonary capillary bed must equal the number of neutrophils leaving it. Furthermore, while there is a greater retention of neutrophils through the upper portion of the lung, the actual number of cells per gram of tissue retained is virtually constant. The volume of cells in each lung region can be estimated by multiplying the average capillary transit time for each region (Table 17) by the number of cells contained in the fraction of the cardiac output delivered to that region (Table 18). The units are in numbers of cells/percentage of blood flow and can be ignored because the fraction of PMNs in blood delivered to all lung regions is identical. The results from top to bottom of the lung are 2.4, 2.0, 2.0, 1.9, 1.9 and indicate that there is little difference in PMN concentration in each region. This result agrees with the measurements of Martin et al (62,63) who showed the number of marginated PMN per gram of tissue changed little with lung height. Therefore, the estimates of regional concentration of marginated PMN obtained in different lung regions, are consistent with the available data.

The electrical network simulations reported here are very similar to earlier studies by West (92) where they also used a resistor grid network to model flows, pressures and resistance in the capillary bed. As with West's earlier work, our simulations show numerous "reverse flow" conditions where electrical current gradients temporarily reversed direction however, it was not possible to determine if this was an artifact of the method used to solve the equations or true reverse flow. West et al (100) and Warrel et al (93) also comment in their studies that the patchy perfusion pattern observed in lungs may be the result of capillary recruitment. The present study suggests an alternative explanation for the mechanism of capillary recruitment. When a single neutrophil stopped within an alveolar wall, the input resistance to the entire wall increased. This would tend to alter the pattern of blood flow away from that alveolar wall to the adjacent walls. Uniform flow would then resume when either the neutrophil plug left the alveolar wall or all alveolar walls in a region of lung developed equal resistances. This mechanism predicts that entire alveolar walls, or portions thereof, could be quite easily recruited or derecruited in relation to the movement of neutrophils. The longer transit time of neutrophils in the upper lungs regions would imply more derecruited regions and possibly account for the known ability of the upper lung regions to increase blood flow remarkably during exercise.

Under conditions of exercise blood vessels become fully dilated as flow rates increase to a maximum (99). This makes neutrophil plugging difficult and prevents derecruitment of vessels by plugging. Several studies (27,68,72) have shown that circulating PMN counts are elevated by almost 42% and that pulmonary vascular resistance decreases by approximately 20% during exercise. The network simulations presented in this study suggest that if the capillary segments

in the pulmonary microcirculation that were blocked, by marginating PMN, were sufficiently dilated to release these cells into the systemic circulation a 20% reduction in resistance would result. A rapid increase in circulating PMN as a result of demargination of PMN from the lung is consistent with the data of Muir et al (68). Although others have suggested that the leukocytesis of exercise is due to demargination from the spleen (73), this seems less likely in our view because a similar WBC response to exercise can be observed in splenectomized subjects (84).

5.3 Total Pulmonary Transit Times

The estimate of total time that PMN and RBC take to traverse the model of the pulmonary vasculature shown in Fig. 36 was obtained by combining the individual models of the capillaries (Fig. 30 and 31), arteries (Fig. 34) and veins (Fig. 35). Fig. 36 also illustrates the difficulty of studying PMN transit using indicator dilution technology because many PMN have the opportunity to recirculate before the remainder complete a single transit through the lung. Comparison of the model results to experimental values obtained in dogs with labelled PMN and RBC (Fig. 37) up to the time of recirculation of the RBC shows important differences. The experimental data shows that the PMN return to baseline whereas the model data shows a shift in the two curves with steadily rising PMN values at the time one might expect RBC recirculation. This suggests that the PMN transit through the lung has a biphasic nature which is not accurately represented by a simple rightward shift of the PMN transit times by the model.

Studies of PMN transit through the pulmonary circulation of humans has been attempted using a gamma camera technique. Although the initial studies (59) suggested a very low retention of PMN during the first transit through the lung, it has now been established that this was the result of an error in technique (42). The correct analysis shows that the extraction and retention obtained using the gamma camera technique in humans are much closer to those observed in the animal studies where blood was sampled directly. Therefore, if it were possible to compare RBC and PMN transit using the indictor dilution technique with direct sampling of blood in humans, the results would be very similar to those obtained in animals. This means

that a simple shift in the distribution of the PMN transit times to the right of the RBC transit times predicted by the model in Fig. 36 is an oversimplification.

The model also predicts a greater proportion of the PMN coming through with the RBC than has been observed experimentally. Recent estimates of RBC and PMN transit times in the human lung (43) suggest that approximately 18% of PMN have transit times similar to RBC. The model predicts values that are much higher than this because there is far less delay in the capillary bed. This means that the model underestimates the time that PMN spend in capillaries for reasons that could relate to the time they need to become actively motile or to a delay produced by adherence between PMN and endothelial cells not taken into account by the modelling process.

6 Summary and Conclusions

The fact that the vascular space contains one pool of white blood cells that circulate and another that marginate along vessel walls was established early in this century (1, 2). The lung has long been recognized as a major site of the marginated pool but in contrast to the systemic circulation where marginated cells are found in post capillary venules, the majority of the cells that marginate in the lung are contained in the capillary bed (20,41). Studies from our laboratory have shown that the pulmonary capillary bed is capable of concentrating PMN 60- to 70-times with respect to the peripheral blood and suggest that this concentration is based on differences in the RBC and PMN capillary transit times (41). The realization that there were differences between erythrocyte and PMN transit of this magnitude led us to consider the possibility of developing a computational model, based on anatomic data, to provide a framework in which to think about the problem of PMN kinetics.

The data presented in this thesis used a set of probabilities to construct a complete model of the arterial vessels from existing information on arterial casts and obtained a model of pulmonary venous system by modifying the process used for the arterial vessels. Many important assumptions were made in order to calculate the pressure drop in the large vessels and the ones that were chosen result in a model that is consistent with the observation that the bulk of the pressure drop occurs across the capillary bed (6) rather than in the large vessels (110).

The distances from the arterioles to the venules and the interconnections between individual segments of the capillary network were modelled assuming that each alveolar wall was

a square grid. Because of the complexity of the system of interconnecting segments joining arterioles and venules, a resistor network simulation was used to investigate the effect of plugging individual segments on the pressure drop across the network of capillaries immediately surrounding an occluded segment. This showed that the pressure drop across individual segments are small and little affected by plugging segments in the network with PMN. Indeed, the fact that the magnitude of the predicted pressure drop across a segment plugged by a PMN is smaller than the required pressure to move individual PMN through micropipettes of capillary sizes (22,76).

The model also allowed us to test the hypothesis that the delay which PMN experience with respect to RBC is solely related to differences in their deformability. The analysis shows that although the erythrocyte transit times were reasonably accurately predicted by the model, the PMN transit times were shorter than those obtained by either direct observation (56,57) in dogs or from the more indirect information available in humans (59,60). This means that all of the mechanisms responsible for delaying PMNs have not been considered in the modelling process and that factors such as the need for PMN to become actively motile to negotiate capillary restrictions or overcome adhesive force between their membranes and the endothelium need to be included to account for the observed delay in PMN traffic. Therefore, the model presented here provides a method for simulating PMN traffic and suggests new avenues of investigation that will provide a better understanding of how circulating cells move through the pulmonary microvessels.

Table 1

Shows data from the four regions of the arterial cast studied by Horsfield and his colleagues. The different regions were chosen with overlapping vessel diameters to assist in the formulation of a Strahler ordering system. As can be seen from this table, the regions from 600μm to 100μm and 90μm to 10μm had relatively few branches recorded. Due to the sparse nature of the data in these two regions the model presented in this thesis consisted of only two regions, 3cm to 100μm and 300μm to 10μm.

Table 1

Summary Description of Horsfield Cast Data

Horsfield's Label	Approximate Range	Number of Vessels
Proximal	3cm to 800μm	2998
Intermediate	600μm to 100μm	765
Upper Distal	300μm to 100μm	3284
Lower Distal	90μm to 10μm	616

Table 2

Shows the number of daughter branches from all parents in either the large vessel or small vessel regions. The NONE column indicates either a terminal branch or branches which are broken and have no daughters. While it is clear that the majority of divisions are bifurcations, a significant fraction are trifurcations and a few parents have more than 3 daughter branches. There are less bifurcations in the small vessel region as compared to the large vessel region.

Table 2

Number of Bifurcations and Trifurcations

	Number of Daughter Branches From Parent			
Zone	NONE	2	3	4+
3cm to 100μm	1640	1223	230	30
100μm to 10μm	490	1251	371	47

Zone	%Bifurcations	%Trifurcations
3cm to 100μm	1223/1483 = 82%	18%
100μm to 10μm	1251/1669 = 75%	25%

Table 3

Shows the branching probability for daughters from a parent branch in the large vessel range, 3cm to 100μm. Bifurcations have a largest daughter and a smallest daughter while trifurcations have an additional second (or middle) daughter. The largest daughter branches to one order smaller than the parent with a probability of 0.89 and 2 orders smaller with a probability of 0.11. The table shows that 58% of the differences between the parent order and the smallest daughter order, are at 5 orders indicating that the daughter branches are quickly approaching the capillary bed. No difference in branching probabilities was detected between bifurcations and trifurcations.

Table 3

Branching Probabilities For 3cm to 100μm Sized Vessels

	Fraction of Daughters Branching 'N' Orders Smaller Than Parent				
	1	2	3	4	5
Largest Daughter	0.890	0.110	0.000	0.000	0.000
Second Daughter	0.231	0.169	0.133	0.123	0.344
Smallest Daughter	0.056	0.067	0.157	0.140	0.580

Table 4

Shows the branching probability for daughters from a parent branch in the small vessel range, 100μm to 10μm. Bifurcations have a largest daughter and a smallest daughter while trifurcations have and additional second (or middle) daughter. The largest daughter branches to one order smaller than the parent with a probability of 0.885 and 2 orders smaller with a probability of 0.115. As seen in table 3 the difference between the parent order and the smallest daughter order is typically 5 orders. No difference in branching probabilities was detected between bifurcations and trifurcations.

Table 4

Branching Probabilities For 100μm to 10μm Sized Vessels

	Fraction of Daughters Branching 'N' Orders Smaller Than Parent				
	1	2	3	4	5
Largest Daughter	0.885	0.115	0.000	0.000	0.000
Second Daughter	0.173	0.133	0.114	0.098	0.482
Smallest Daughter	0.030	0.052	0.068	0.143	0.707

Table 5

The largest vessels of the arterial cast data in the regions 3cm to 100μm are not well represented by the proposed branching probabilities in this work. Therefore, the first four divisions of the large vessel region were recorded exactly as they occured in the cast data. This table shows how each parent in the first four divisions, branched. Within each divison, the largest vessels are displayed first. As an example, the first parent, order 48, divides into two order 47 branches. The first order 47 vessel is the largest and is therefore the first line of data from the 2nd divison values. The second order 47 vessel is the next line of data in the 2nd divison region.

Table 5

Branching Pattern of Large Arterial Branches

		Daughters			
Region	Parent	1st	2nd	3rd	Diameter(um)
1st Division					
	48	47	47		30000
2nd Division					
	47	44	46		19000
	47	46	42		18500
3rd Division					
	44	43	39		10000
	46	45	44	41	15500
	46	45	40		18000
	42	41	40	38	8000
4th Division					
	43	42	40		8500
	39	38	35		7000
	45	44	42	42	11000
	44	43	42		8500
	41	40	40	38	6500
	45	44	41		13500
	40	39	39		7000
	41	40	34		5000
	40	39	35		4500
	38	37	36		4000

Table 6

Shows the estimates for the number of bifurcations, trifurcations and diameter for vessels ordered 44 to 1 obtained using the model. While not shown in this table, the variability about the mean diameter (displayed in Figure 10) is about 30%.

Table 6 (Part 1 of 2)
Branching Pattern for Arterial Tree Orders 44 to 1

Orders	Bifurcations (# of vessels)	Trifurcations (# of Vessels)	Diameter(um)
44	2	0	9036
43	2	1	7840
42	6	1	6759
41	7	1	5697
40	11	3	5015
39	20	4	4351
38	30	6	3671
37	42	9	3163
36	59	13	2732
35	89	20	2359
34	134	29	2038
33	196	43	1760
32	285	63	1520
31	418	92	1313
30	613	135	1134
29	900	198	979
28	1324	291	846
27	1945	427	731
26	2853	626	631
25	4188	919	545
24	6147	1349	471
23	9021	1980	407
22	13241	2906	351
21	19433	4266	303
20	26088	8696	262
19	40160	13386	226
18	62067	20689	195
17	96394	32131	169
16	149632	49877	146
15	228133	76044	126
14	349232	116410	109

Table 6 (Part 2 of 2)
Branching Pattern for Arterial Tree Orders 44 to 1

Orders	Bifurcations (# of vessels)	Trifurcations (# of Vessels)	Diameter(um)
13	535204	178401	94
12	820817	273606	81
11	1259282	419760	70
10	1930967	643655	60
9	2960802	986934	52
8	4539909	1513303	45
7	6961409	2320470	39
6	10674757	3558252	34
5	16368734	5456244	29
4	25099811	8366604	25
3	38487988	12829328	22
2	59017388	19672462	19
1			13

Table 7

Shows the ratio of the arterial vessel number, diameter and length to the venous values. Clearly a larger number of precapillary arterioles exist than postcapillary venules. In general, the ratio of arterial diameter to capillary diameters tends to be within the variation of arterial diameter (30%).

Table 7
Ratio Between Number of Vessels, Vessel Diameter and Vessel Length for Arterial and Venous Cast Data Using Strahler Ordering

All values are Arteries/Veins

Order	#Vessels	Diameter	Length
1	411.4%	100.0%	100.0%
2	53.1%	110.5%	104.2%
3	57.7%	117.2%	102.5%
4	60.8%	125.6%	105.3%
5	64.1%	134.4%	105.3%
6	67.5%	143.8%	100.0%
7	71.1%	160.0%	103.0%
8	73.6%	159.5%	106.1%
9	77.7%	134.6%	124.4%
10	124.3%	139.3%	146.6%
11	136.1%	109.9%	60.0%
12	128.5%	110.0%	56.8%
13	124.5%	125.9%	70.5%
14	142.9%	111.3%	53.1%
15	200.0%	58.1%	29.7%

Table 8

Shows the percent decrease in the number of vessels in either the arterial or venous tree from the smallest pre or post capillary vessels to the larger proximal vessels. Except for the discrepancies between values from order 1 to 2, the rate of reduction of vessels appears quite similar in both the arterial and venous trees when a Strahler scheme is used.

Table 8
Percent Decrease in Number of Vessels Between Adjacent Orders for Arterial and Venous Trees Using Strahler Ordering

	Arteries	Veins
1 to 2	95.9%	83.2%
2 to 3	65.5%	68.3%
3 to 4	66.6%	68.3%
4 to 5	66.6%	68.3%
5 to 6	66.6%	68.3%
6 to 7	66.6%	68.3%
7 to 8	66.6%	67.7%
8 to 9	66.6%	68.4%
9 to 10	60.9%	75.6%
10 to 11	70.5%	73.1%
11 to 12	69.9%	68.1%
12 to 13	67.5%	66.5%
13 to 14	69.7%	73.6%
14 to 15	60.0%	71.4%
15 to 16	62.5%	
16 to 17	66.7%	

Table 9

Shows the number of vessels and predicted diameters for a venous network model obtained using the branching probabilities from tables 2,3 and 4 which were determined from arterial cast data. The number of orders, and the starting number of vessels, were chosen to agree with previously published results (45).

Table 9 (Part 1 of 2)
Summary Data for Venous Tree Branching Orders 43 to 1

Orders	Number of Vessels	Diameter(um)
43	4	7840
42	4	6759
41	8	5697
40	10	5015
39	16	4351
38	25	3671
37	37	3163
36	51	2732
35	72	2359
34	110	2038
33	163	1760
32	239	1520
31	348	1313
30	510	1134
29	748	979
28	1098	846
27	1615	731
26	2372	631
25	3479	545
24	5107	471
23	7496	407
22	11001	351
21	16147	303
20	23699	262
19	34784	226
18	53546	195
17	82756	169
16	128525	146

Table 9 (Part 2 of 2)
Summary Data for Venous Tree Branching Orders 43 to 1

Orders	Number of Vessels	Diameter(um)
15	199509	126
14	304177	109
13	465642	94
12	713605	81
11	1094423	70
10	1679042	60
9	2574622	52
8	3947736	45
7	6053212	39
6	9281879	34
5	14233009	29
4	21824978	25
3	33466415	22
2	51317314	19
1	78689850	13

Table 10

Shows the resistance in a network of resistors from each node to ground. Each grid is intended to represent a single alveolar wall where nodes represent the junction of capillary segments and capillary segments are replaced by resistors. Arteriole flow input is replaced by a voltage source and venule outflow by ground. These tables show that the resistances within each network have similar values and the total resistance across each grid is weakly related to the size of the grid.

Table 10
Resistance from Node to Output for Electrical Grids

4x4 Grid Total Resistance = 4.7

6.9	6.5	5.7	4.2
6.5	6.0	5.2	3.8
5.7	5.2	4.6	3.5
4.2	3.8	3.5	3.1

5x5 Grid Total Resistance = 4.2

6.7	6.7	6.2	5.5	4.1
6.7	6.5	6.0	5.2	3.8
6.2	6.0	5.5	4.8	3.6
5.5	5.2	4.8	4.4	3.5
4.1	3.8	3.6	3.5	3.0

6x6 Grid Total Resistance= 3.9

6.6	6.7	6.4	6.0	5.3	4.0
6.7	6.8	6.4	5.9	5.1	3.8
6.4	6.4	6.1	5.6	4.9	3.7
6.0	5.9	5.6	5.2	4.6	3.6
5.3	5.1	4.9	4.6	4.3	3.5
4.0	3.8	3.7	3.6	3.5	3.0

═══ indicates input borders (arterioles)
——— indicates output borders (venules)

Table 11

Shows the relative increase in resistance at each node in a resistor grid if 10% of the resistors have been replaced by open circuits (which are meant to represent capillary blockages by PMN). In these tables infinite resistances are not seen due to the vast number of alternative pathways. It can be seen in these tables that while the resistance very close to capillary blockages increases, this increased resistance is not transmitted back into the network grid more than one or two segments. Blockages in this model have a greater affect in the 4x4 grid than the larger 6x6 grid due the relatively fewer number of alternative pathways.

Table 11

Relative Increase in Resistance at Each Node with 10% Blockages

4x4 Grid Total Resistance = 1.2

1.3	1.2	1.3	1.1
1.3	1.3	2.0	1.1
1.2	1.5	1.4	1.1
1.2	2.2	1.8	1.1

5x5 Grid Total Resistance 1.2

1.3	1.3	1.2	1.0	1.2
1.3	1.3	1.3	1.0	1.0
1.1	1.1	1.2	1.0	1.0
1.1	1.0	1.0	1.0	1.0
1.1	1.0	1.0	1.0	1.0

6x6 Grid Total Resistance = 1.2

1.1	1.1	1.1	1.0	1.0	1.0
1.2	1.1	1.1	1.1	1.0	1.0
1.2	1.2	1.8	1.2	1.1	1.1
1.1	1.1	1.3	1.1	1.1	1.6
1.0	1.1	1.4	1.1	1.1	1.1
1.0	1.0	1.2	1.0	1.0	1.0

═══ indicates input borders (arterioles)
——— indicates output borders (venules)

Table 12

Shows the relative increase in resistance at each node in a resistor grid if 25% of the resistors have been replaced by open circuits (which are meant to represent capillary blockages by PMN). In these tables infinite resistances are not seen due to the vast number of alternative pathways. Although the resistance very close to capillary blockages increases, this increased resistance is not transmitted back into the network grid more than one or two segments but with this large number of open circuits resistances throughout the grid networks have increased relative to table 10.

Table 12

Relative Increase at Each Node with 25% Blockages

4x4 Grid Total Resistance = 3.2

3.9	2.5	2.7	2.9
3.0	3.1	3.8	1.5
1.8	2.4	2.3	1.2
1.8	1.6	1.3	1.0

5x5 Grid Total Resistance = 2.0

2.0	1.5	1.4	1.3	1.2
1.8	1.6	1.5	1.6	1.3
2.3	1.5	1.3	1.3	1.7
2.2	1.4	1.2	1.5	1.9
2.6	1.3	1.1	1.2	2.0

6x6 Grid Total Resistance = 2.6

2.1	2.3	2.0	2.0	2.0	1.6
2.0	2.3	2.6	2.1	2.2	2.1
2.4	2.4	4.4	2.3	2.6	1.5
2.4	2.5	2.5	2.4	2.9	2.4
3.8	5.9	3.7	2.9	3.0	1.5
5.0	2.6	4.9	3.8	3.0	1.8

═══ indicates input borders (arterioles)
——— indicates output borders (venules)

Table 13

Shows how the pattern of resistance varies when blockages are present in the resistor grid network. From table 12 each node resistance was divided by the total network resistance, then a corresponding table of these relative resistancse were computed for 10% or 25% blockages. The two tables shown here display the results for the scaled resistance with no blockages to those with either 10% or 25% blockages. Values of 1.0 indicate no differnce in the resistance at a given node relative to ground when blockages were present, values greater than 1 indicate an increased relative resistance. These data show that when only 10% of the capillary segments within a single alveolar wall are blocked that no effect on the pattern of pathway resistance can be seen. Also, when a larger number of pathways are blocked, 25%, only those nodes at or near the blockages are affected.

Table 13

Resistance Pattern for 5x5 Grid Scaled to Total Grid Resistance

10% Blockages

1.1	1.1	1.0	0.8	1.0
1.1	1.0	1.1	0.8	0.8
0.9	0.9	1.0	0.8	0.8
0.9	0.8	0.8	0.8	0.8
0.9	0.8	0.8	0.8	0.8

20% Blockages

1.0	1.3	1.4	1.5	1.7
1.1	1.2	1.3	1.3	1.5
0.9	1.3	1.5	1.5	1.2
0.9	1.4	1.7	1.3	1.1
0.8	1.5	1.8	1.7	1.0

═══ indicates input border (arterioles)
——— indicates output border (venule)

Table 14

Shows the relative increase in resistance in an electrical grid network, similar to table 13, except that current (flow by analogy) is limited to travel in a unidirectional manner in each segment. This network simulates the condition of two vessels flowing into each network node and two out from each node. Values of INF indicate an infinite resistance, meaning that both vessels leading from that node are plugged. Note that with 10% blockages, the infinite resistance at a completely occluded node is only transmitted back one or at most two segments into the capillary network.

Table 14

Relative Increase in Resistance at Each Node with 10% Blockages Relative to No Blockages: This Model Allows Unidirectional Flow in Each Segment

4x4 Grid Total Resistance (Relative Change) = 1.2

2.2	1.4	1.6	1.0
1.5	3.2	INF	1.1
1.3	2.4	1.3	1.0
1.3	4.7	2.6	1.0

5x5 Grid Total Resistance (Relative Change) = 1.3

1.4	1.9	1.2	1.0	1.0
1.7	1.1	1.7	1.0	1.0
1.0	1.0	1.0	1.0	1.0
1.0	1.0	1.0	1.0	1.0
1.0	1.0	1.0	1.0	1.0

6x6 Grid Total Resistance (Relative Change) = 1.0

1.4	1.1	1.2	1.0	1.0	1.0
2.0	1.3	1.7	1.0	1.0	1.0
1.2	1.8	INF	1.1	1.1	1.2
1.1	1.2	1.5	1.1	1.4	2.8
1.0	1.1	2.2	1.0	1.0	1.0
1.0	1.0	1.0	1.0	1.0	1.0

INF indicates an INFINITE resistance, all pathways to exit blocked

═══ indicates input border (arteriole)
——— indicates output border (venule)

Table 15

Shows the relative increase in resistance in an electrical grid network, similar to table 14, except that current (flow by analogy) is limited to travel in a single direction in each segment. This network simulates the condition of two vessels flowing into each network node and two out from each node. Values of INF indicate an infinite resistance, meaning that both vessels leading from that node are plugged. In contrast to table 16, when 25% of the segments are plugged relatively large increases in vessel resistances are seen throughout the network. In this simulation the greater increase in total grid resistance for the 4x4 model is merely a reflection of the close proximity of the blocked segments. In general, the total network resistance was similar for all network sizes.

Table 15

Relative Increase in Resistance at Each Node with 25% Blockages Relative to No Blockages: This Model Allows Unidirectional Flow in Each Segment

4x4 Grid Total Resistance (Relative Change) = 3.5

4.0	3.3	2.9	2.9
INF	INF	INF	1.0
1.3	3.0	1.9	1.0
1.5	1.0	1.0	1.0

5x5 Grid Total Resistance (Relative Change) = 2.3

1.9	1.2	1.2	1.2	1.0
2.7	1.9	1.6	2.9	1.2
INF	1.1	1.2	1.6	3.4
2.9	1.0	1.2	2.0	1.6
2.9	1.0	1.0	1.1	2.0

6x6 Grid Total Resistance (Relative Change) = 2.6

10.7	2.5	1.9	1.3	1.7	1.2
8.1	7.9	INF	2.1	2.3	3.1
7.4	6.5	INF	4.3	6.6	1.2
7.9	5.7	4.1	3.8	5.0	2.9
INF	INF	6.6	3.7	3.8	1.1
INF	1.5	8.2	5.6	3.5	2.0

INF indicates an INFINITE resistance, all pathways to exit blocked

═══indicates input border (arteriole)
———indicates output border (venule)

Table 16

Shows the values used for regional capillary diameters based on the data of Glazier (33) (figures 25 and 26). The first column shows the relative amount the capillary segment diameters are decreased compared to fully distended values. Also shown are the mean and standard deviation of the capillary segment diameters using the fully distended values estimated in section 3.1 of the thesis.

Table 16

Regional Capillary Diameters

	%Maximum	Mean μm	SD μm
Upper Lung	67%	5.01	1.55
Slice 2	75%	5.61	1.73
Slice 3	83%	6.21	1.92
Slice 4	89%	6.66	2.06
Lower Lung	94%	7.03	2.17

Table 17

Shows the results of the model of the capillary bed. The different regional responses were estimated by varying only the capillary segment diameters based on values from table 16. These data show that relatively little effect on the number of stops (number of vessels encountered with diameters less than that of the PMN) is seen regionally. However, the median time per stop and the median transit time is significantly increased when the PMN is forced to travel through small diameter vessels.

Table 17

Summary of Capillary Bed Simulations

Region	Median Stops (#)	Median Time per stop (secs)	Median Transit Time (sec)
Upper Lung	5	12.8	63.9
Slice 2	5	4.0	18.2
Slice 3	4	2.3	10.2
Slice 4	4	1.5	6.8
Lower Lung	4	1.1	5.3

Table 18

Shows the fraction of total pulmonary flow delivered to different lung regions based on the data of Anthonisen and Milic-Emili (3). When estimating total pulmonary transit times these values were used to determine what fraction of the cells traversed each of the different lung regions where capillary segment diameter varied.

Table 18

Fraction of Cardiac Output Delivered to Each Region

Upper Lung	3.7%
Slice 2	11.1%
Slice 3	19.9%
Slice 4	28.5%
Lower Lung	36.8%

Figure 1

Shows a radiographic image of the human pulmonary arterial tree obtained 3 seconds after an injection of dye into the right ventricle. Comparison of this picture to those in Fig. 2 and 3 provides an overview of the complexity of the pulmonary vasculature and the diversity of pathlengths from the pulmonary artery to pulmonary veins.

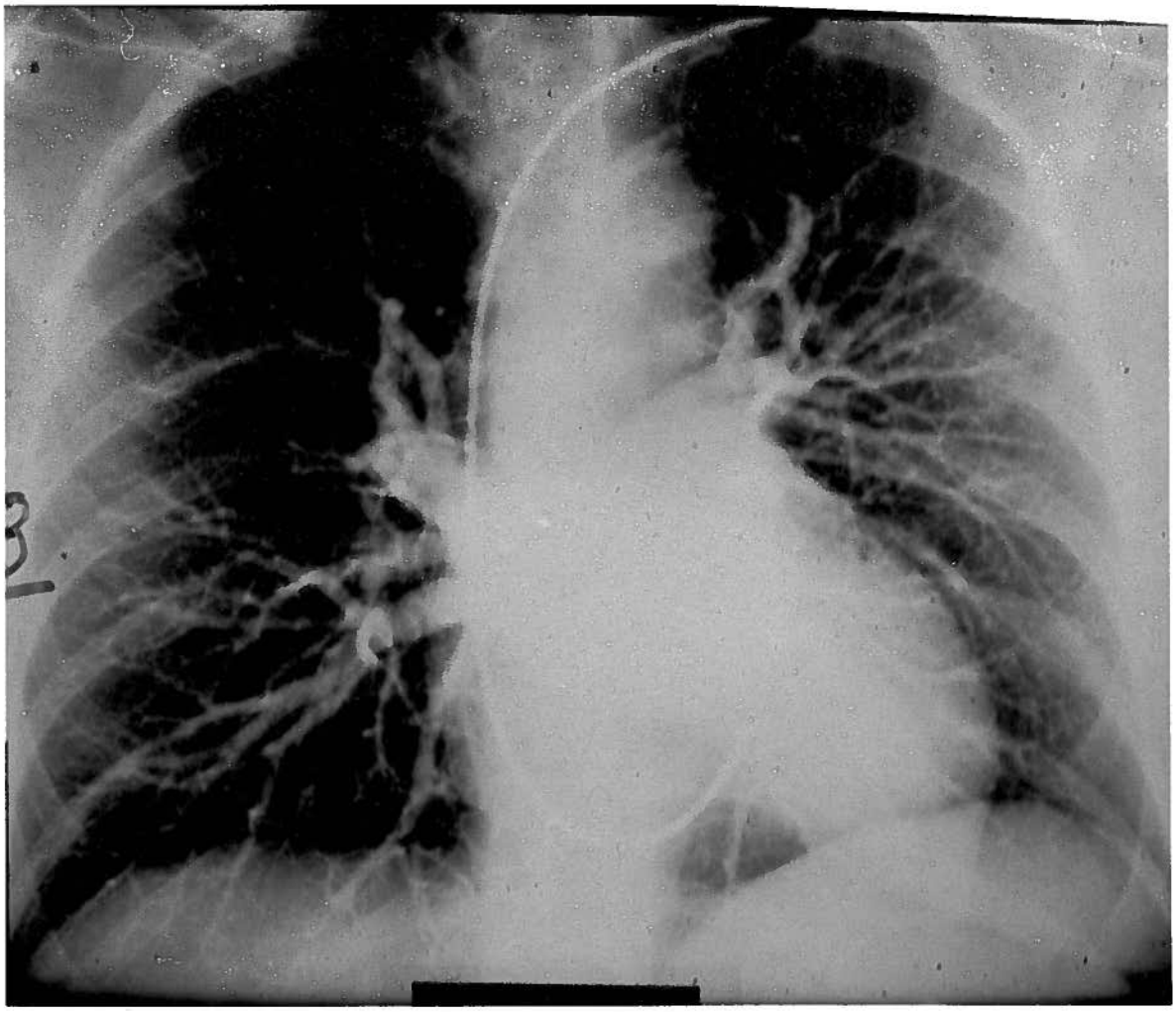

Figure 2

From the same series as Figure 1 showing a second radiographic image taken 8 seconds after the injection of dye in the right ventricle. The venous circulation is shown to advantage in this image.

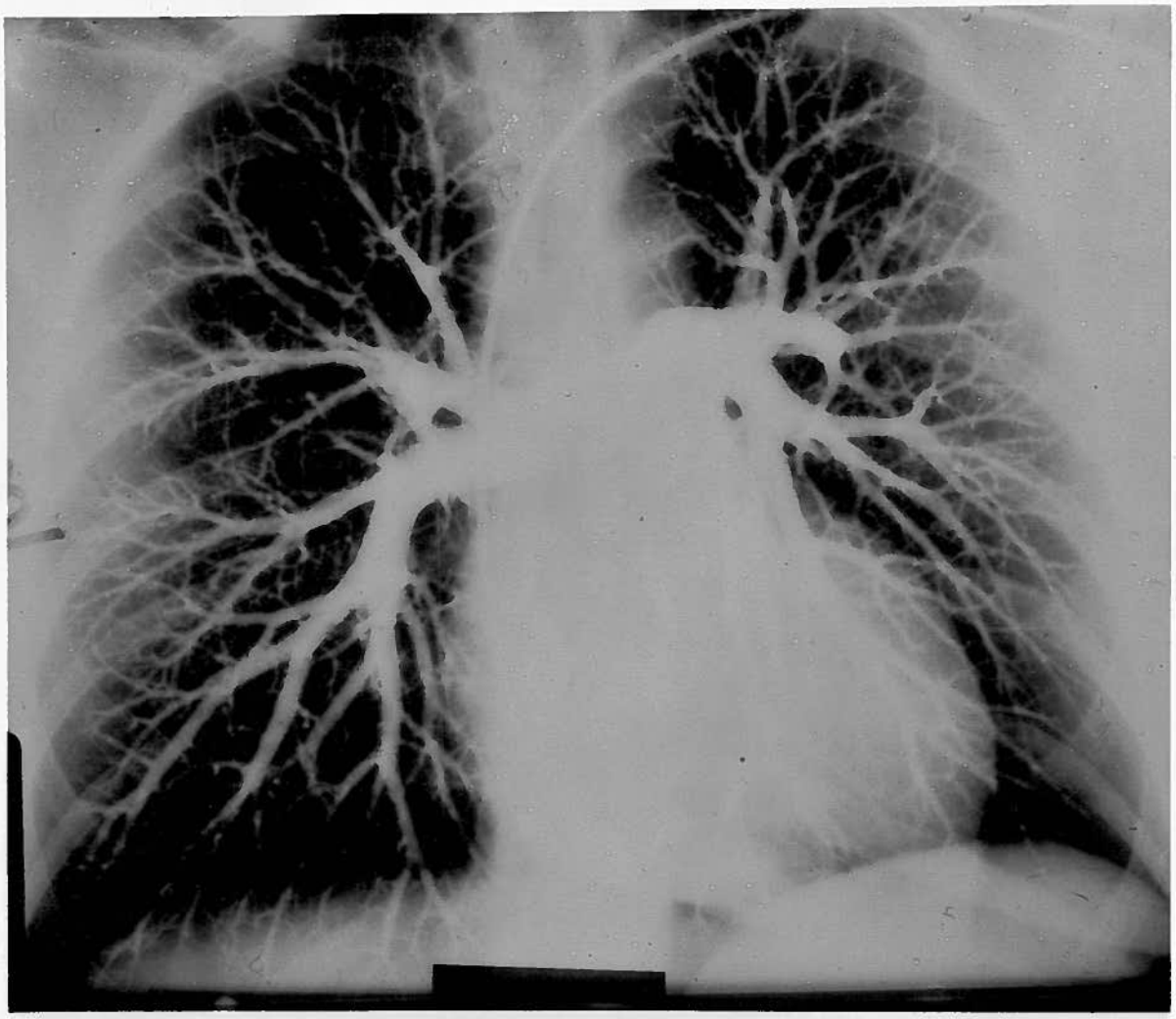

Figure 3

Shows a third radiographic image from the same series as Figs. 1 and 2 taken 20 seconds after the dye was injected in the right ventricle. It demonstrates that the dye has almost completely cleared from the venous circulation at this phase.

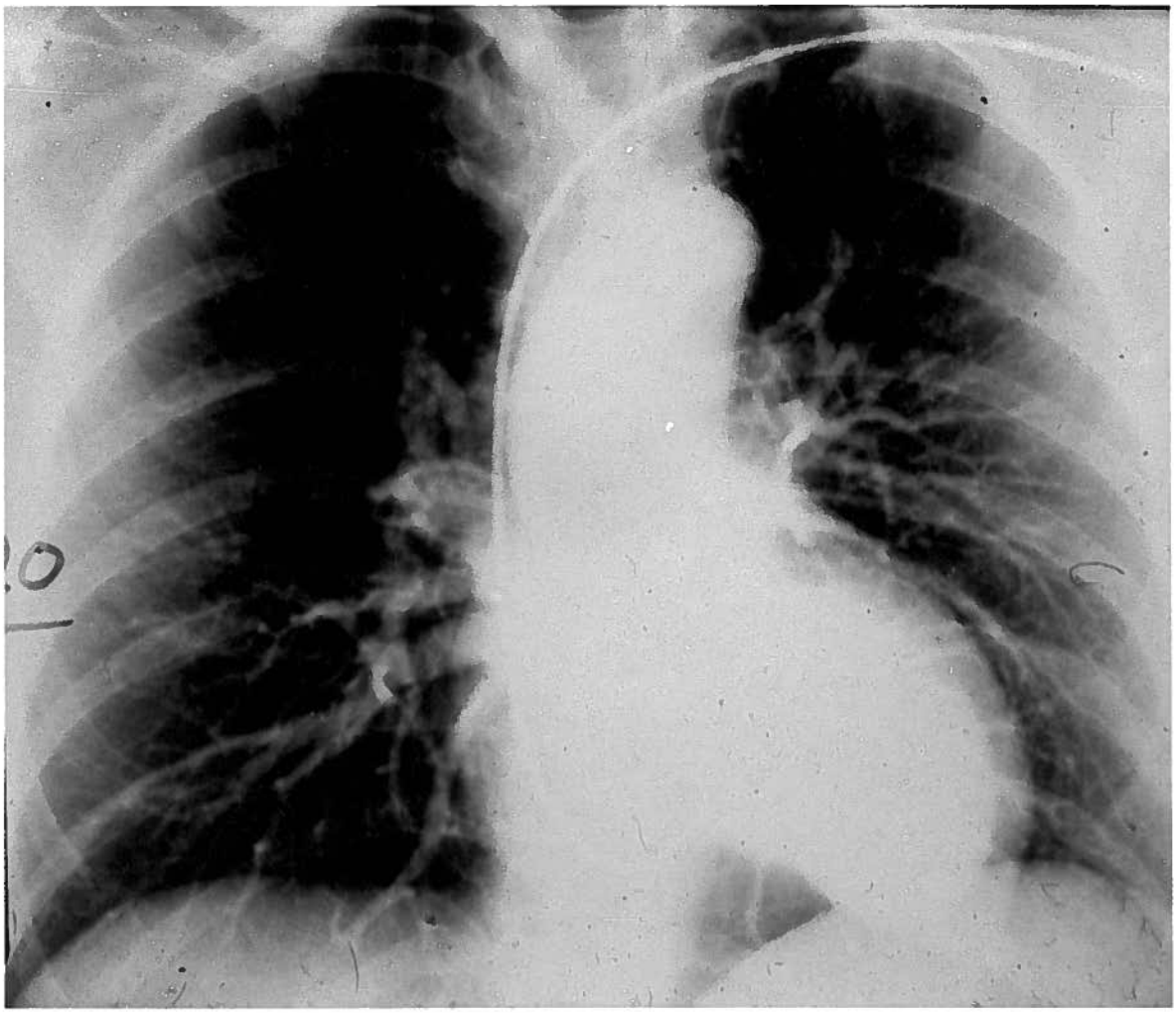

Figure 4

Shows the results of an indicator dilution study from reference 62 which compares ^{99M}Tc RBC to ^{51}Cr RBC during a single pass through the lung. The labelled cells were injected into the right ventricle and sampled at the aorta and the data show that the two procedures used to label the RBC had no effect on their transit through the pulmonary circulation.

Figure 4

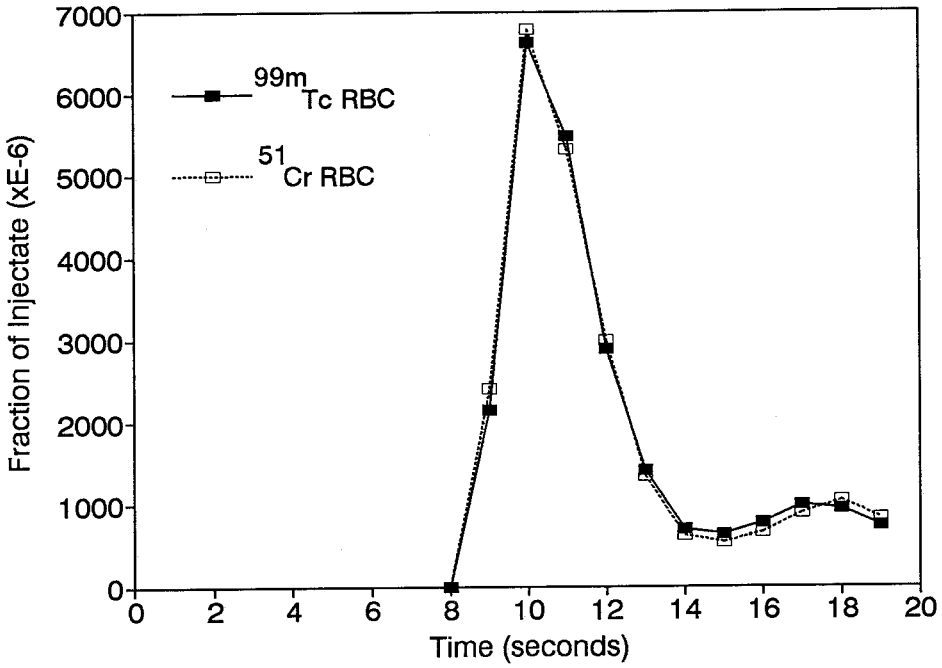
7000
6000
5000
4000
3000
2000
1000
0
Fraction of Injectate (xE-6)
99m Tc RBC
51 Cr RBC
0
2
4
6
8
10
12
14
16
18
20
Time (seconds)

Figure 5

Data from reference 62 comparing ^{99}Tc RBC to ^{51}Cr PMN with the same injection and sampling sites as in Figure 4. It shows that only about 20% of the PMN came through with the RBC which means that 80% were delayed in the lung.

Figure 5

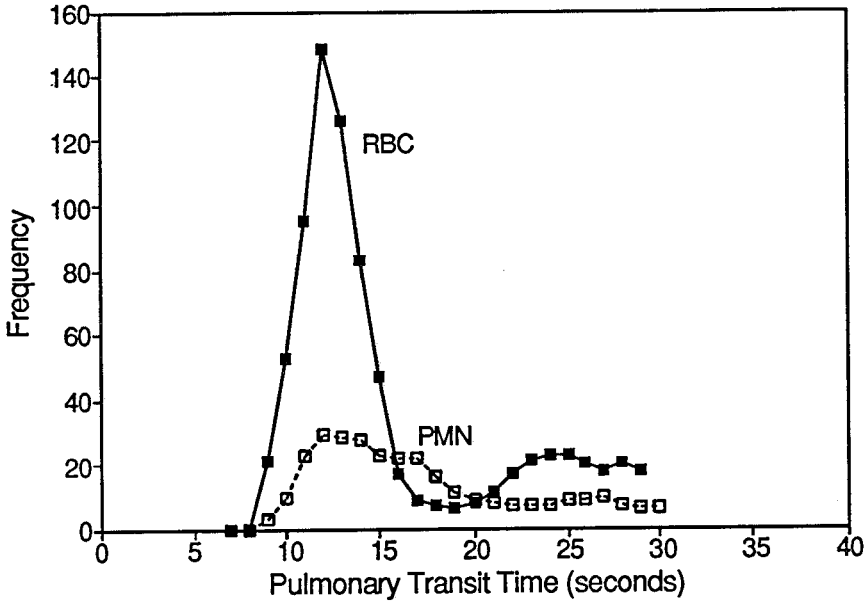
160
140
120
100
80
60
40
20
0
Frequency
RBC
PMN
0
5
10
15
20
25
30
35
40
Pulmonary Transit Time (seconds)

Figure 6

This figure shows a branching network labelled using Strahler ordering rules. In this labelling scheme, the smallest vessels (at the ends of the tree) are labelled as order 1. When two vessels meet the parent vessel is labelled one order larger than the daughters if both daughters have the same order. If the two daughter branches have different orders then the parent branch is given the order of the largest daughter branch. This branching scheme makes it impossible to track vessel length for a random path through the tree and therefore is not practical for a fluid mechanics approach to studing the pulmonary vasculature.

Figure 6

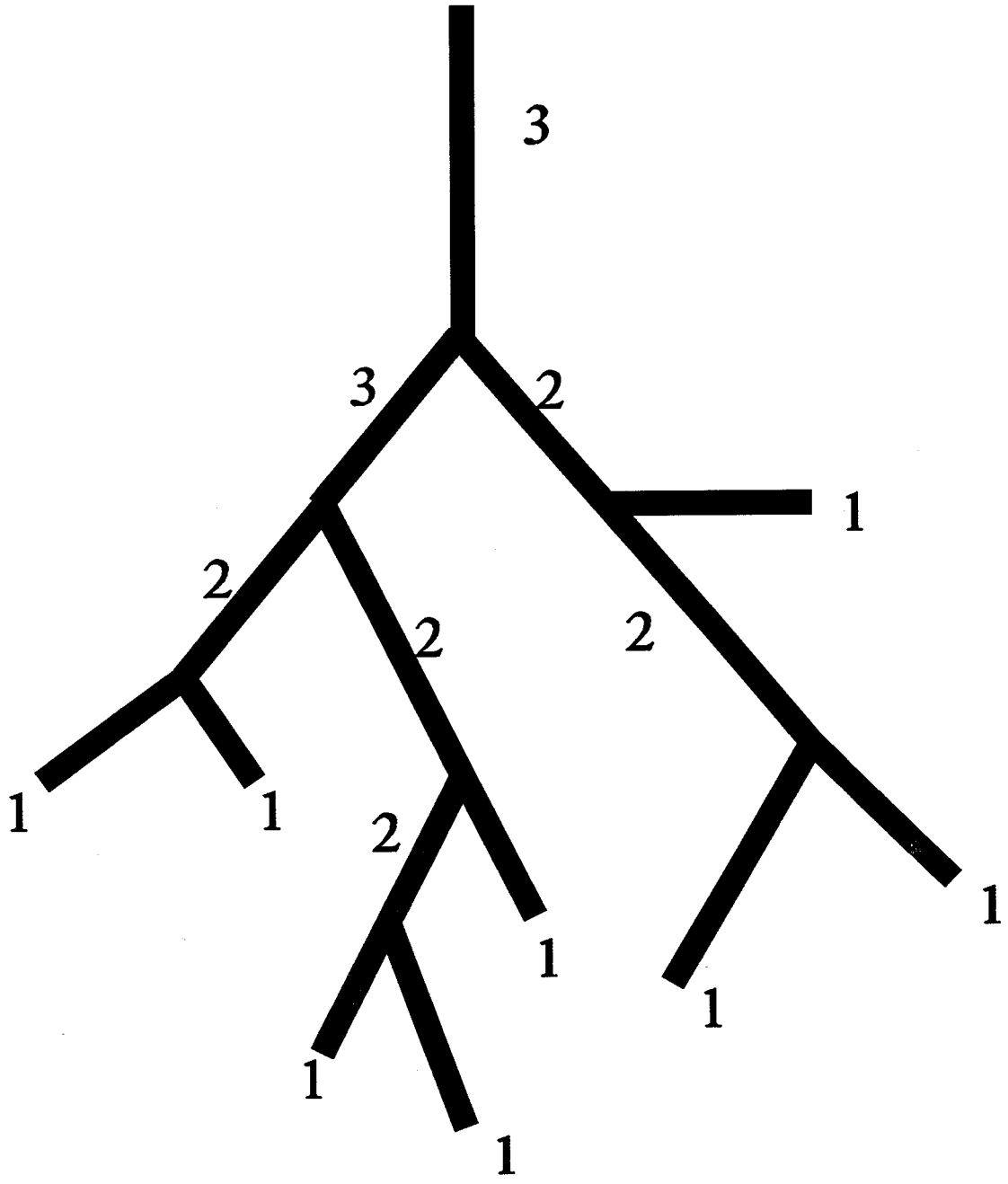

Figure 7

This figure shows the same tree as in Figure 6 ordered using a symmetrical branching system. In this scheme, the largest branch at the top of the tree is labelled an order 0 vessel. Each daughter at each division is then assigned an order, one less than the parent vessel. This symmetric branching method cannot accurately represent the very asymmetric branching structure present in the pulmonary angiogram (see Figures 1-3) and is not practical for ordering a pulmonary vasculature tree.

Figure 7

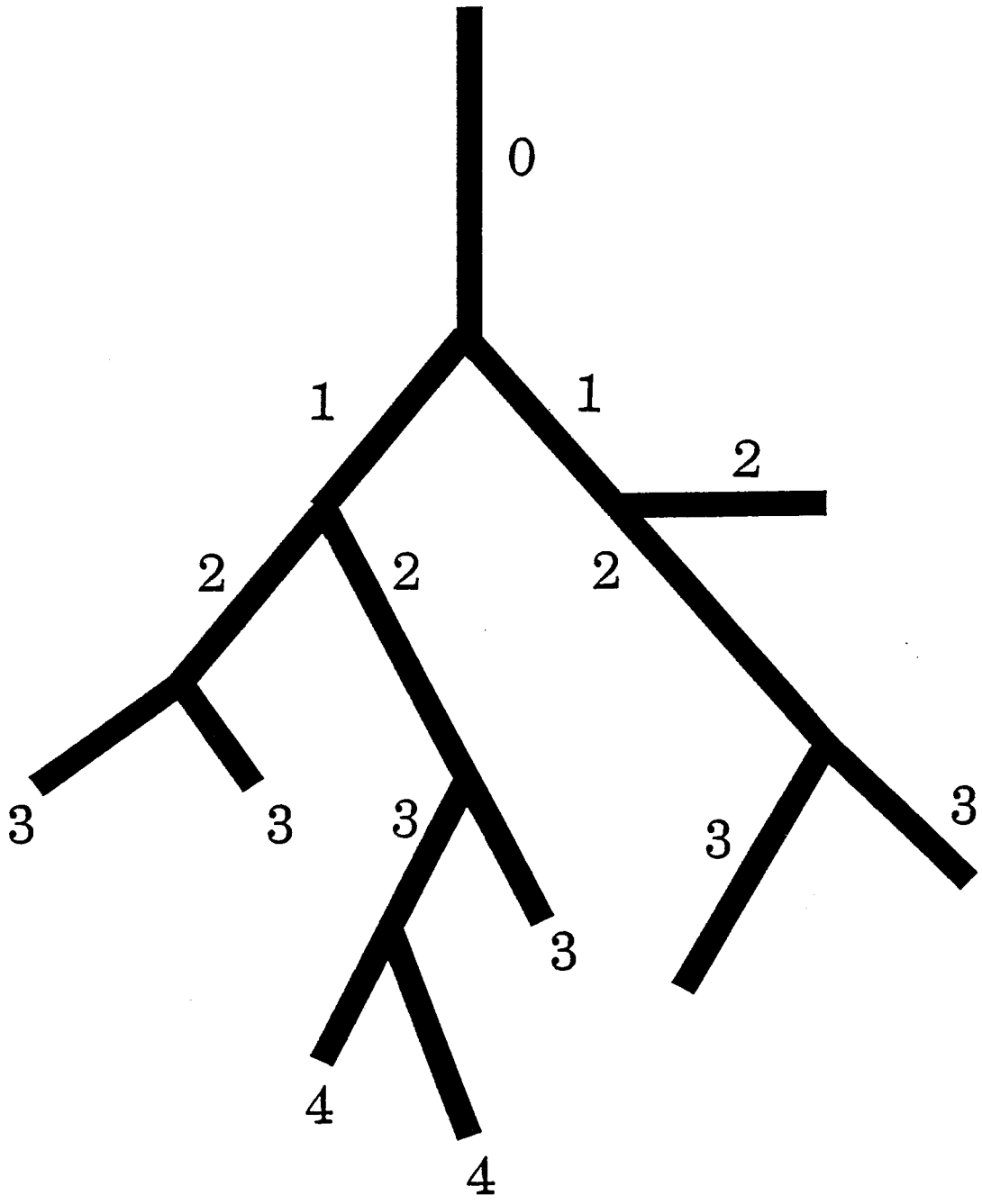

Figure 8

Shows a Horsfield ordering scheme for the same tree as in Figures 6 and 7. In Horsfield ordering each terminal end branch is given an order 1 as in Strahler ordering. When two (or more daughters) meet at a division, the parent branch is assigned an order one larger than the largest daughter. Unlike the Strahler ordering, this method makes it possible to accurately record total path lengths and allows a very asymmetric branching pattern to be modelled. This system was used to order the pulmonary vessels in this thesis.

Figure 8

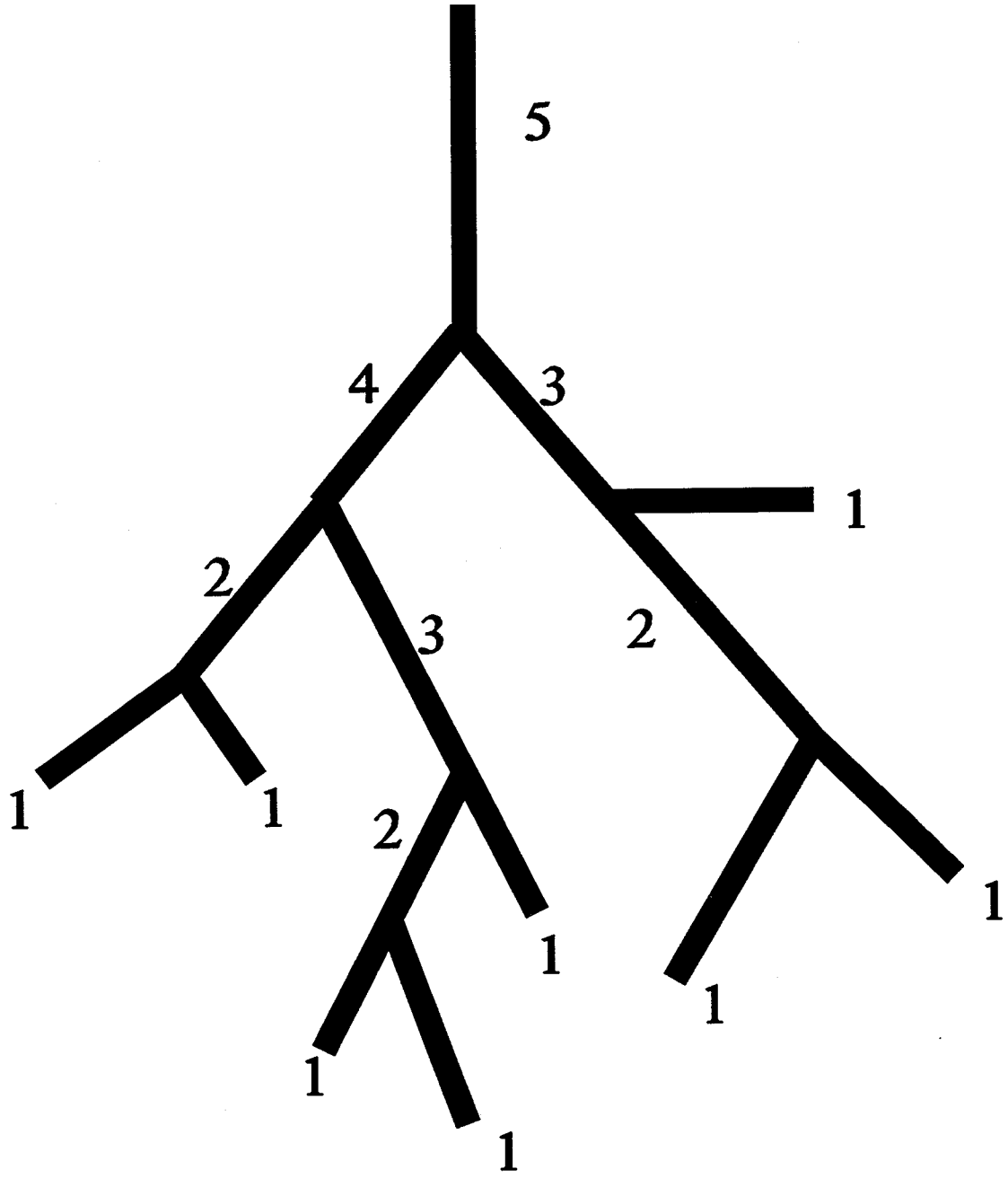

Figure 9

Shows the results of ordering each of the four regions of the available cast data (Table 1) using the Horsfield scheme in Figure 8. Each region of cast data has been artificially separated for display purposes. The curvilinear drop in each region is due to broken branches providing biased estimates of vessel diameter.

Figure 9

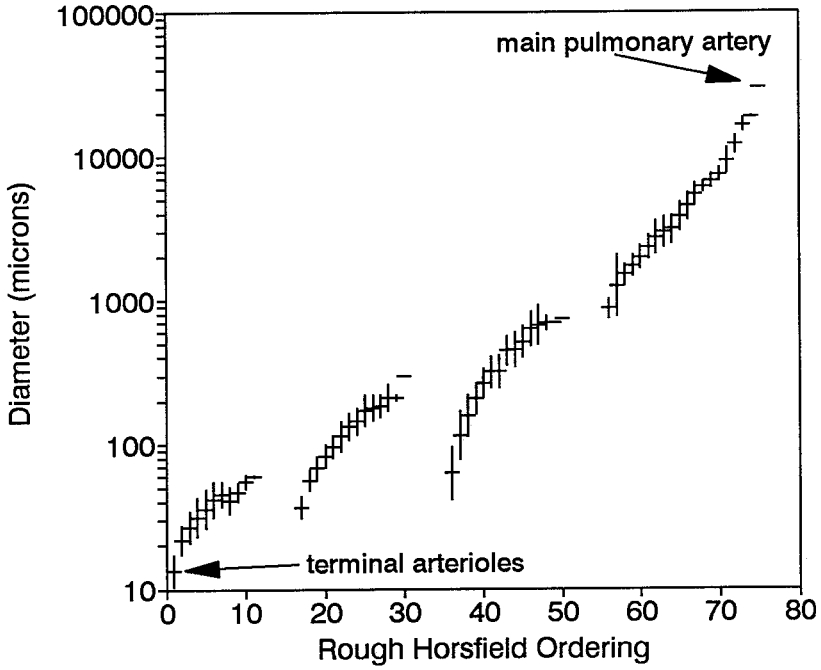
100000
10000
1000
100
10
Diameter (microns)
main pulmonary artery
terminal arterioles
0
10
20
30
40
50
60
70
80
Rough Horsfield Ordering

Figure 10

Shows the complete cast data ordered by the Horsfield branching scheme. The separate cast regions have been aligned by matching vessels of similar diameters in the proximal end of one region with those in the distal end of another. These data show a log-linear relationship between diameter and order which is a common characteristic of naturally occurring branching patterns. The variability in diameters at each order is about 30%.

Figure 10

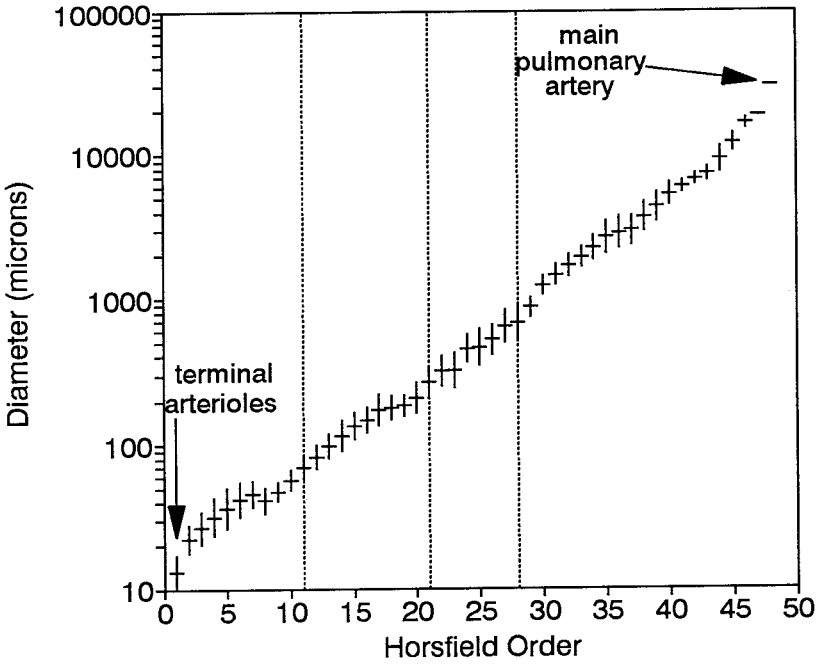
100000
10000
1000
100
10
Diameter (microns)
main
pulmonary
artery
terminal
arterioles
0
5
10
15
20
25
30
35
40
45
50
Horsfield Order

Figure 11

Shows an estimate of the number of branches in a given order for a simulated arterial tree. The probabilities in tables 2,3 and 4 were used to estimate these values. The number of terminal arterioles in this model is $3x10^{11}$ agrees with previous estimates (95).

Figure 11

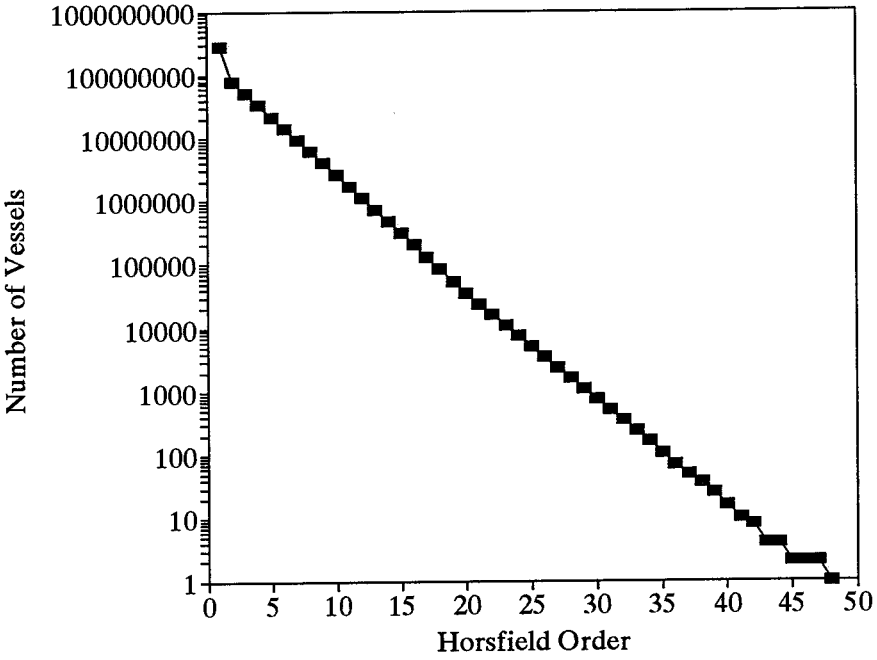
Number of Vessels
1000000000
100000000
10000000
1000000
100000
10000
1000
100
10
1
0
5
10
15
20
25
30
35
40
45
50
Horsfield Order

Figure 12

Shows the cross-sectional area available for blood flow at each order in the simulated arterial tree. These values are based on the estimated vessel diameter (figure 10) and the estimated number of vessels (figure 11) at each order. It is interesting that there is a reduction in cross-sectional area at approximately order 44. A similar reduction in cross-sectional area has been recorded in the tracheobronchial tree (see references 46,96) but as the estimates are made on casts from different lungs, the location of these constrictions cannot be compared.

Figure 12

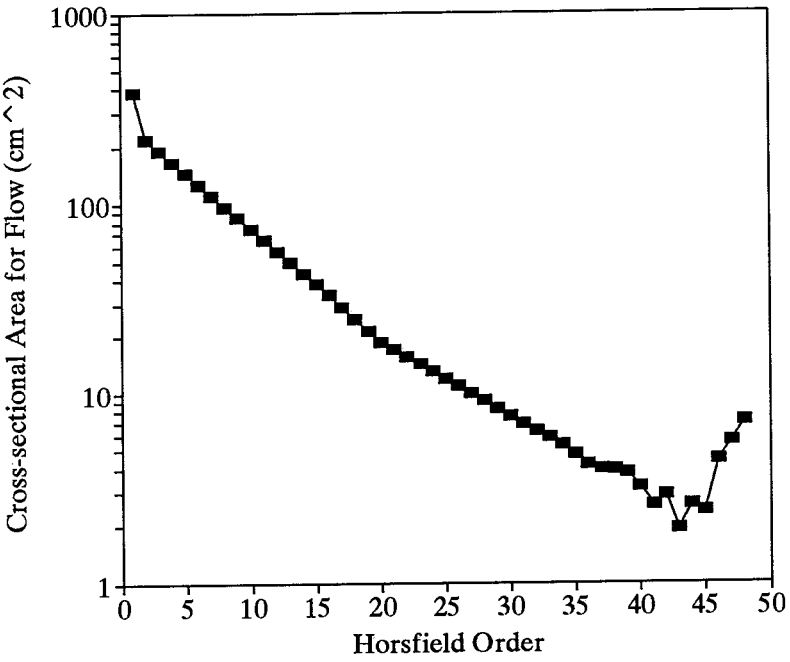
1000
100
10
1
Cross-sectional Area for Flow (cm ^ 2)
0
5
10
15
20
25
30
35
40
45
50
Horsfield Order

Figure 13

Using the concept of flow continuity, which states that all the fluid flowing into a bifurcation or trifurcation must flow out of the division we can estimate the possible amount of flow that a particular order vessel could carry. If it is assumed that each terminal arteriole carries 1 unit of flow then each order 2 arteriole must carry 2 units (for a bifurcation) or 3 units (for a trifurcation) since this model has assumed that all branching terminates at order 1 vessels. With flow now solved for all possible order two vessels, the same logic can be extended to predict possible flows in order 3 vessels etc. This pattern of tracking was computed up to order 20 vessels. These data show that as vessels become larger they can carry more flow but that the variation in the amount of flow per vessel also increases.

Figure 13

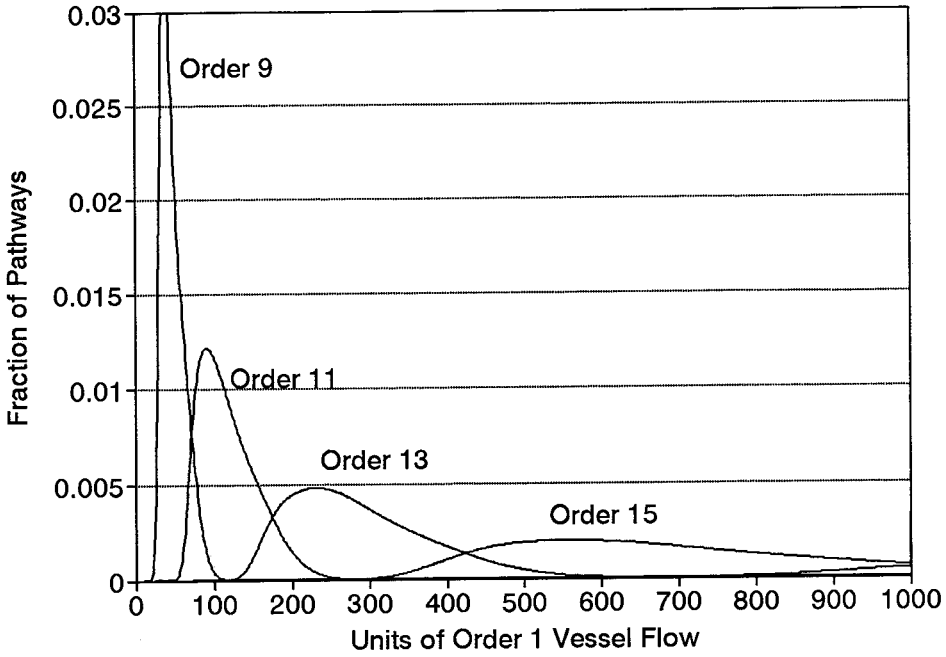
0.03
0.025
0.02
0.015
0.01
0.005
0
Fraction of Pathways
Order 9
Order 11
Order 13
Order 15
0
100
200
300
400
500
600
700
800
900
1000
Units of Order 1 Vessel Flow

Figure 14

This figure shows the estimated average flow in a vessel of a given order as a fraction of the total cardiac output. The average flow for orders 1-20 was estimated as described in Figure 13. Average flow in vessels from order 21 to 48 are extrapolated based on the values for the smaller vessels. While not evident from this figure, by multiplying the average flow per vessel shown here by the number of vessels of a given order (figure 11) it is estimated that each order carries approximately 50% of the total cardiac output. This means that because the branching is not symmetrical, all of the flow does not go through each order of branching.

Figure 14

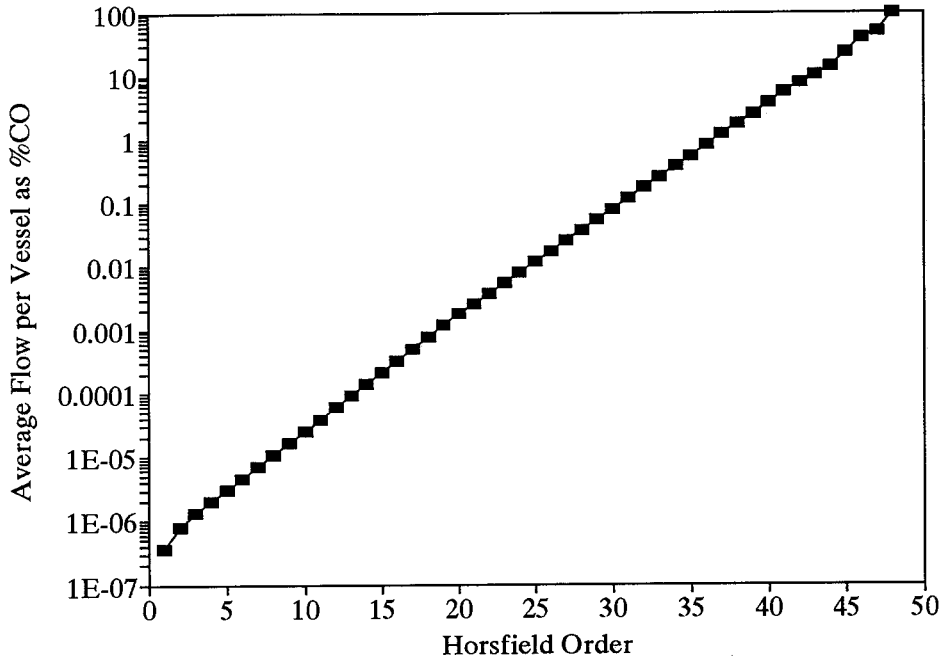
Average Flow per Vessel as %CO
100
10
1
0.1
0.01
0.001
0.0001
1E-05
1E-06
1E-07
0
5
10
15
20
25
30
35
40
45
50
Horsfield Order

Figure 15

Shows the distribution of pressure drops for numerous simulated pathways from the main pulmonary artery to the precapillary vessels. The different pressures reflect the different pathways that the flow can take from the main pulmonary artery to the capillary network. While pressure drops as large as 4 or 5 mmHg can occur, the average pressure drop is only 1.8 mmHg.

Panel B shows the average pressure drop for the vessels of each arterial order.

Figure 15A

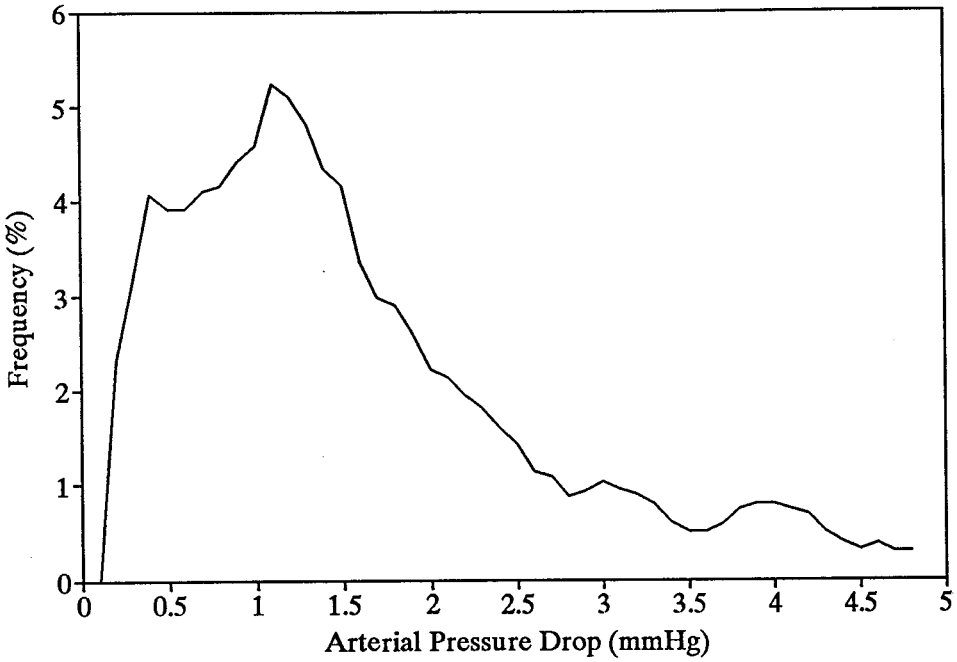

Figure 15B

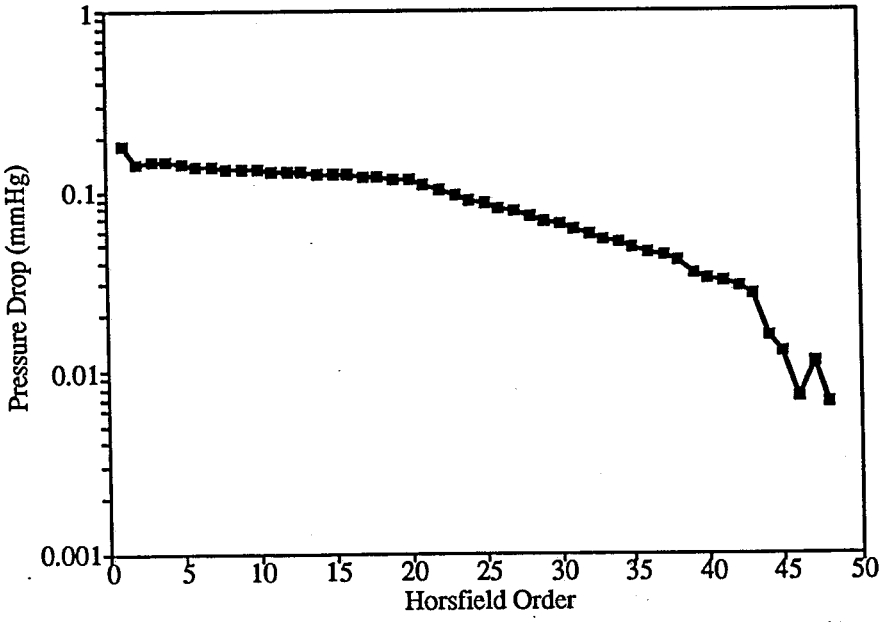

Figure 16

Shows the distribution of arterial vessel path lengths from the main pulmonary artery to the precapillary vessels. As is apparent from the angiographic images of the vessels (see Figures 1-3), a wide distribution of pathways should be expected. The maximum predicted pathways are approximately 10cm in length which are reasonable for a human lung.

Figure 16

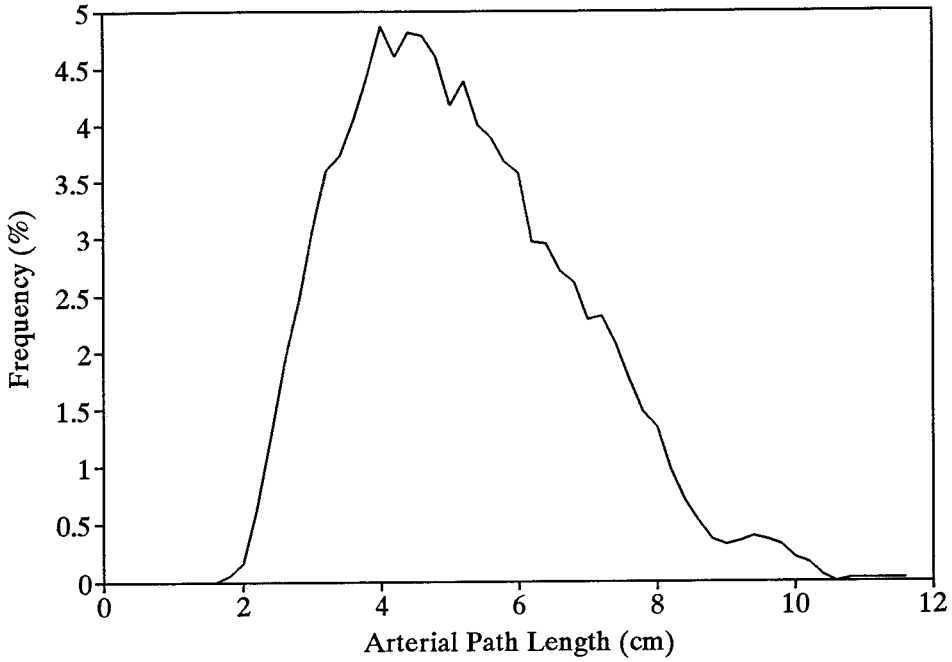
Frequency (%)
5
4.5
4
3.5
3
2.5
2
1.5
1
0.5
0
0
2
4
6
8
10
12
Arterial Path Length (cm)

Figure 17

Shows an estimate of precapillary blood velocity based on the computational estimates described in the text. The majority are included in the range from 500 to 2000μm/s which is in good agreement with published results (83). This indicates that the rules used to divide flow at divisions and the computed pressure drops in the arterial system are reasonable.

Figure 17

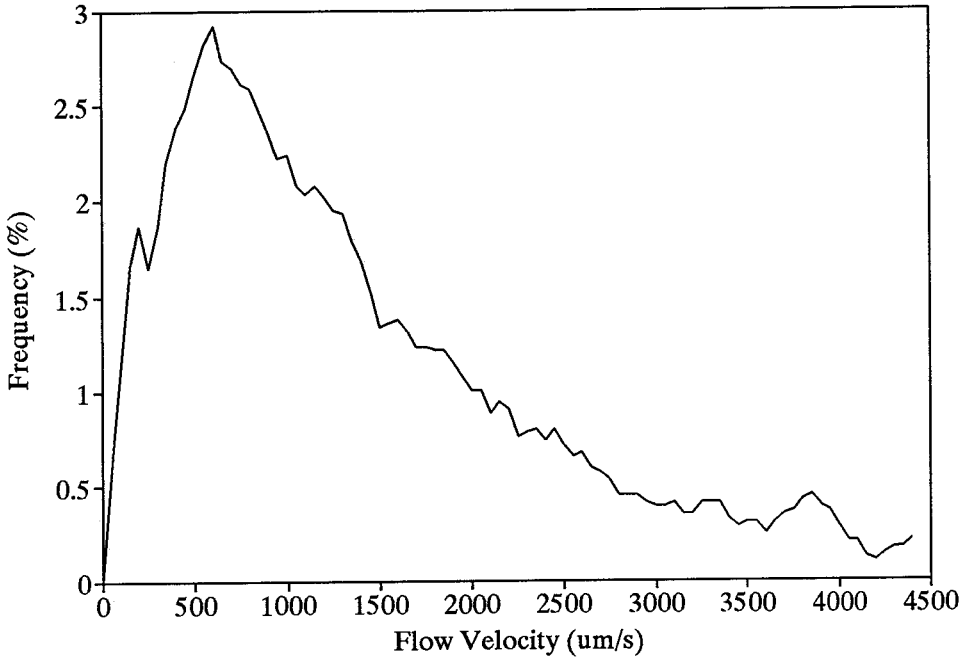
Frequency (%)
3
2.5
2
1.5
1
0.5
0
0
500
1000
1500
2000
2500
3000
3500
4000
4500
Flow Velocity (um/s)

Figure 18

Shows the estimated distribution of path lengths for the simulated venous tree. The slight differences from the arterial system (Figure 16) are due to the fact that the arterial tree was trimmed to represent the venous system.

Figure 18

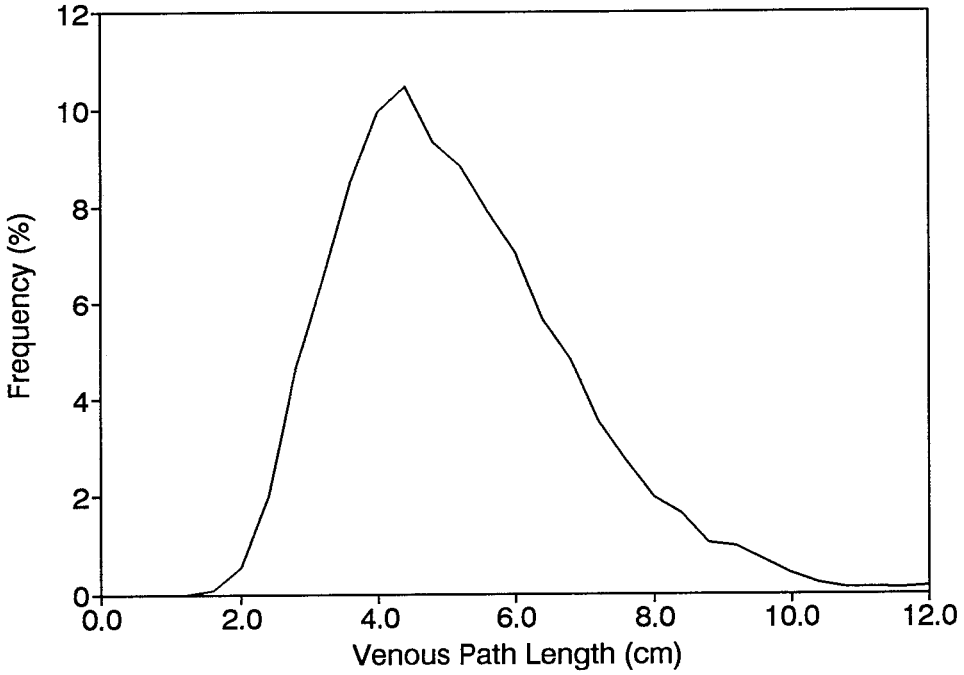
12
10
8
6
4
2
0
Frequency (%)
0.0
2.0
4.0
6.0
8.0
10.0
12.0
Venous Path Length (cm)

Figure 19

Shows the distribution of pressure drops in the venous network. The average pressure drop of about 1.3 mmHg is slightly less than that of the arterial tree due to selective pruning of the arterial data to obtain this model of the pulmonary veins.

Figure 19

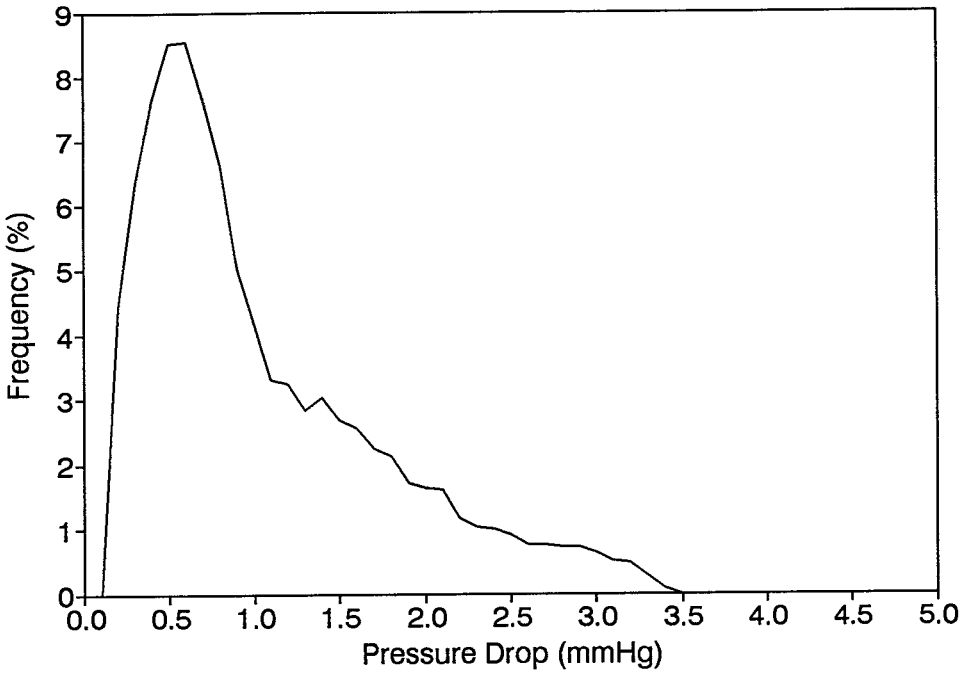
Frequency (%)
9
8
7
6
5
4
3
2
1
0
0.0
0.5
1.0
1.5
2.0
2.5
3.0
3.5
4.0
4.5
5.0
Pressure Drop (mmHg)

Figure 20

Compares the cumulative pressure drop in the large vessels (arteries and veins). The data have been arbitrarily placed at an initial pressure of 15mmHg to match that of Zhuang (110). The solid line represents the maximum possible pressure drop calculated when blood is allowed to pass through every order of both the arterial and venous tree. The dotted line represents the estimate obtained using the model system described in this thesis. The distance between these lines graphically displays the potential range of pressures at every order. The pressure drop between orders can be infered by the slope of the lines but this should be done with caution as it is clear that most of the blood does not flow through sequential orders. The discrepancy between the pressure at the terminal arteriole and post capillary venules provides an estimate of the pressure drop across the capillary bed.

Figure 20

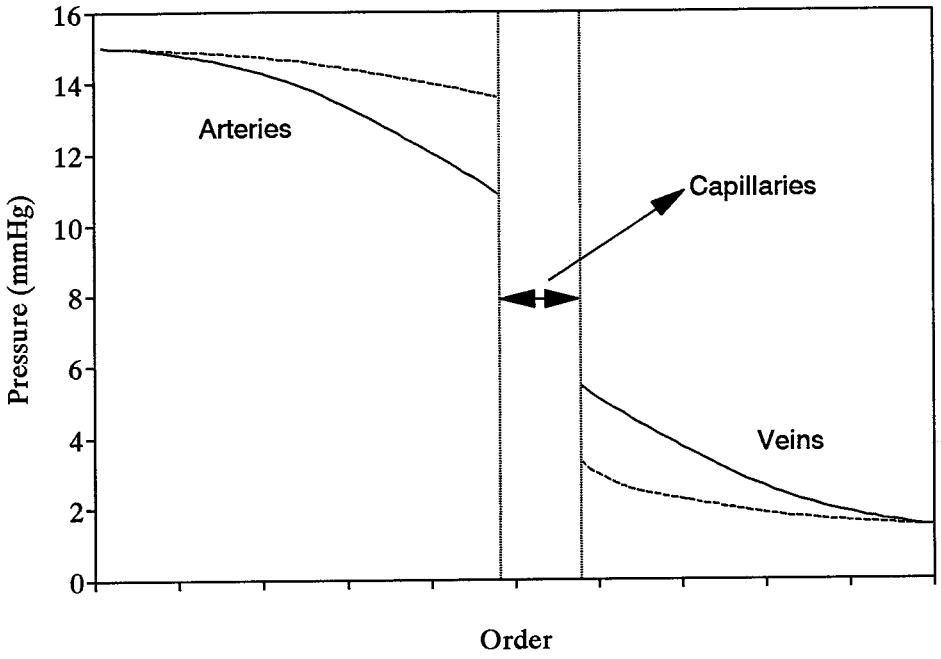
16
14
12
10
8
6
4
2
0
Pressure (mmHg)
Arteries
Capillaries
Veins
Order

Figure 21

Shows the distribution of human capillary segment diameters (solid bars) and human PMN diameters (open bars) obtained using morphometric techniques. The capillary segment diameters have a wider distribution than the PMN and many segments, at least 58%, have diameters smaller than the average PMN diameter. This difference in PMN size and pulmonary capillary size forces PMN to stop and deform as they attempt to traverse the pulmonary microvasculature.

Figure 21

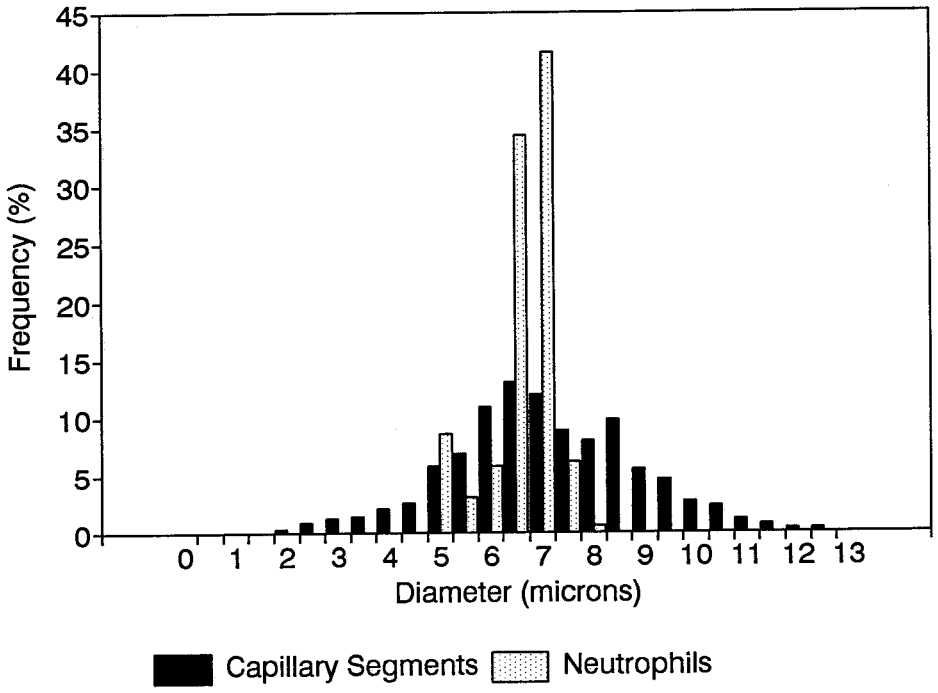
45
40
35
30
25
20
15
10
5
0
Frequency (%)
0 1 2 3 4 5 6 7 8 9 10 11 12 13
Diameter (microns)
Capillary Segments
Neutrophils

Figure 22

This photograph is a 25μm thick section of a human alveolar wall. Several RBC and PMN can be identified within the segments.

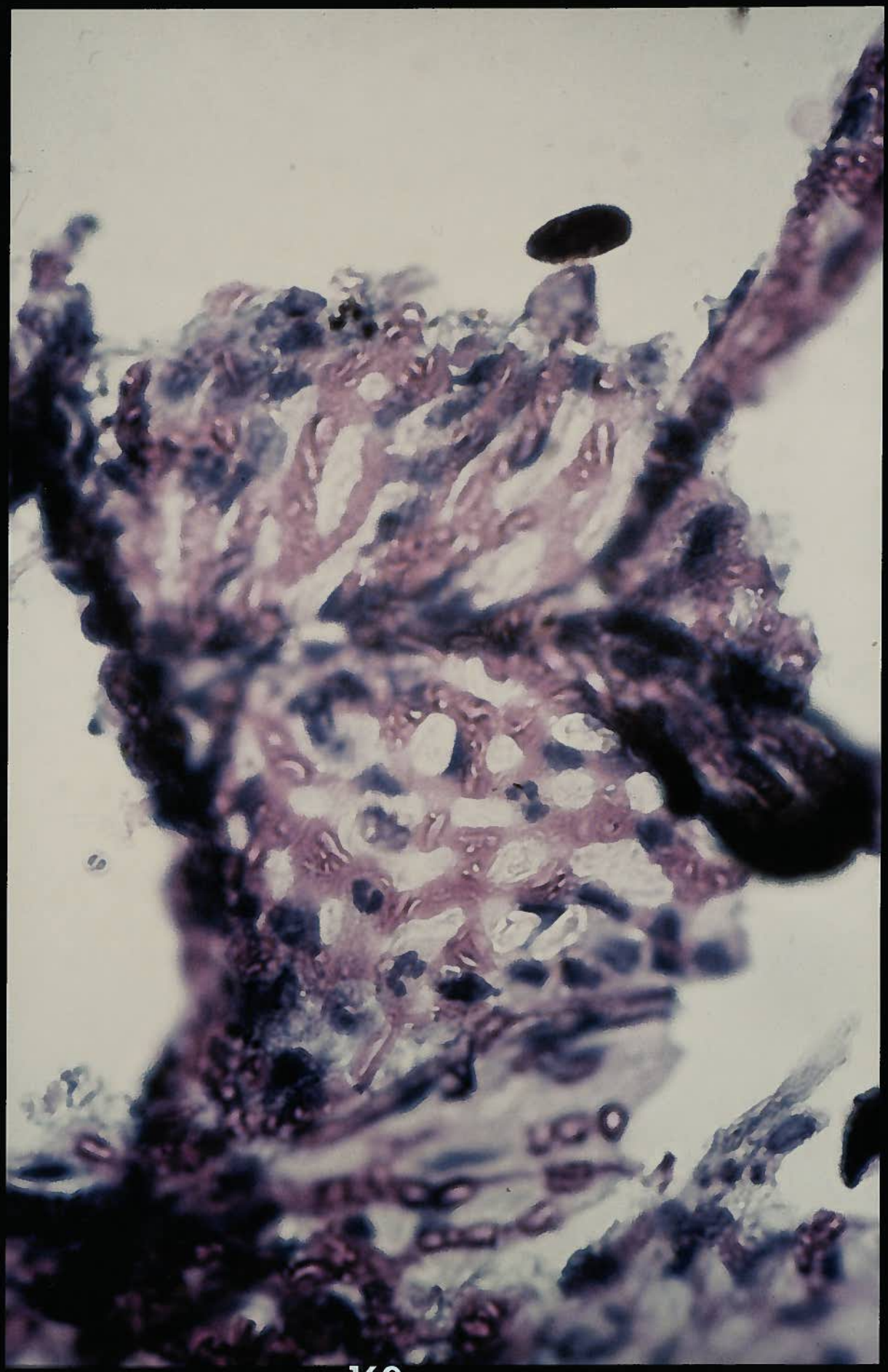

Figure 23

This diagram shows the network design used to simulate a single alveolar wall. Two walls were randomly chosen (not necessarily adjacent walls) to represent arteriole or corner vessel input and the remaining two walls venule or corner vessel outputs. Capillary segments were taken to be each small line segment, there are 60 segments of line in this 5x5 grid, and nodes are where four capillary segments meet. Blood is assumed to flow along the solid black lines in this diagram and the open white spaces would represent the posts in a sheet flow model. No attept has been made to draw the grid to anatomical scale. In the electrical simulations computed, the arterial inputs were voltage sources, the venous return were grounds. Each capillary segment was replaced by a resistor and flow was allowed in a single direction through each segment.

Figure 23

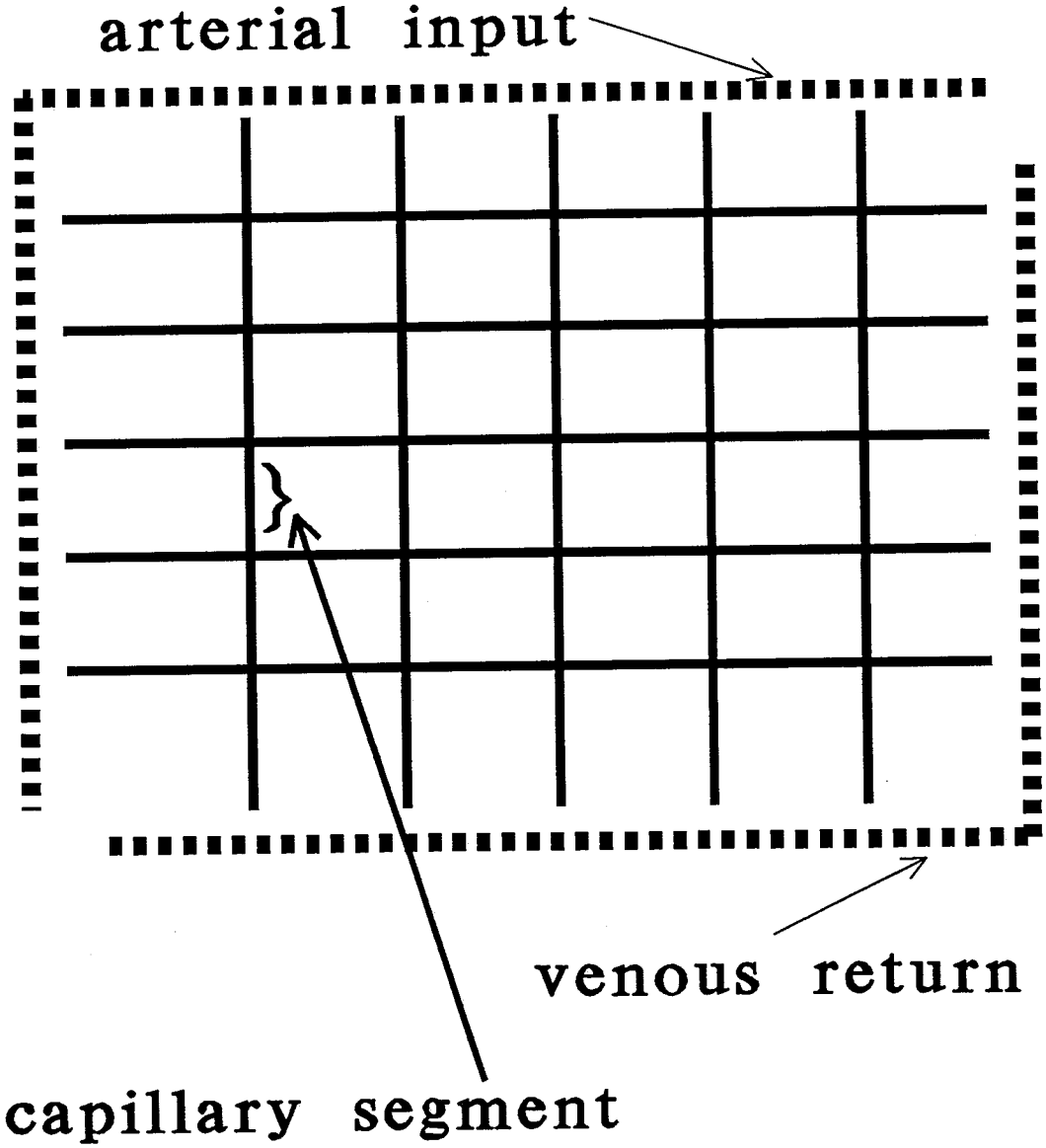

Figure 24

Shows an example where capillary segments blocked by PMN were modelled by replacing them with open circuits. The **O** indicates the situation with 10% of segments randomly plugged. The **X** denote the additional segments that are removed from the circuit when 25% capillary segments are plugged.

Figure 24

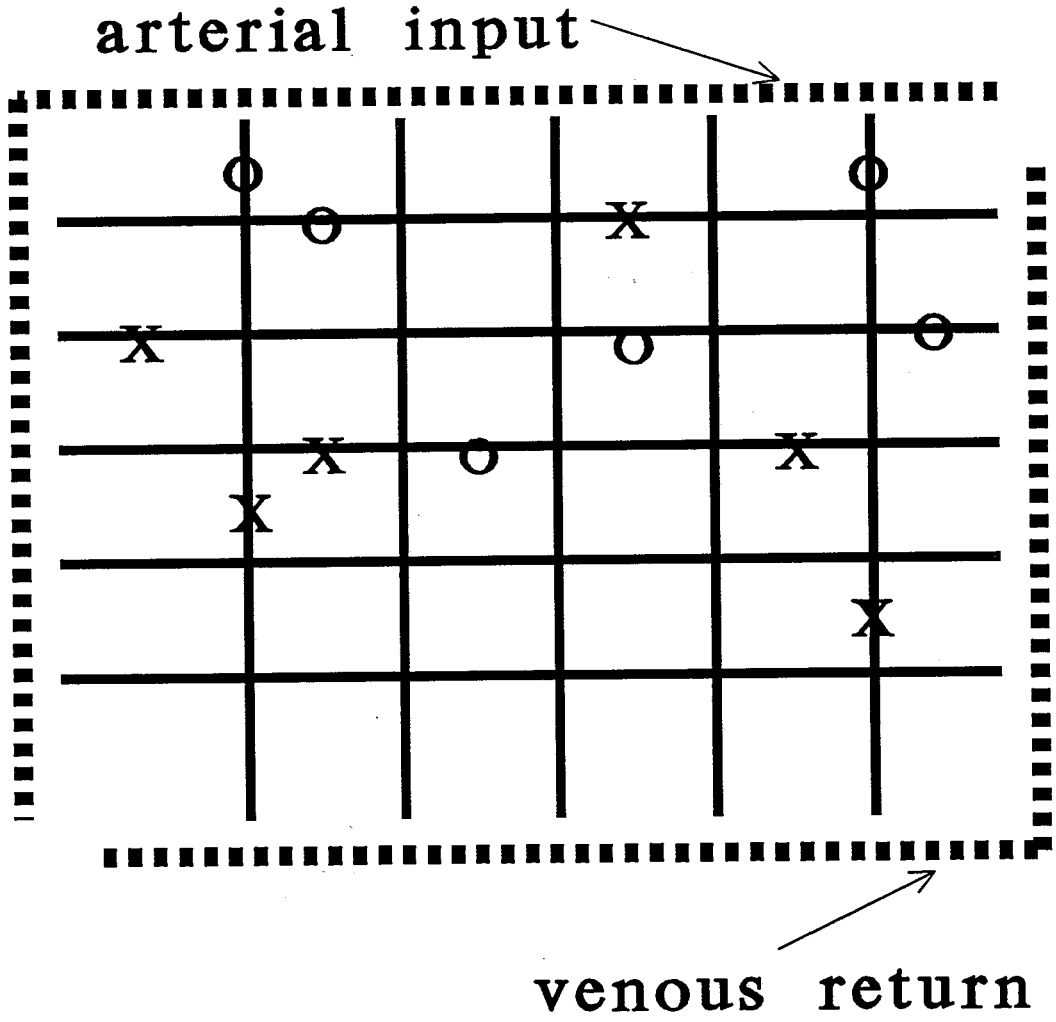

O location of 10% blockages

X location of 25% blockages

Figure 25

Data modified from Glazier et al showing capillary segment diameters in different gravitational planes. The large distance down Zone III was achieved by controlling arterial and venous pressures to keep the entire lung under Zone III conditions.

Figure 25

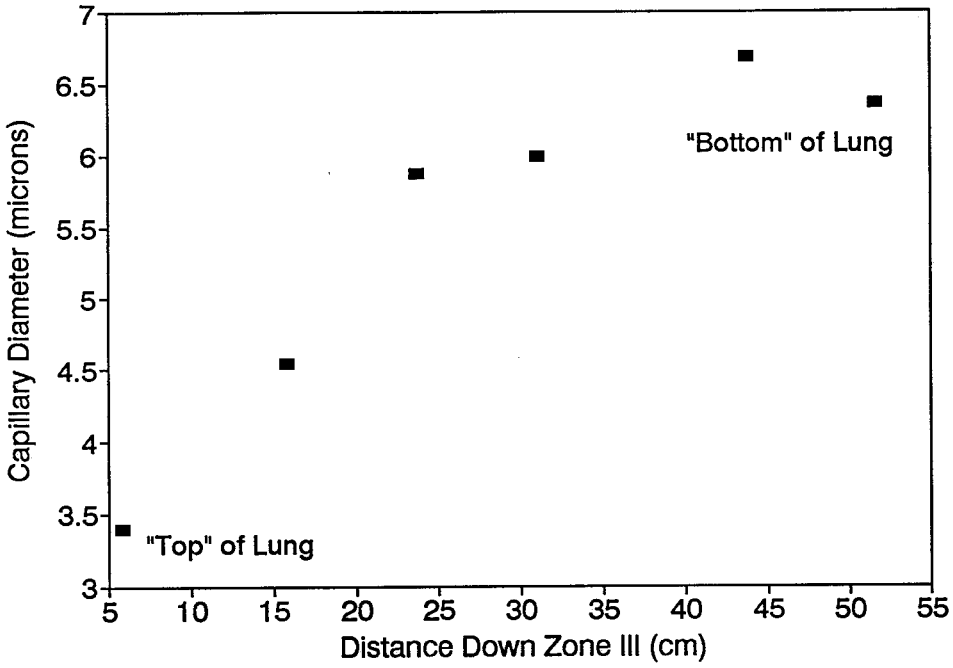
Capillary Diameter (microns)
7
6.5
6
5.5
5
4.5
4
3.5
3
"Bottom" of Lung
"Top" of Lung
5
10
15
20
25
30
35
40
45
50
55
Distance Down Zone III (cm)

Figure 26

Data from figure 25 which has been scaled to show capillary segment diameter as a percent of its maximum. The average capillary segment diameter, relative to the maximally dilated values, was determined for each of 5 six cm sections selected to represent a 30 cm human lung. The numerical values for each of these regions are shown in Table 16.

Figure 26

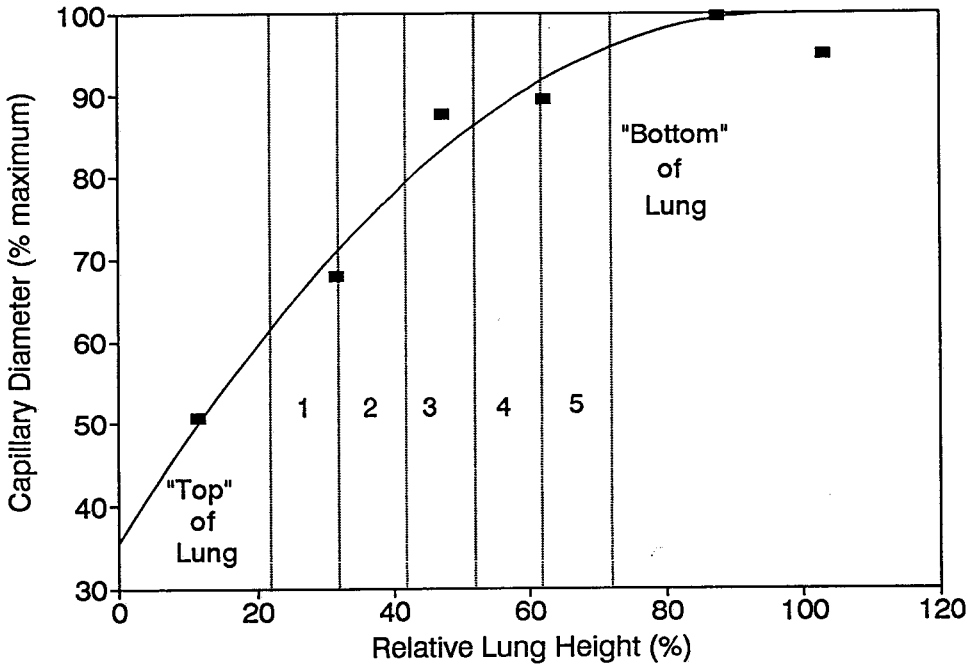
Capillary Diameter (% maximum)
100
90
80
70
60
50
40
30
0
20
40
60
80
100
120
Relative Lung Height (%)
"Top" of Lung
"Bottom" of Lung
1
2
3
4
5

Figure 27

Shows a line derived from the equation, empirically determined by Fenton et al (26), for the time required for a WBC to deform and enter a pipet. This equation was chosen because it was imperically derived without a pressure term which allowed it to be used to model events across individual capillary segments where no pressure data is available.

Figure 27

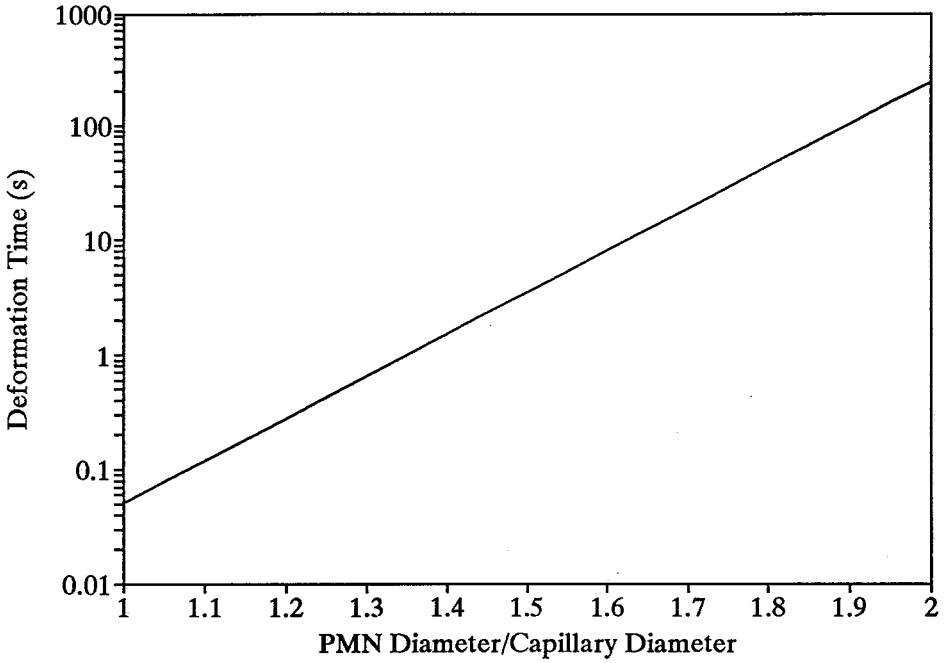
1000
100
10
1
0.1
0.01
Deformation Time (s)
1
1.1
1.2
1.3
1.4
1.5
1.6
1.7
1.8
1.9
2
PMN Diameter/Capillary Diameter

Figure 28

Shows the estimated number of capillary segments traversed by cells moving from a terminal arteriole to a post capillary venule. On average each PMN passes through 90 segments, with the majority of pathways containing between 70 and 120 segments.

Figure 28

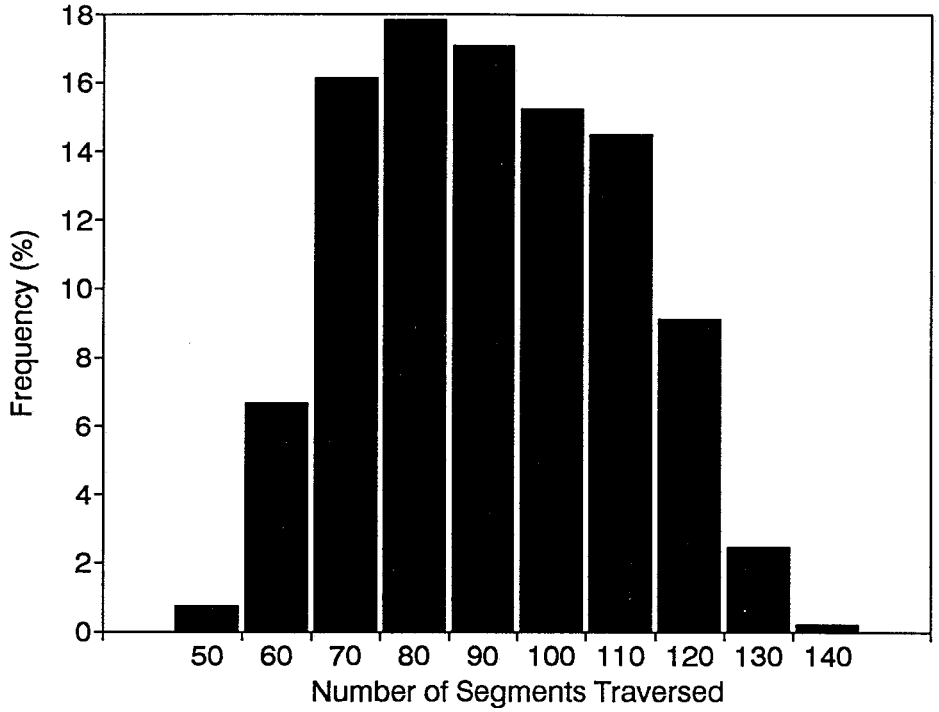
18
16
14
12
10
8
6
4
2
0
Frequency (%)
50
60
70
80
90
100
110
120
130
140
Number of Segments Traversed

Figure 29

Shows the estimate of the total capillary path length that a PMN travels from a terminal arteriole to a post capillary venule. This length can not be measured directly using current experimental techniques but Staub and Schultz (83) have measured the minimum arteriole to venule distance in a straight line between an arteriole and venule on a planar section. The values shown in this figure are slightly larger than those recorded by Staub and Schultz (83) in dogs, cats and rabbits.

Figure 29

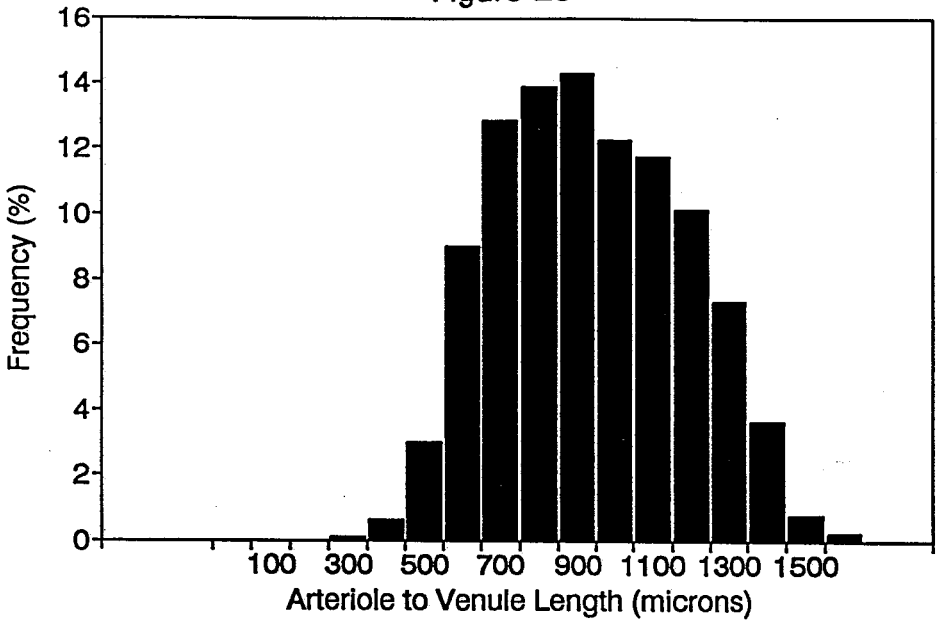
16
14
12
10
8
6
4
2
0
Frequency (%)
100
300
500
700
900
1100
1300
1500
Arteriole to Venule Length (microns)

Figure 30

Shows the RBC transit time estimated using the model where the median value of 0.8 seconds compares well with estimated capillary transit times in normal seated subjects using physiologic techniques.

Figure 30

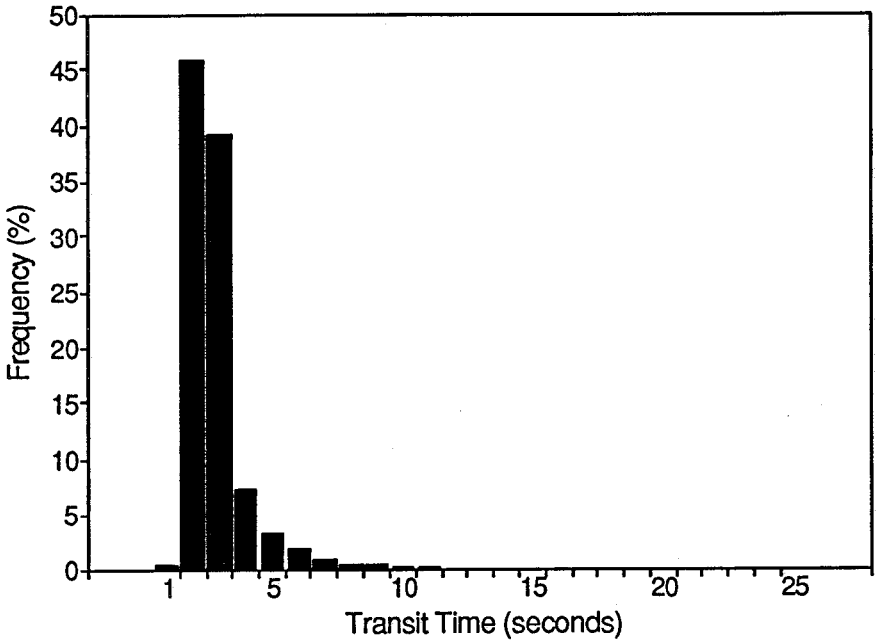
50
45
40
35
30
25
20
15
10
5
0
Frequency (%)
1
5
10
15
20
25
Transit Time (seconds)

Figure 31

This figure shows the estimated transit time for PMN travelling through the pulmonary capillary bed where the median value is 7.8 sec a mean of 145.7 sec with a range of 0.6-10000 sec. The PMN transit times are much longer than those obtained for RBC (Fig. 30) because the PMN were required to stop (based on equation 15) and deform before they could enter a restriction imposed by narrow capillaries.

Figure 31

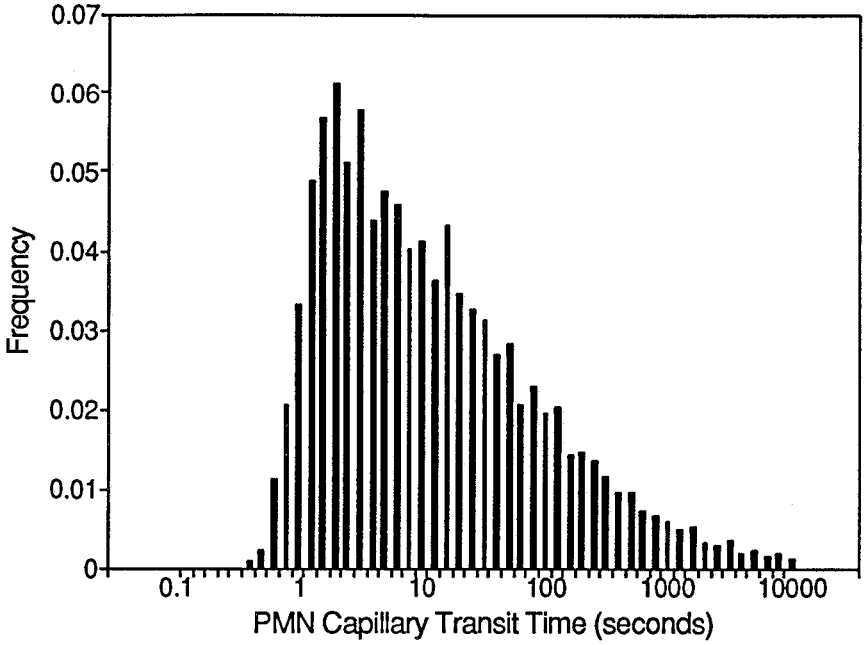
0.07
0.06
0.05
0.04
0.03
0.02
0.01
0
Frequency
0.1
1
10
100
1000
10000
PMN Capillary Transit Time (seconds)

Figure 32

Shows the number of stops made by a PMN as it traversed through the model of the capillary bed. The median number of stops in each of 5 lung regions is shown in Table 17.

Figure 32

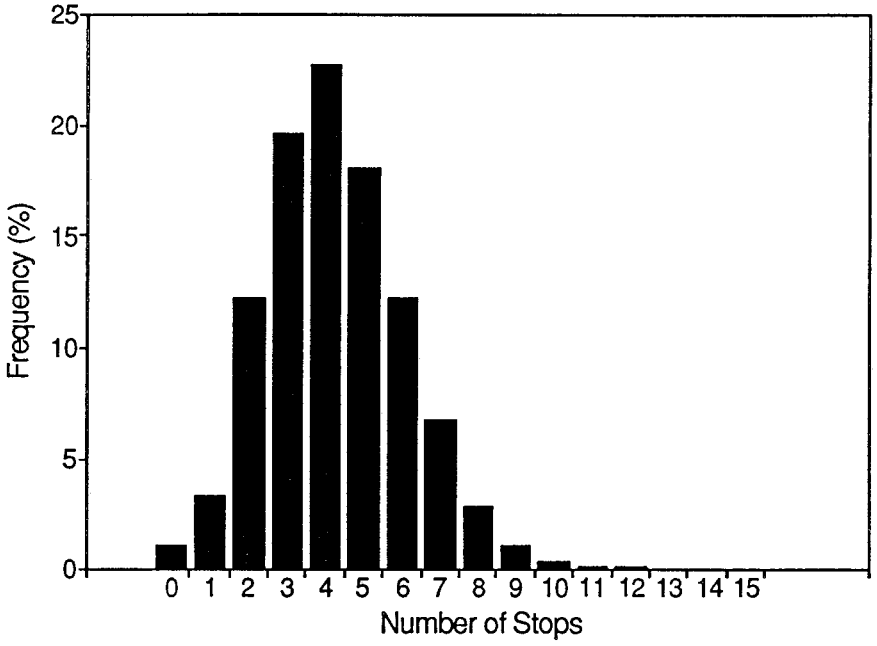
25
20
15
10
5
0
Frequency (%)
0 1 2 3 4 5 6 7 8 9 10 11 12 13 14 15
Number of Stops

Figure 33

Shows the average length of time per PMN stop as they traverse the capillary network. These values are the ratio of the total length of time required for the PMN to traverse the bed divided by the total number of stops.

Figure 33

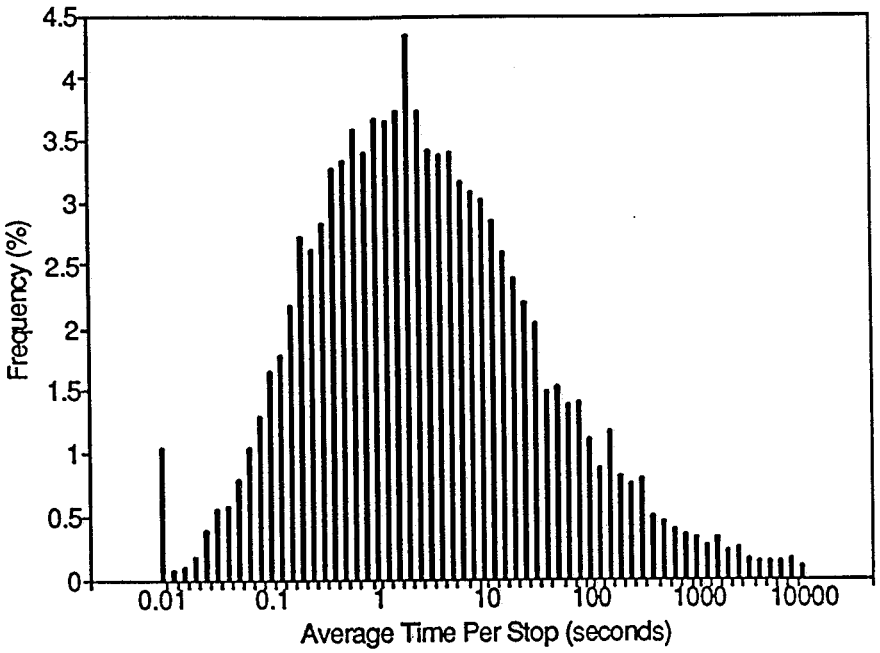
4.5
4
3.5
3
2.5
2
1.5
1
0.5
0
Frequency (%)
0.01
0.1
1
10
100
1000
10000
Average Time Per Stop (seconds)

Figure 34

Shows the distribution of arterial transit times where the median value was 0.7 seconds

.

Figure 34

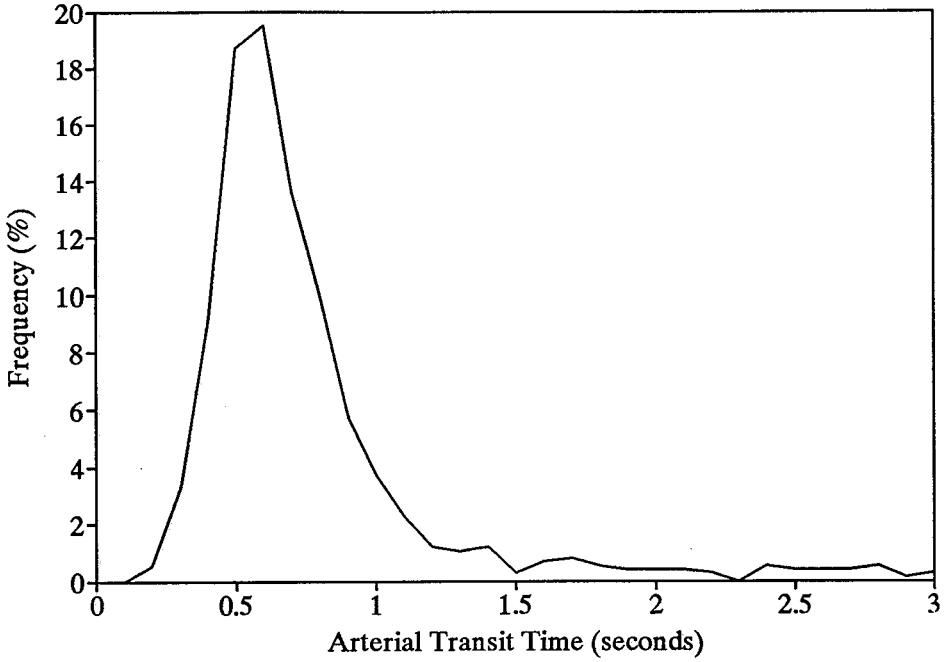
Frequency (%)
20
18
16
14
12
10
8
6
4
2
0
0
0.5
1
1.5
2
2.5
3
Arterial Transit Time (seconds)

Figure 35

Shows the estimated distribution of venous transit times where the median value was 0.8 seconds.

Figure 35

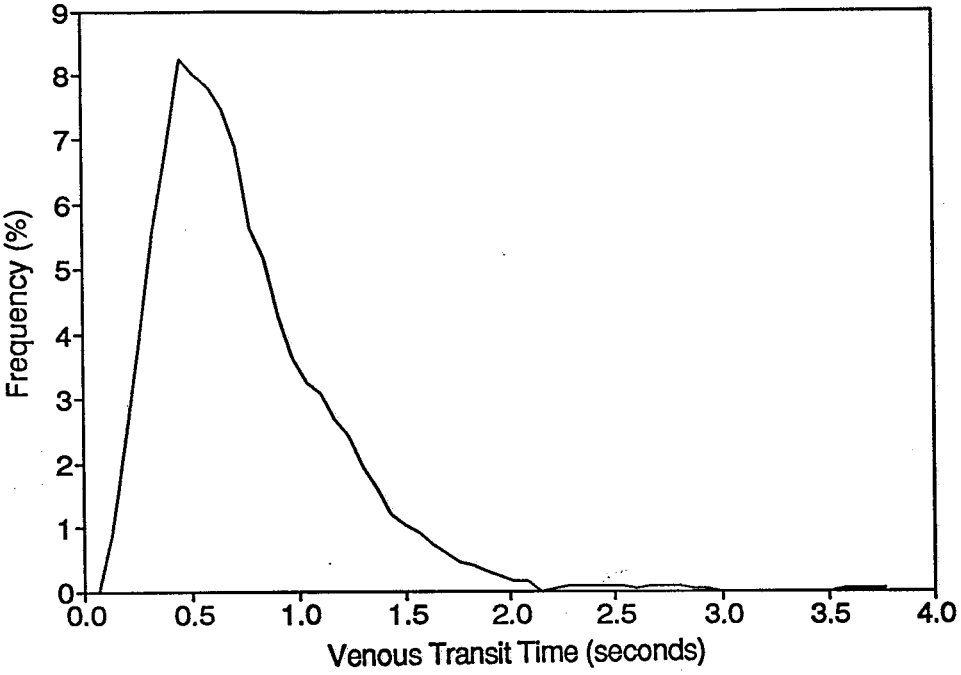
Frequency (%)
9
8
7
6
5
4
3
2
1
0
0.0
0.5
1.0
1.5
2.0
2.5
3.0
3.5
4.0
Venous Transit Time (seconds)

Figure 36

Shows the total pulmonary transit times obtained by connecting the arterial path lengths and venous path lengths and summing their two transit times. This resultant "large vessel" transit time was then convolved with the distribution of capillary transit times for either RBC or a flow weighted distribution of PMN transit times. The median RBC transit time is 2.1 seconds with a range of 0.8-15.4 sec and median PMN transit times of 8.6 seconds with a range of 1.1-9862 sec. The majority of the PMN transit times fall within the range of the RBC transit times.

Figure 36

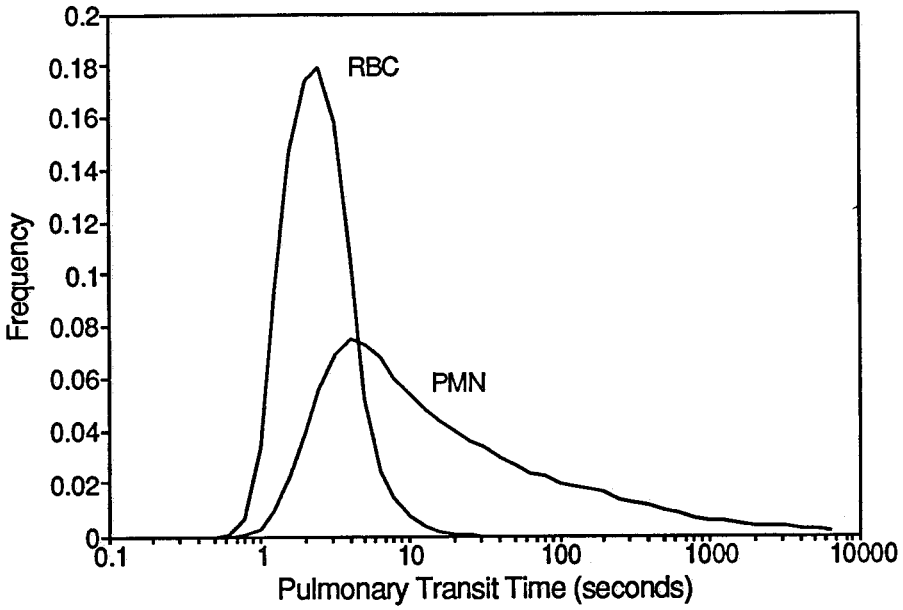
0.2
0.18
0.16
0.14
0.12
0.1
0.08
0.06
0.04
0.02
0
Frequency
RBC
PMN
0.1
1
10
100
1000
10000
Pulmonary Transit Time (seconds)

Figure 37

Compares the time activity curve from reference 62 obtained by direct sampling of central arterial blood following an injection of ^{51}Cr PMN and ^{99Tc}RBC into the central venous circulation (panel A) to the data obtained for PMN and RBC using the model (panel B). Note that in the experimental data, the PMN appearing prior to the recirculation of RBC fall to 0, whereas in the PMN data obtained using the model remains high. This suggests that in vivo one population of PMN traverses the pulmonary circulation with the RBC and the remainder come through more slowly. This is consistent with a biphasic distribution of PMN transits in life which is different from the simple shift of the distribution of PMN transit times to the right of the RBC transit times predicted by the model. It also suggests that far more cells are slowed down in the living circulation than in the model. Note that the data in panel A has been scaled to show frequencies and the model response (panel B) has been shifted by 8 seconds to coincide with the experimental conditions.

Figure 37A

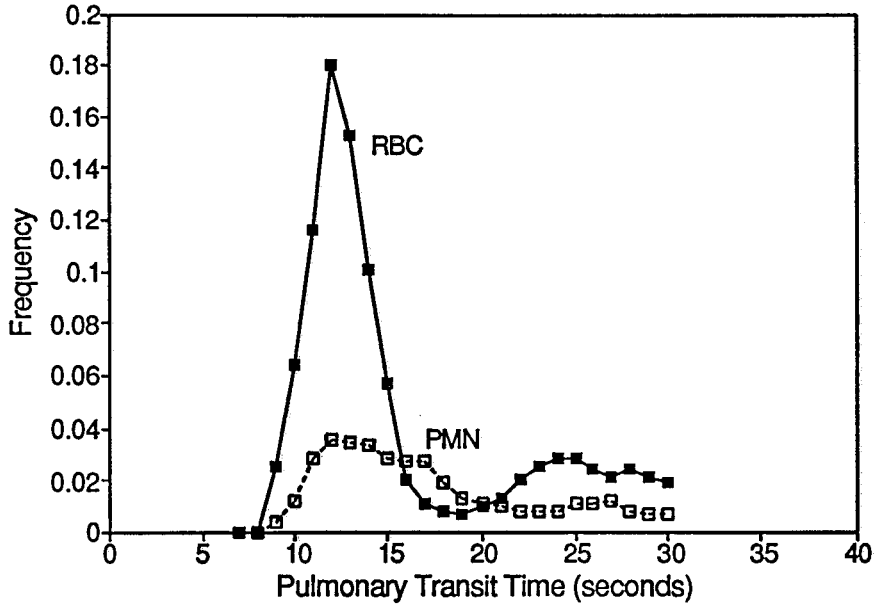

Figure 37B

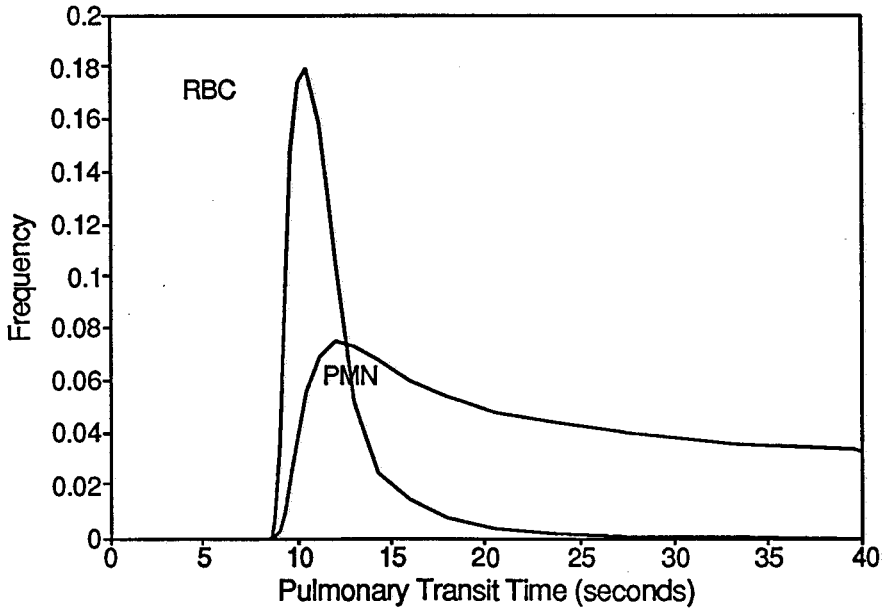

References

1) Andrewes, F.W. Behaviour of the leukocytes in infection and immunity: lecture I. Lancet 1:1737-1734, 1910.

2) Andrewes, F.W. Behaviour of the leukocytes in infection and immunity: lecture II. Lancet 2:8-16, 1910.

3) Anthonisen, N. and Milic-Emili, J. Distribution of pulmonary perfusion in erect man. Journal of Applied Physiology, 21:760-766, 1966.

4) Bassingthwaighte, J.B. and vanBeek, J.H.G. Lightning and the heart: Fractal behavious in cardiac function. Proc IEEE 76:693-699, 1988.

5) Bassingthwaighte, J.B., King, R.B. and Roger, S.A. Fractal nature of regional myocardial blood flow heterogeneity. Circulation Res. 65:578-590, 1989.

6) Bhattacharya, J. and Staub, N. Direct measurement of microvascular pressures in the isolated perfused dog lung. Science, 210:327-328, 1980.

7) Bird, R, Armstrong, R. and Hassager, O. Dynamics of Polymeric Liquids, Volume 1, Fluid Mechanics. John Wiley and Sons, Toronto, 1987

8) Brumwell, M.L., MacNee, W., Doerschuk, C.M., Wiggs, B. and Hogg, J.C. Neutrophil kinetics in normal and emphysematous regions of human lungs. In: Pulmonary Emphysema: The Rationale for Therapeutic Intervention. Weinbaum, G., Giles, R. and Krell, R. (Eds). NY Academy of Sciences, Volume 624, NY, 1991.

9) Burton, A. Physiology and Biophysics of the Circulation. Year Book Medical Publishers, New York, 1972.

10) Capen, R., Hanson, W., Latham, L., Dawson, C. and Wagner Jr., W. Distribution of pulmonary capillary transit times in recruited networks. Journal of Applied Physiology, 69(2):473-478, 1990.

11) Capen, R.L., Graham, J.A., Godbey, P.S., Doerschuk, C.M., Hanger, C.C., Gebb, S.A. and Wagner, W.W. Jr. Comparison of subpleural and interior pulmonary capillary diameters in dogs. FASEB J.7:A541 (Abstract #3137) , 1993.

12) Charm, S. and Kurland, G. Blood flow and microcirculation: A guide to quantitating flow and its clinical significance. John Wiley and Sons, Toronto, 1974.

13) Chien, S. The Microcirculatory Society Eugene M. Landis award lecture. Microvascular Research, 29:129-151, 1985

14) Chien, S., Schmid-Schonbein, G., Sung, K., Schmalzer, E. and Skalak, R. Viscoelastic properties of leukocytes, In: White Cell Mechanics: Basic Science and Clinical Aspects. Meiselman, H., Lichtman, M. and LaCelle, P. (eds) Alan R. Liss, Inc., New York, NY, pp19-51, 1984.

15) Christaller, W. Die Zentralen Orte in Suddeutschland, Gustav Fischer Verlag, Jena. 1933. Translation: Central Places in southern Germany.

16) Collins, J.M., Shapiro, A.H., Kimmel, E. and Kamm, R.D. The Steady Expiratory Pressure-Flow Relation in a Model Pulmonary Bifurcation. Accepted, Journal of Biomechanical Engineering

17) Dewey, C.F. Jr. Biomedical Fluid Mechanics,Unpublished notes for course 2.277, 1991. MIT Mech Eng Dept.

18) Doerschuk, C., Allard, M. and Hogg, J. Neutrophil kinetics in rabbits during infusion of zymosin-activated plasma. Journal of Applied Physiology, 67:88-95, 1989.

19) Doerschuk, C., Allard, M., Lee, S., Brumwell, M. and Hogg, J. Effect of epinephrine on neutrophil kinetics in rabbit lungs. Journal of Applied Physiology, 65:401-407, 1988.

20) Doerschuk, C., Allard, M., Martin, B., McKenzie, A., Autor, A. and Hogg, J. Marginated pool of neutrophils in rabbit lungs. Journal of Applied Physiology, 63:1806-1815, 1987.

21) Doerschuk, C.M., Beyers, N., Coxson, H.O., Wiggs, B. and Hogg, J.C. Comparison of neutrophil and capillary diameters and their relation to neutrophil sequestration in the lung. Journal of Applied Physiology. In press. 1993

22) Evans, E. and Yeung, A. Apparent viscosity and cortical tension of blood granulocytes determined by micropipet aspiration. Biophysics Journal, 56:151-160, 1989.

23) Evans, E. Structural model for passive granulocyte behaviour based on mechanical deformation and recovery after deformation tests. In: White

Cell Mechanics: Basic Science and Clinical Aspects. Meiselman, H., Lichtman, M. and LaCelle, P. (eds) Alan R. Liss, Inc., New Yrok, NY, pp53-71, 1984.

24) Fahraeus, R. and Lindqvist, T. The viscosity of the blood in narrow capillary tubes. American Journal of Physiology, 96:562-568, 1931.

25) Fei, D., Kraft, K. and Fatouros, P. Model studies of nonsteady flow using magnetic resonance imaging. Journal of Biomechanical Engineering, 112:93-99, 1990.

26) Fenton, B., Wilson, D. and Cokelet, G. Analysis of the effects of measured white blood cell entrance times on hemodynamics in a computer model of a microvascular bed. Pflugers Archives, 403:396-401, 1985.

27) Foster, N.K., Martyn, J.B., Rangno, R.E., Hogg, J.C. and Pardy, R.L. Leukocytosis of exercise: role of cardiac output and catecholamines. Journal of Applied Physiology. 61(6):2218-2223, 1986.

28) Fox, R. and McDonald, A. Introduction to Fluid Mechanics, 4th Edition. John Wiley and Sons, Toronto, 1992.

29) Fung, Y. Biodynamics: Circulation. Springer Verlag.. Toronto, 1984.

30) Fung, Y. and Sobin, S. Circulation Research, 30:451-490, 1972.

31) Fung, Y.C., Dynamics of Blood Flow and Pressure-Flow Relationship, in The Lung, ED: Crystal, R.G. and West, J.B. Raven Press, New York 1991

32) Gelin, L. A method for studies of aggregation of blood cells, erythrostasis and plasma skimming in branch capillary tubes. Biorheology, 1:119, 1963.

33) Glazier, J., Hughes, J., Maloney, J. and West, J. Measurements of capillary dimensions and blood volume in rapidly frozen lungs. Journal of Applied Physiology, 26:65-76, 1969.

34) Glenny, R.W., Lamm, W.J.E., Albert, R.K. and Robertson, H.T. Gravity is a minor determinant of pulmonary blood flow distribution. Journal of Applied Physiology, 71:620-629, 1991.

35) Glenny, R.W. Spatial correlation of regional pulmonary perfusion. Journal of Applied Physiology, 72(6), 2378-2386, 1992.

36) Glenny, R.W. and Robertson, H.T. Fractal properties of pulmonary blood flow: charcaterization of spatial heterogeniety. J. Appl. Physiol. 69(2):532-545, 1990

37) Glenny, R.W. and Robertson, H.T. Fractal modeling of pulmonary blood flow heterogeneity. J. Appl. Physiol. 70:1024-1030, 1991

38) Harris, P. and Heath, D. The measurement of blood volume in the lungs. In: The human pulmonary circulation. Churchill Livingstone, Edinburgh, 2nd edition, 1977.

39) Hatabu, H., Gefter, W., Kressel, H., Axel, L. and Lenkinski, R. Pulmonary microvasculature: high resolution MR imaging. Radiology, 171:391-395, 1989.

40) Hogg, J. Neutrophil kinetics in lung injury. Physiological Review. 67:1249-1295, 1987.

41) Hogg, J., McLean, T., Martin, B. and Wiggs, B. Erythrocyte transit and neutrophil concentration in the dog lung. Journal of Applied Physiology, 65(3):1217-1225, 1988.

42) Hogg, J.C., Doerschuk, C.M., Wiggs, B., Minshall, D. Neutrophil retention

during a single transit through the pulmonary circulation. J. Appl. Physiol. 73(4):1683-1685, 1992.

43) Hogg, J.C., Coxson, H.O., Brumwell, M-L, Beyers, N., Doerschuk, C.M., MacNee, W., MacKenzie, A., Opazo Saez, A. and Wiggs, B.R. Polymorphonuclear (PMN) cell transit time and concentration in human pulmonary capillaries. Submitted.

44) Horsfield, K. and Woldenberg, M. Diameters and cross-sectional areas of branches in the human pulmonary arterial tree. Anatomical Record, 223:245-251, 1989.

45) Horsfield, K. Morphometry of the small pulmonary arteries in man. Circulation Research, 42:593-597, 1978.

46) Horsfield, K. and Cumming, G. Morphology of the bronchial tree in man. Journal of Applied Physiology, 24:373-383, 1968.

47) Horsfield, K. and Gordon, W. Morphometry of pulmonary veins in man. Lung, 159:211-218, 1981.

48) Inano, H., English, D. and Doerschuk, C. Effect of zymosan-activated

plasma on the deformability of rabbit polymorphonuclear leukocytes and the role of the cytoskeleton. Accepted. Journal of Applied Physiology, 1992.

49) Johnson, R.L., Spicer, W.S., Bishop, J.M., and Forster, R.E. Pulmonary capillary blood volume flow and diffusing capacity during exercise. Journal of Applied Physiology, 15:893-902, 1960.

50) Kiani, M. and Hudetz, A. A semi-emperical model of apparent blood viscosity as a function of vessel diameter and discharge haematocrit. Biorheology, 28:65-73, 1991.

51) Kolega, J. Effects of mechanical tension on protrusive activity and microfilament and intermediate filament organization in an epidermal epithelium moving in culture. J. Cell Biology 102:1400-1411, 1986.

52) Krenz, G.S., Linehan, J.H. and Dawson, C.A. A fractal continuum model of the pulmonary arterial tree. J. Appl. Physiol. 72(6):225-2237, 1992.

53) Krenz, G.S., Linehan, J.H. and Dawson, C.A. A fractal continuum model of the pulmonary arterial tree. Technical Report No. 362 April 1992 Marquette University.

54) Ku, D., Biancheri, C., Pettigrew, R., Peifer, J., Markou, C. and Engels, H. Evaluation of magnetic resonance velocimetry for steady flow. Journal of Biomechanical Engineering, 112:464-472, 1990.

55) Lewis, B.M., Forster, R.E., and Beckman, E.L. Effect of inflation of a pressure suit on pulmonary diffusing capacity in man. Journal of Applied Physiology, 12:57-64, 1958.

56) Lien, D., Wagner Jr, W., Capen, R., Haslett, C., Hanson, P. and Worthen, S. Physiological neutrophil sequestration in the lung: visual evidence for localization in capillaries. Journal of Applied Physiology, 62:1236-1243, 1987.

57) Lien, D., Worthen, S., Capen, R., Hanson, W., Checkley, L., Janke, S., Hensen and Wagner Jr., W. Neutrophil kinetics in the pulmonary microcirculation. ARRD, 141:953-959, 1990.

58) Lipowsky, H. and Zweifach, B. Network analysis of microcirculation of cat mesentery. Microvascular Research, 7:73-83, 1974.

59) MacNee, W., Martin, B., Wiggs, B., Belzberg, A. and Hogg, J. Regional pulmonary transit times in humans. Journal of Applied Physiology, 66:844-850, 1989.

60) MacNee, W., Wiggs, B., Belzberg, A. and Hogg, J. The effects of cigarette smoking on neutrophil kinetics in human lungs. New England Journal of Medicine, 321:924-928, 1989.

61) Manderino, G.L., Suarez, A.F., Hirata, A.A. and Ward, P. Chemotaxis under agarose utilizing human serum depleted of C-5 derived peptides. Journal of Immunological Methods, 45:283-299, 1981.

62) Martin, B., Wright, J., Thommasen, H. and Hogg, J. Effect of pulmonary blood flow on the exchange between circulating and marginating pool of polymorphonuclear leukocytes in dog lungs. Journal of Clinical Investigation, 69:1277-1285, 1982.

63) Martin, B., Wiggs, B., Lee, S. and Hogg, J. Regional differences in neutrophil margination in dog lungs. Journal of Applied Physiology, 63(3):1253-1261, 1987.

64) Maseri, A., Caldini, P., Permutt, S. and Zierler, K.L. Frequency function of

transit times through dog pulmonary circulation. Circulation Research, 26:527-543, 1970.

65) Mayrovitz, H.N. and Rubin, R. Leukocyte distribution to arteriolar branches: dependence on microvasculature blood flow. Microvascular Research 29:282-294, 1985.

66) McNeill, R.S., Rankin, R.S. and Forster, R.E. The diffusing capacity of the pulmonary membrane and the pulmonry capillary blood volume in cardiopulmonary disease. Clinical Science 17:465-82.

67) Milic-Emili, J, Henderson, J.A.M., Dolovich, M.B., Trop, D. and Kaneko, K. Regional distribution of inspired gas in the lung. J. Appl. Physiol. 21:749-759, 1966.

68) Muir, A.L., Cruz, M., Martin, B., Thommasen. Belzberg, A. and Hogg, J.C. Leukocyte kinetics in the human lung: role of exercise and catecholamines. Journal of Applied Physiology, 57(3), 711-719, 1984.

69) Murray, C.D. The physiological principle of minimum work. I. The vascular system and the cost of blood volume. Proc. Nat. Acad. Sci. 12:207-214, 1926.

70) Needham, D. and Hochmuth, R. Rapid flow of passive neutrophils into a 4μm pipet and measurement of cytoplasmic viscosity. Journal of Biomechanical Engineering, 112:269-276, 1990.

71) Parker, S. Fluid Mechanics source book. McGraw-Hill, Toronto, 1987.

72) Pedley, T., Schroter, R. and Sudlow, M. Energy losses and pressure drop in models of human airways. Respiration Physiology, 9:371-386, 1970.

73) Peters, A.M., Allsop, P., Stuttle, A.W.J., Arnot, R.N., Gwilliam, M. and Hall, G.M. Granulocyte margination in the human lung and its response to strenous exercise. Clinical Science, 82:237-244, 1992.

74) Reeves, J., Dempsey, J. and Grover, R. Pulmonary circulation during exercise. In: Pulmonary Vascular Physiology and Pathophysiology, Weir, K. and Reeves, J. (Eds) Marcel Dekker, Inc, New York, pp107-134, 1989.

75) Schmid-Schonbein, G., Shik, Y. and Chien, S. Morphometry of human leukocytes. Blood, 56:866-875, 1980.

76) Schmid-Schonbein, G. Capillary plugging by granulocytes and the no-

reflow phenomenon in the microcirculation. Federation Proceedings 46:2397-2401, 1987.

77) Schowalter, W.R. Mechanics of non-newtonian fluids. Pergammon Press. Toronto, 1978.

78) Singhal, S., Henderson, R., Horsfield, K., Harding, K. and Cumming, G. Morphometry of the human pulmonary arterial tree. Circulation Research, 33:190-197, 1973.

79) Singhal, S., Cumming, G., Horsfield, K., and Harding, L. Morphometric study of pulmonary arterial tree and its hemodynamics. Journal of the Association of Physicians of India, 21:719-722, 1973.

80) Skalak, R., Dong, C. and Zhu, C. Passive deformation and active motions of leukocytes. Journal of Biomechanical Engineering, 112:295-302, 1990.

81) Skalak, T. A mathematical hemodynamic network model of the microcirculation in skeletal muscle, using measured blood vessel distensibility and topology. PhD Thesis, University of California, San Diego, 1984.

82) Sobin, S., Fung, Y., Tremer, H. and Rosenquist, T. Circulation Research, 30:440-450, 1972.

83) Staub, N. and Schultz, E. Pulmonary capillary length in dog, cat and rabbit. Respiration Physiology, 5:371-378, 1968.

84) Steel, C.M., French, E.B., and Aitchison, W.J.R. Studies on adrenalin-induced leukocytosis in normal man. 1. The role of the spleen and the thoracic duct. British Journal of Hematology, 21:413, 1971.

85) Strahler, A. Quantitative analysis of watershed geomorphology. Transactions of the American Geophys. Union. 38:913-920, 1957.

86) Sweadner, J.K. and Goldin, S.M. Active transport of sodium and potassium ions: mechanism, function and regulation. New England Journal of Med. 302:777-783, 1980.

87) Tompsett, P. Anatomical Techniques. London, Livingstone, 1956.

88) Uylings, H. Optimization ofdiameters and bifurcation angles in lung and vascular tree structures. Bull. Math. Biol. 39: 509-520, 1977.

89) Wagner, P.D., Saltzman, H.A. and West, J.B. Measurements of continuous distributions of ventilation-perfusion ratios: theory. J. Appl. Physiol. 36:588-599, 1974.

90) Warnke, K. and Skalak T. *In vivo* measurement of leukocyte viscosity during capillary plugging. Journal of Biomechanical Engineering, November, 1992. In Press.

91) Warnke, K. and Skalak, T. Leukocyte plugging in vivo in skeletal muscle arteriolar trees. American Journal of Physiology, 262:H1149-H1155, 1992.

92) Warnke, K. and Skalak, T. The effects of leukocytes on blood flow in a model skeletal muscle capillary network. Microvascular Research, 40:118-136, 1990.

93) Warrell, D., Evans, J., Clarke, R., Kingaby, G. and West, J. Pattern of filling in the pulmonary capillary bed. Journal of Applied Physiology, 32:346-356, 1972.

94) Watson, J.D. and Crick, F.H.C. Genetic implications of the structure of deoxyribonucleic acid. Nature 171:964-967, 1953

95) Weibel, E. Morphometry of the human lung.Academic Press Inc, New York, New York, 1963.

96) Weibel, E. and Gomez, D. Architecture of the human lung. Science, 137:577-585, 1962.

97) Welsh, M.J. Electrolyte transport by airway epithelia. Physiol. Review 67:1143-1184, 1987.

98) West, J.B. Ventilation-perfusion inequality and overall gas exchange in computer models of the lung. Respir. Physiol. 7:88-110, 1969

99) West, J. Ventilation/Blood Flow and Gas Exchange, 4th Edition. Blackwell Scientific, Boston, 1985.

100) West, J., Schneider, A. and Mitchell, M. Recruitment in networks of pulmonary capillaries. Journal of Applied Physiology, 39:976-984, 1975.

101) Wiggs, B.R. Modelling the resistance to airflow in the human lung. University

of BC, MSc Thesis, 1989.

102) Wiggs, B.R., Moreno, R., Hogg, J., Hilliam, C. and Pare, P. A model of the mechanics of airway narrowing. Journal of Applied Physiology, 69(3):849-860, 1989.

103) Wiggs, B.R., Bosken, C., Pare, P.D., James, A.J. and Hogg, J.C. A model of airway narrowing in asthma and in chronic obstructive disease. Amer. Rev. Resp. Dis. 145:1251-1258, 1992.

104) Williams, M. Stereological Techniques. In: Practical Methods in Electron Microscopy, Ed. Glauert, A. North-Holland, Amsterdam, Vol. 6, 5-84, 1980.

105) Woldenberg, M. A periodic table of spatial hierarchies. In: *Philosophy in Geography* Ed: Gale, S and Olsson, G. D. Reidel Publishing. 429-456, 1979.

106) Woldenberg, M. The average hexagon in spatial hierarchies. In: *Spatial Analysis in Geomorphology.* Ed: Chorley, R.J. Springfield Press. pp323-352, 1972.

107) Woldenberg, M. A structural taxonomy of spatial hierarchies. In: *Regional*

Forecasting, Proceedings of the Colston Research Society #22 Ed: Chisholm, M., Frey, A. and Haggett, P. Butterworths, London, pp147-175, 1971.

108) Yen, R.T. and Fung, Y.C. Effect of velocity distribution on red cell distribution in capillary blood vessels. Am. J. Physiol. (Heart Circ. Physiol): H251-H257, 1978.

109) Yen, R.T., Zhuang, F.Y., Fung, Y.C., Ho, H.H., Tremer, H. and Sobin, S.S. Morphometry of cats pulmonary arterial tree. J. Biomech. Eng. 106:131-136, 1984

110) Zhuang, F., Fung, Y. and Yen, R. Analysis of blood flow in cat's lung with detailed anatomical elasticity data. Journal of Applied Physiology: Respiration, Environmental and Exercise Physiology, 55:1341-1348, 1983.